鋼コンクリート複合構造の力学特性解析法確立に関する研究

（１１４５０１６９）

平成 11 年度～13 年度科学研究費補助金（基盤研究(B)(2)）研究成果報告書

平成１４年３月

研究代表者　町田篤彦
（埼玉大学工学部教授）

埼大コーナー
埼玉大学附属図書館
998005243

１．はしがき

近年、構造物が巨大化するとともに、供用中の構造物のごく近傍あるいは水深の深い水中に建設し、騒音・振動など環境に及ぼす影響を最小限に抑え、その上、経済的になど、構造物に対する要求条件がますます複雑多岐にわたるようになってきた。従来、一つの構造物は、鋼構造あるいは鉄筋コンクリート構造というように、一種類の材料を用いて建設されることが極めて多かったが、それぞれの材料特性に応じて、鋼とコンクリートを適宜に組み合わせた複合構造とすれば、力学的に合理的な構造とすることが可能となり、構造物に要求される複雑多岐な性能を満足させるのが容易となる場合が少なくない。このため、橋梁をはじめとする各種の構造物に複合構造を適用しようとする技術開発が盛んに行われるようになってきた。

このようなメリットがある鋼コンクリート複合構造に対しては、これを合理的に設計すべく、設計基準類が整備されつつはあるが、現状では、その力学的な挙動を的確に予測できる解析手法は確立されていないといって過言でない。これは、一方では、複合構造が多岐にわたるため、従来の知見を一般化するのが困難であることに起因しているが、もう一方では、基本特性の解明が徹底的に遅れていることに大きな原因がある。このため、新たな複合構造を建設しようとするときには、大規模な実験を行うことが余儀なくされている状況を招いている。

本研究「鋼コンクリート複合構造の力学特性解析法確立に関する研究」は、このような背景のもとに立案したもので、鋼コンクリート複合構造全般にわたって、その通常の使用状態下および地震その他の荷重を受ける極限状態下の力学的挙動を的確に予測できる解析法を確立することを目標とした。これを達成するため、まず、鋼材とコンクリートの付着特性、ずれ止めの挙動といった、複合構造の挙動を左右する鋼材とコンクリートとの力の伝達メカニズムに着目して、その基本的解明を図り、力学モデルを作成した。ついで、鋼コンクリート接合部の挙動を、上記に基づいた解析および実験により解明し、接合部内における力の伝達メカニズム、接合部の構造細目が力学的特性に及ぼす影響などを明らかにしようと検討を重ねた。これらの成果に基づいて、全体構造の力学的特性を解析する場合のモデル化の方法、接合部の取り扱いなどを明らかにする研究に歩を進め、解析法の方法論を確立することに努めた。

研究組織

本研究の研究組織は、下記のようである。この種の研究は、鋼構造の研究者、コンクリート構造の研究者および構造解析の研究者が密接な連携を保って進める必要があり、このため、研究代表者が連携をとりやすい研究者に参加を求め、下記ような研究組織としたのである。

研究代表者：町田篤彦　　埼玉大学工学部教授
研究分担者：山口宏樹　　埼玉大学工学部教授
研究分担者：睦好宏史　　埼玉大学工学部教授
研究分担者：奥井義昭　　埼玉大学工学部助教授
研究分担者：牧　剛史　　埼玉大学工学部助手

研究経費

平成１１年度	３，２００千円
平成１２年度	３，３００千円
平成１３年度	１，８００千円
計	８，３００千円

研究発表

（１）学会誌等

Chakree Bamrungwong, Finite Element analysis of steel girder-concrete pier rigid connection コンクリート工学年次論文報告集、Vol.22-3、pp.997-1002, 2000

Chakree Bamrungwong, Finite Element analysis of steel Girder-Concrete Pier Composite Connection with Application of Interface Element, コンクリート工学年次論文報告集,Vol.23-1、pp.763-768, 2001

（２）口頭発表

（３）出版物

なし

2. 研究成果

（１）穴あき鋼板が伝達し得るせん断力について既往の文献を調査した結果、終局せん断力は、穴の面積およびコンクリート強度に概ね比例すること、このことを仮定した場合、実験値は穴径が小さい場合やや大きく、大きい場合やや小さい傾向があること、実験値の回帰曲線を０．７倍すれば、終局せん断力を安全側に評価できることが明らかになった。

（２）一般鋼材とコンクリートとの付着特性に関する既往の文献を調査した結果、付着強度は摩擦係数によって整理するのが便利であり、かぶりの影響は側圧に換算して、これを表すことが可能であって、その力学特性は鋼板とコンクリートの接触問題として定式化できることが判明した。

（3） スタッドジベルに関し、これを溶植した鋼材をコンクリートに埋め込んだ供試体につき載荷実験を行った結果、本研究の準備となる研究で得たスタッドジベルの解析プログラムは十分な精度でその挙動を予測できるが、これを全体構造の解析に用いるには、単純化する必要が認められた。単純化の一つの方法として、一端を鋼板に他端をコンクリートに固定した梁要素とし、その曲げ剛性を前述の解析プログラムであらかじめ求めておく方法が有望であるが、なお検討が必要である。

（4） 鋼桁を鉄筋コンクリート橋脚に剛結する形式の複合構造について、小型供試体を用いた載荷実験の結果と有限要素解析を対比した結果、鋼板とコンクリートを完全付着とし、相互の剥離を考慮しない場合、コンクリートの構成則として、分散ひび割れモデルを用いてひずみ軟化を考慮し、等方性材料として破壊基準をモールクーロン則、混合硬化とすれば、満足できる程度に接合部の挙動を推定できるが、大変形領域での精度を向上させるには、鋼板とコンクリートのすべりならびに剥離を考慮する必要があることが明らかとなった。

（5） コンクリートと鉄筋の付着およびコンクリートと鋼板の付着をより厳密に取り扱うため、既往のモデルをもとに、付着特性をバネで表現する付着要素の開発を行った。特に、コンクリートと鋼板の付着要素は、すべりおよび剥離を考慮できるようにした。

（6） 開発した有限要素プログラムによる解析結果と載荷実験の結果と対比した結果、このプログラムによれば、大変形領域まで精度よく力学挙動を追跡できることが示された。このプログラムは、開発で主に対象とした複合構造以外の複合構造にも用いることができる。

（7） 開発した有限要素プログラムを用い、鋼桁を鉄筋コンクリート橋脚に剛結する複合橋梁の挙動解析を重ねた結果、接合に特別の工夫をしない限り、上部構造からの荷重の大部分は接合部近傍に伝達され、横方向には分散しないことが明らかとなった。また、横桁にダイヤフラムを設け、そのダイヤフラムにフランジを付ければ、荷重は横方向へ効果的に分散伝達されることも明らかとなった。

（8） 解析結果を基に、より簡便に接合部の力学挙動を解明し、設計に結びつけることができるストラット・タイモデルを開発した。

以上の成果の詳細を、以下に示す。なお、このような成果が得られ、鋼コンクリート複合構造の開発に貢献できたことは、科学研究費補助金が与えられたことと研究分担者各位の熱心なご協力によるところが大きい。ここに記して、厚くお礼申し上げる次第である。

鋼桁とRC橋脚を剛結した複合ラーメン橋接合部の力学特性に関する研究

石澤 徹[1]・町田 篤彦[2]・長谷 俊彦[3]・佐藤 徹[4]

[1]正会員　埼玉大学大学院　理工学研究科（〒336-0907　埼玉県浦和市道祖土4-34-4-203）
[2]正会員　工博　埼玉大学教授　工学部建設工学科（〒338-8570　埼玉県浦和市下大久保255）
[3]正会員　JH試験研究所　橋梁研究室（〒194-8508　東京都町田市忠生1-4-1）
[4]正会員　(株) 宮地鐵工所　技術本部　技術部技術開発課（〒290-8580　千葉県市原市八幡海岸通3）

鋼桁とRC橋脚を剛結した複合ラーメン橋接合部の設計を行なう場合，合理的に主桁断面力をRC橋脚に伝達させることが重要となるが，その荷重伝達機構は解明されてはいない．本研究では複合ラーメン橋接合部の実験結果と解析結果の比較により解析の妥当性を検討した後，実構造物をモデルとした3次元FEMを行ない接合部コンクリート，横桁，橋脚の各部に関して詳細な検討を行なうことで，合理的な接合部構造形式の提案と荷重伝達機構の解明を試みた．

***Key Words** : load transfer mechanism , concrete in connection , cross girder , RC column , 3-dimensional finite element method*

1．はじめに

鋼桁とRC橋脚を剛結した複合ラーメン橋が日本道路公団を中心としてこれまでいくつか建設されており，さらに近年では鋼2主桁形式の標準化へ向けた検討が行われている．しかし複合ラーメン橋接合部の設計法については，鋼桁からRC橋脚への荷重伝達機構が解明されておらず，また合理的に荷重を伝達させる接合部の構造形式が確立されていない．そのための共通の設計法が示されていないのが現状である．

本研究では3次元FEM解析と複合ラーメン橋接合部の実験結果とを比較することによって解析手法の妥当性を検討した後，実構造物を対象とした解析を行なった．この解析結果をもとに接合部を構成する部材である接合部コンクリート，横桁に着目した検討を行なうことで，より合理的な接合部構造形式の提案と荷重伝達機構を解明しようとした．

2．複合ラーメン橋接合部の実験

(1) 実験供試体

実験供試体は鋼鈑桁とRC柱を剛結し，RC柱を取り囲む形で横桁を配し横桁ウェブにはスタッドを配置したものである．供試体外観を図−2.1 に，供試体寸法を図−2.2 に示す．実験にあたってはRC柱から鋼桁への荷重伝達機構を明確にする目的で，荷重の伝達に主要な役割を果た

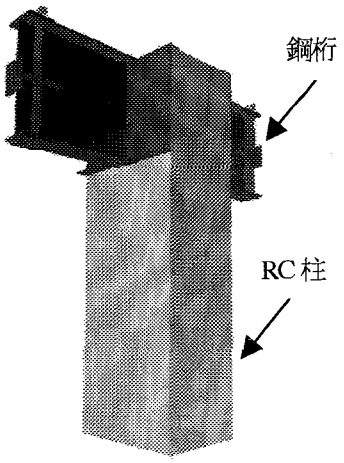

図−2．1　実験供試体外観（TYPE-1B）

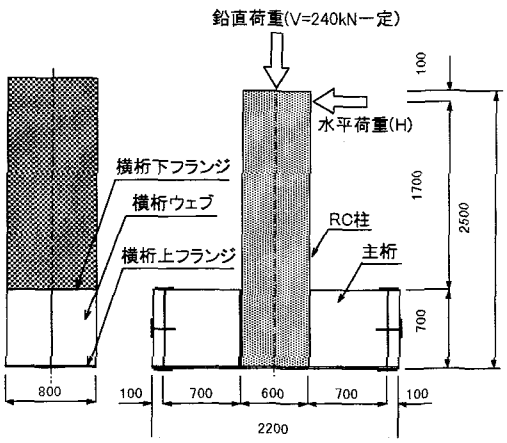

図−2.2 供試体寸法

表−2.1 実験供試体の種類

供試体No	横桁のスタッド	横桁形状
TYPE-1A	30本	下フランジ外向き
TYPE-1B	16本	下フランジ外向き
TYPE-1C	16本	下フランジ内向き
TYPE-1C'	なし	下フランジ内向き
TYPE-1D	16本	横桁は主桁と定着せず 帯鉄筋が横桁を貫通
TYPE-2	なし	RC柱内部に埋め込み 横桁間隔300mm
TYPE-3	16本	RC柱幅から張り出す 横桁間隔760mm

表−2.2 実験供試体の材料特性

コンクリート (早強コンクリート)	弾性係数 23.4 kN/mm^2 圧縮強度 31.6 N/mm^2
鋼板 (SM400A)	弾性係数 212.1 kN/mm^2 降伏強度 304.6 N/mm^2 引張強度 457.8 N/mm^2
鉄筋 (SD345)	弾性係数 191.7 kN/mm^2 降伏強度 380.7 N/mm^2 引張強度 557.2 N/mm^2

すとされる横桁，横桁ウェブのスタッドに着目し横桁形状，スタッド本数，横桁･スタッドの有無をパラメータとした．表−2.1 にこれらの供試体の種類を示す．また用いた材料の特性は表−2.2 に示す．

(2) 実験方法

実験は供試体をローラー上に横向きの状態で設置し，主桁端部（片側可動，片側固定）を支点とし RC 柱に載荷する方法で行なった．上部工自重分（V=240kN）を鉛直荷重として一定載荷した状態で水平荷重を加える方法で載荷を行ない，単調載荷試験と正負交番載荷試験を行なった．図−2.3 に実験レイアウトを示す．

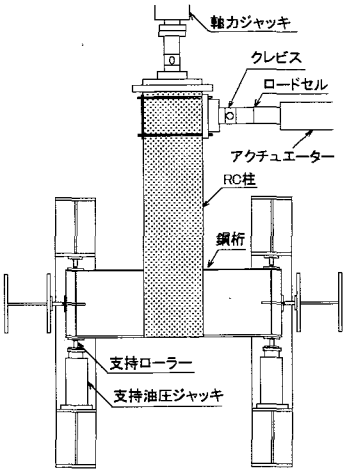

図−2.3 実験レイアウト

(3) 実験結果

実験結果の概要を表−2.3 に示す．単調載荷試験では横桁下フランジ内向きの TYPE-1C とスタッド本数の多い TYPE-1A の変位が比較的小さく接合部構造形式により変位の差がみられた．正負交番載荷試験では 20δy 付近まで TYPE-1D を除いては十分なじん性を有していることが示された．

表−2.3 実験結果

供試体No	鉄筋降伏荷重 (kN)	降伏変位δy (mm)	最大荷重 (kN)	終局変位 (最大変位)	破壊形状
計算値*	336.4	4.73	−	−	−
TYPE-1A	289.0	5.77	459.0	+23δy	RC柱の曲げ破壊
TYPE-1B	298.5	7.61	489.5	+20δy	RC柱の曲げ破壊
TYPE-1C	283.0	5.97	458.5	+23δy	RC柱の曲げ破壊
TYPE-1C'	313.5	6.92	449.0	+20δy	RC柱の曲げ破壊
TYPE-1D	297.5	7.89	352.0	+3δy	接合部のせん断破壊
TYPE-2	311.0	7.99	463.5	+20δy	RC柱の曲げ破壊
TYPE-3	349.5	7.85	466.5	+20δy	接合部せん断破壊 RC柱曲げ破壊

＊RC 柱断面計算による

3．解析の概要と実験結果との比較

(1) 解析方法

解析には非線型有限要素法汎用プログラム MARC を使用した．

コンクリート部分には 8 節点ソリッド要素を使用し，その破壊条件は Mohr-Coulomb 則とした．図−3．1 にコ

ンクリートの構成曲線を示す．これは実験供試体で用いたコンクリートの圧縮強度試験の結果から得られた曲線を直線との差を考慮し試験値に 0.85 を乗じた値を用いた．なお図のように，圧縮域ではひずみが 0.002 に達すると

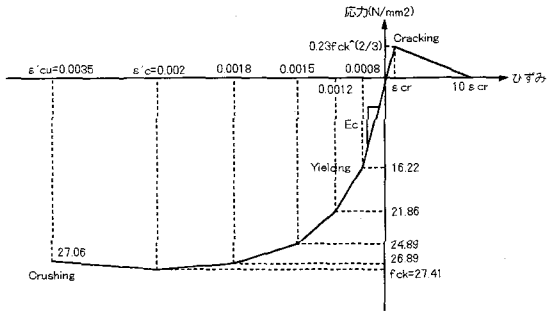

図−3.1 コンクリートの構成曲線

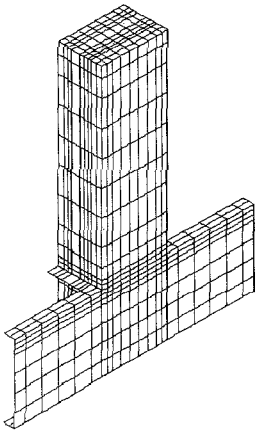

図−3.2 解析モデル（TYPE-1B）

ひずみ軟化が発生し，0.0035 では圧壊が生ずるとした．また引張域ではひび割れは主応力が引張強度（$0.23f'ck^{2/3}$ (N/mm^2)）に達した時点で主応力と直角方向に発生し，その後ひび割れひずみの 10 倍に達するまで直線的にひずみ軟化が発生すると定義した．

鋼板には 4 節点厚肉シェル要素を使用し，コンクリートとの接合面ではすべりのみを考慮し剥離は考慮しない条件とした．鉄筋には 2 節点 3 次元トラス要素を，スタッドには 2 節点 3 次元弾性はり要素を使用し，どちらもコンクリートとは完全付着とした．鋼材の降伏条件は von - Mises とし，応力−ひずみ曲線は完全弾塑性体とした．

(2) 解析モデル

解析モデルは実験供試体を主桁ウェブ中央で分割した 1/2 モデルとした．解析モデルを図−3．2 に示す．解析は TYPE-1A を除く 6 供試体の単調載荷試験について行ない，荷重は実験と同様に鉛直荷重を与えた後水平荷重を節点に作用させる方法で，単調載荷試験の最大荷重付近まで載荷した．

(3) 実験結果との比較

a) 変位

図−3.3 に一例として TYPE-1C の水平荷重−水平変位

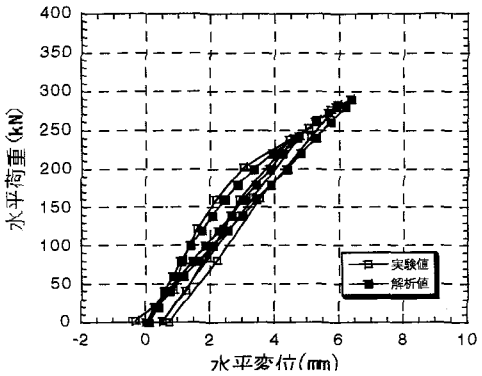

図−3.3 水平荷重−水平変位関係（TYPE-1C）

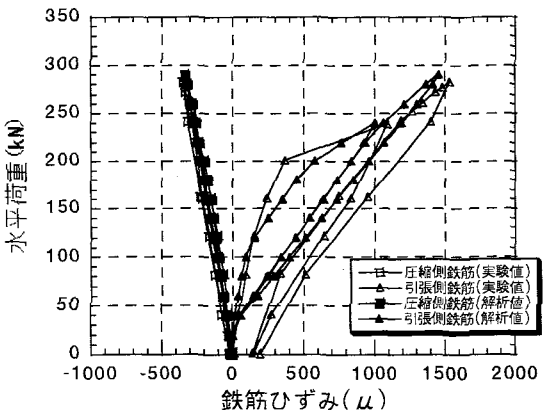

図−3.4 水平荷重−主鉄筋ひずみ関係（TYPE-1C）

関係を示す．この図のように，4 タイプの解析による荷重−変位関係は実験と比較して全てよく一致した．

b) 鉄筋のひずみ

図−3.4 に TYPE-1C の水平荷重−鉄筋ひずみ関係を示す．この図は主桁に近い側の鉄筋であるが，主桁から離れた側の鉄筋についても同様に全て実験値とよく一致した．

c) 鋼板の主ひずみ

図−3．5，図−3．6 に単調載荷試験の最大荷重時における鋼桁の主ひずみ分布を示す．主桁，横桁とも主ひずみ方向はよく合っており特に横桁では大きさ，方向ともよく一致しているといえる．

これらのことから本研究の解析は妥当な結果を与える

と判断される．

4．実構造物を対象とした解析

(1) 解析方法および解析モデル

ここでは2主桁鈑桁形式の複合ラーメン橋を対象とした実構造物モデルについて解析を行なった．解析モデル

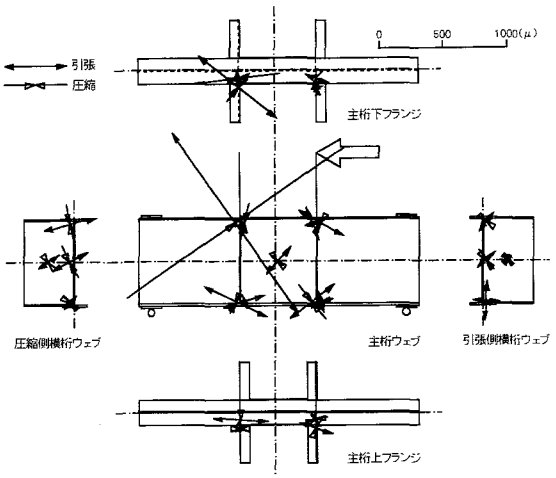

図−3.5 鋼桁主ひずみ実験値（TYPE-1B）

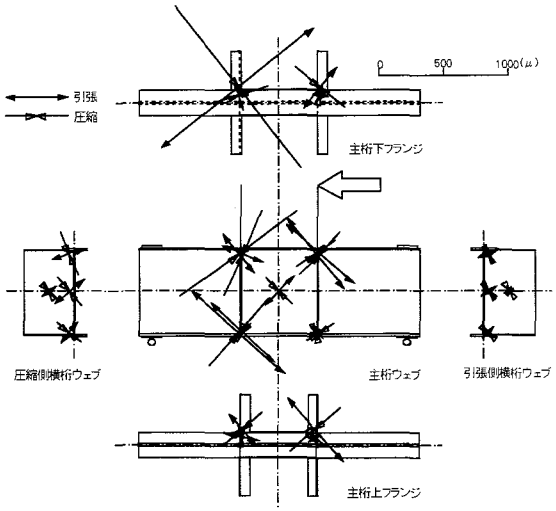

図−3.6 鋼桁主ひずみ解析値（TYPE-1B）

では接合部をT字型に取り出し主桁ウェブと平行な面で2主桁の中間部で橋脚を分割した．接合部コンクリートは，主桁ウェブ，横桁ウェブで取り囲んだ形式とし，荷重伝達に及ぼすスタッドの働きを考え，スタッドは横桁ウェブのみに配置し他には一切配置していない．使用要素，材料定数などの解析方法は前章の解析と同一とした．図−4.1に解析モデルを示す．

載荷方法は上部工の自重分（約62kN/m^2）を主桁上フランジに分布荷重として一定載荷した状態で，主桁端部に鉛直方向に等価な偶力を与え接合部に曲げモーメントが作用するよう，主鉄筋が降伏するまで単調増分載荷を行なった．支点条件はRC橋脚下面を完全固定とし，切断面では面の法線方向の変位，および面の接線まわりの回転を拘束した．

解析モデルは，横桁構造の違いにより以下の3モデルについて比較検討を行なった．

Model-1：横桁が接合部コンクリートを取り囲む形で配置され、横桁上下フランジが外向きで接合部コンクリート

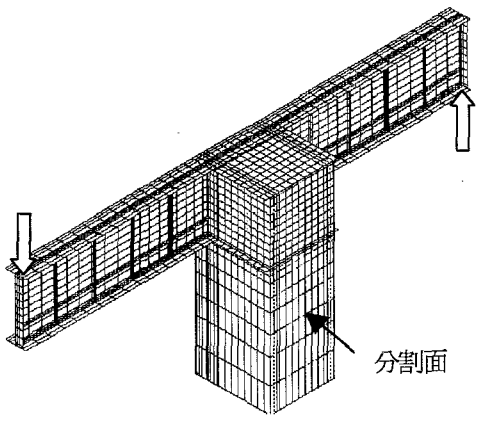

図−4.1 解析モデル

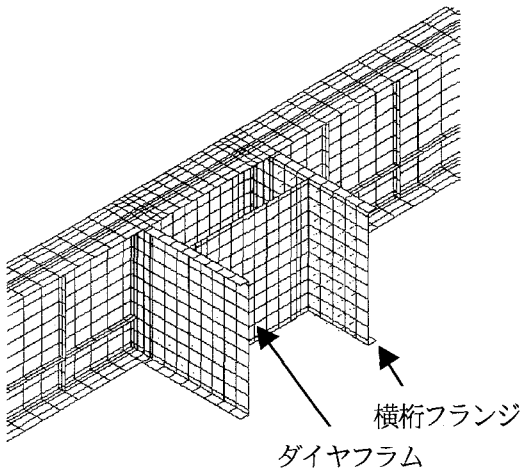

図−4.2 解析モデルの横桁構造（Model-3）

と横桁がスタッドのみで接合されており，3モデルの中で鋼桁からコンクリートへの荷重伝達作用が最も低いと予想される．

Model-2：横桁上下フランジが内向きで下フランジがRC橋脚内に埋め込まれており，フランジを貫通して主鉄筋が配置されている．Model-1と比較して横桁から接合部コンクリートへのモーメントの伝達作用が増加し接合部コンクリートの圧縮ストラット形成作用が高まると予想される．

Model-3：横桁フランジの向きはModel-1と同様とし，横桁間にダイヤフラムを配置し両側の横桁を接合することによって横桁の剛性を高めたため，横桁からの接合部コンクリートへの荷重伝達作用が増すと予想される．ダイ

ヤフラムの寸法は2900×3000mmで厚さは主桁ウェブと同様の 18mm とし，主桁位置から 1450mm（主桁間隔 5900mm を想定）の位置に配置した．

図−4．2に Model-3 の接合部構造を示す．

5．接合部コンクリートの挙動

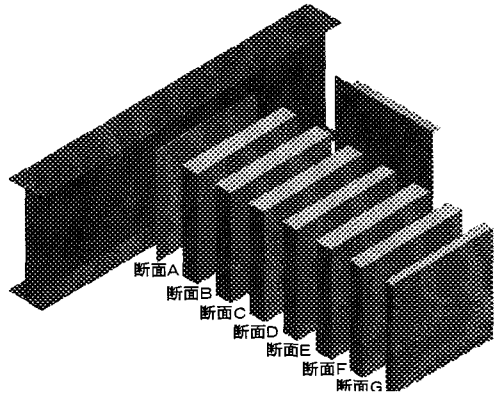

図−5.1 荷重計算断面

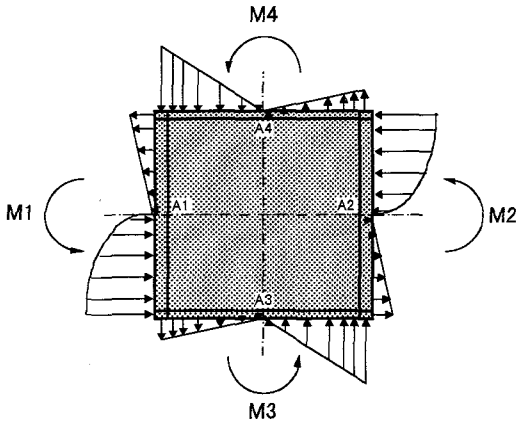

図−5.3 断面のモーメント計算

(1) 接合部コンクリートに作用するモーメント

この種の構造において，主桁から橋脚への荷重伝達は主桁の近傍に限られるといった問題が報告されている点を確かめるため，接合部コンクリートにおける主桁直角方向の荷重分布状況について検討を行なった．この検討は，図−5．1に示すようにほぼ主桁フランジ幅の1/2間隔に切断した断面における接合部コンクリートに作用するモーメントを計算することによって行なった．曲げモーメントの計算にあたっては，図−5．2に示すように断面の外側の要素（A1〜A4）にのみ着目し要素の鉛直，水平方向応力に要素断面積を乗じ荷重とした．次にこの荷重をもとに力の釣り合いを考え図−5.2 に示すモーメント（M1〜M4）の向きを正と仮定して，断面中央に関するモーメントを求めた．その結果を図−5．3に示す．

ここでは断面内の要素において高い応力が発生する外側要素のみを考慮した計算を行なったため，実際はこれよりやや低い値を示すと思われる．コンクリート要素に圧壊などが生ずると応力の出力が不可能となるため，荷重と断面に作用する曲げモーメントの関係は必ずしも比例しない．したがって着目した要素の全積分点での応力の出力が可能な範囲である荷重が 25200kN･mまでを対象とした．

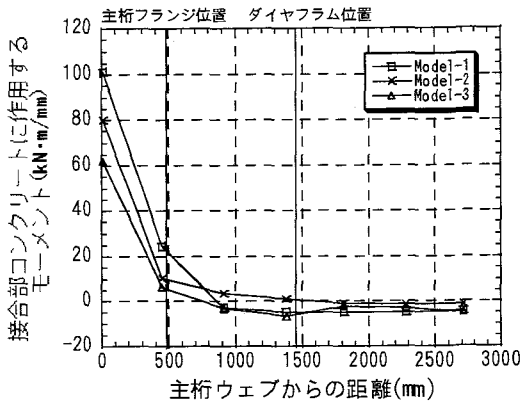

図−5.3 接合部コンクリートに作用するモーメント分布

この結果から明らかなように全てのモデルについて断面Bにおいてすでに急激なモーメントの低下が見られ，断面C以降ではモーメントの値が負となり，ほとんど作用していない．このことは圧縮ストラットの機構による荷重伝達作用が，主桁近傍の狭い範囲に限られていることを表している．断面C以降でモーメントの値が負となっているのは，図−5.2 で示した M3 において圧縮側で橋脚コンクリートからの支圧，および引張側で主鉄筋の定着作用によって図中で仮定した向きとは逆向きのモーメントが発生し，M1, M2, M4 と打ち消し合うためである．全てのモデルで同様にモーメントが低下していることから，主桁近傍で発生したモーメントが主桁から離れた位置に効率良く伝達される働きには横桁構造はそれほど関与しないといえる．しかし断面Aでのモーメントで比較した場合，Model-1 と比べると Mdoel-2, Model-3 ではやや低減されており，主桁近傍のモーメントが接合部コンクリート以外の他の部分（横桁など）に負担されているとみなすことができる．

(2) モーメント成分の分布

前節で述べたように図−5．3に示したモーメント分布の値は図−5.2 における M1〜M4 を足し合わせたものであった．ここでは各断面に作用するモーメントを M1〜M4 の各成分に分け荷重25200kN･m における断面ごとの分布を示したものが図−5．7〜図−5．9である．

これらの図に示すように，いずれのモデルも断面A, B

ではM1，M2のモーメントが比較的大きいのに対し，断面C以降ではM1，M2，M4がほとんど発生せずM3のみがわずかに負の値を示したまま一様に分布している傾向を示している．モーメントM3とは橋脚と接合部コンクリートの境界において作用するモーメントであり，したがって主桁近傍で発生したモーメントが断面C以降に伝達されるのに対し，橋脚コンクリートの支圧力と主鉄筋の引張力による伝達機構によって橋脚にモーメントを伝達していることを表している。

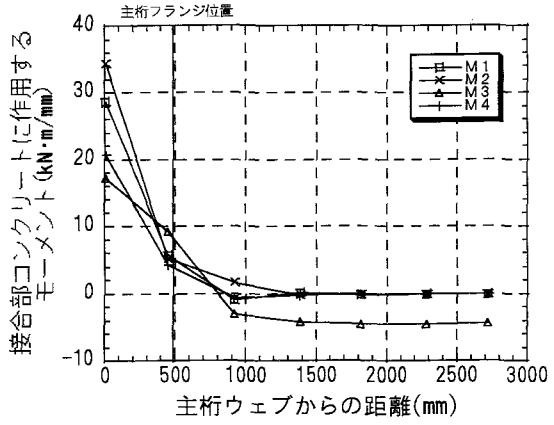

図−5.7 モーメント成分分布（Model-1）

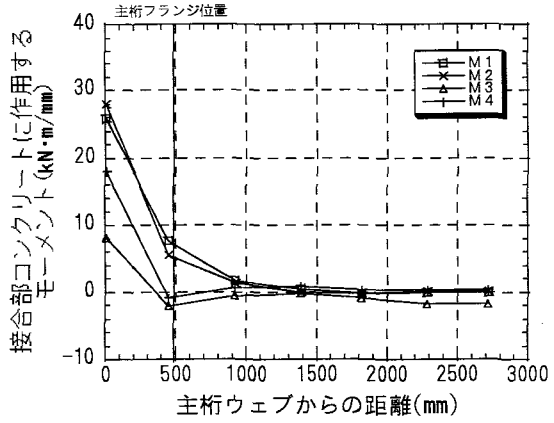

図−5.8 モーメント成分分布（Model-2）

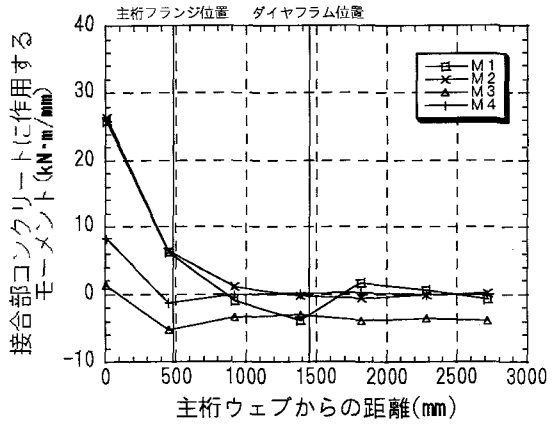

図−5.9 モーメント成分分布（Model-3）

(3) 断面の主応力の流れ

図−5．10～図−5．13に断面A，Gのコンクリート要素における断面に投影表示した最大主応力、最小主応力の流れを示す．

モデルによって主応力の流れに違いはみられないが，断面ごとで比較した場合主桁フランジ内の要素の断面A，B

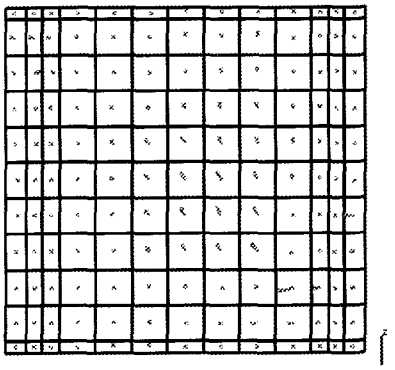
図−5.10 断面Aでの最大主応力の流れ（Model-1）

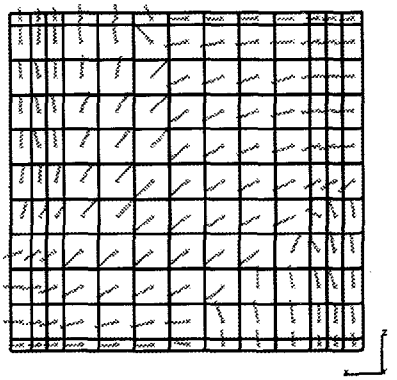
図−5.11 断面Aでの最大主応力の流れ（Model-1）

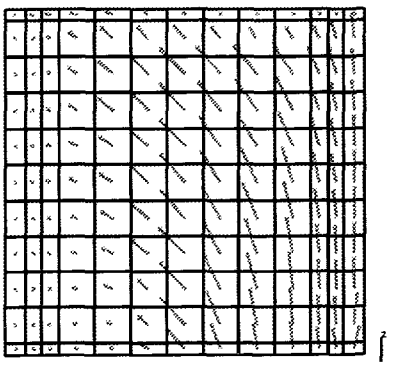
図−5.12 断面Gでの最大主応力の流れ（Model-1）

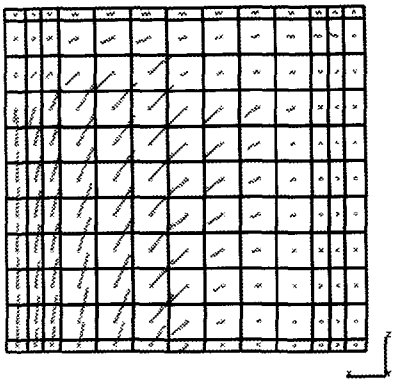

図−5.13 断面Gでの最小主応力の流れ（Model-1）

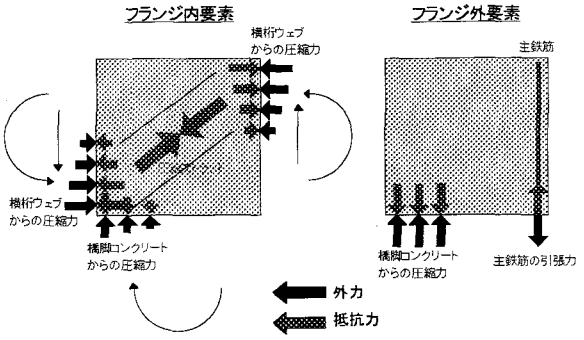

図−5.14 接合部コンクリートの荷重伝達機構

とフランジ外の要素の断面 C〜F はそれぞれほぼ同様の性状を示し，その 2 つには明らかな違いがみられる．断面Aでの最小主応力の流れから判断すると主桁上下フランジからの圧縮力が鉛直方向に，横桁ウェブからの圧縮力が水平方向に作用しており，このうち主として横桁からの圧縮力と橋脚からの圧縮力によってよって断面の対角方向に圧縮ストラットが形成され，これが荷重伝達機構となっていることがわかる．断面 A での最大主応力の目立った分布は見られないことから，圧縮ストラット方向と直角方向に発生する引張力が主桁ウェブによって負担されているとみなすことができる．

一方，断面 C〜F では最大主応力，最小主応力の流れから判断して横桁から作用するモーメントと，鋼桁から主桁フランジ内の要素に作用する圧縮力によって主桁近傍で発生したねじりモーメントが伝達され，これが橋脚コンクリートの支圧と主鉄筋の引張力によって抵抗することで曲げが作用していることがわかる．

(4) 荷重伝達機構における接合部コンクリートの役割

これまでの接合部コンクリートにおけるモーメントの分布と最大，最小主応力の流れの結果から明らかとなった力学性状から，接合部コンクリートを主桁フランジ内の要素とフランジ外の要素に分けて別の荷重伝達機構を考える必要がある．主桁フランジ内の要素では橋脚コンクリートからの鉛直方向の圧縮力，および横桁ウェブからの水平方向の圧縮力が作用することで圧縮ストラットが形成されこれが荷重伝達機構となる．一方，主桁フランジ外の要素では横桁から作用するモーメントと主桁近傍から伝達するモーメントを，圧縮側で橋脚コンクリートの支圧力および引張側主鉄筋の引張力によって橋脚に曲げとして伝達する機構を有しているといえる．以上のことから明らかとなった接合部コンクリートの荷重伝達機構を模式的に示したものが図−5.14 である．

6．横桁の挙動

(1) 横桁に作用する鉛直荷重分布

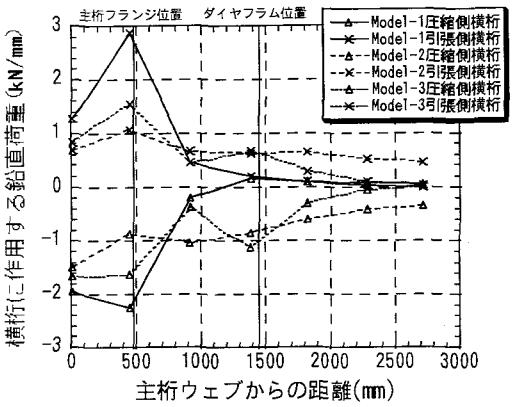

図−6.1 横桁に作用する鉛直荷重分布

次に横桁の挙動について考えるため，横桁が負担する鉛直荷重を接合部コンクリートの場合と同様の断面ごとに計算した．断面内で最大の応力が発生する最下部の要素の鉛直応力に鉛直方向の要素断面積を乗じ荷重としたものを横桁に作用する鉛直荷重とした．荷重 25200kN･m 時におけるその分布を図−6.1 に示す．図中において鉛直下向きに荷重が作用する側を圧縮側横桁，上向きの側を引張側とし，横桁に作用する鉛直荷重の符号は鋼板の引張力を正，圧縮力を負とした．

その結果，主桁下フランジを外向きとすることで横桁ウェブに配置したスタッドによってコンクリートに荷重を伝達するとした Model-1，Model-3 では断面 C ですでに鉛直荷重の低下が生じ，Model-1 では断面 D 以降では鉛直荷重がほとんど作用しておらず，逆に主桁フランジ内の断面 A，B に集中的に作用している．横桁上下フランジを内向きとすることでフランジのずれ止め効果によってコンクリートに荷重を伝達することを期待した Model-2 では，圧縮側，引張側横桁とも鉛直荷重は緩やかに減少するもののそれほど急激な低下は見られず一様な分布を示している．また断面 A，B に作用する荷重も他のモデルと比較して小さく，横桁に作用する荷重が効果的に主桁直角方向に分散され負担されていることが分

かる．Model-3 ではダイヤフラム近傍で荷重の増加が見られるものの，それ以外の断面では Model-1 とそれほど変わらない分布を示している．

(2) 合理的な横桁構造

スタッド本数が等しく横桁フランジ形状の異なる Model-1 と Model-2 を比較した結果，鉛直荷重の分布に大きな差が見られたことは，横桁の役割としてスタッドを介して荷重を伝達する部材と考えた場合に合理的な構造とはいえないことを表している．主桁から横桁→スタッド接合部コンクリート→主鉄筋→橋脚コンクリートという従来の荷重伝達経路を考えるとともおり，横桁と

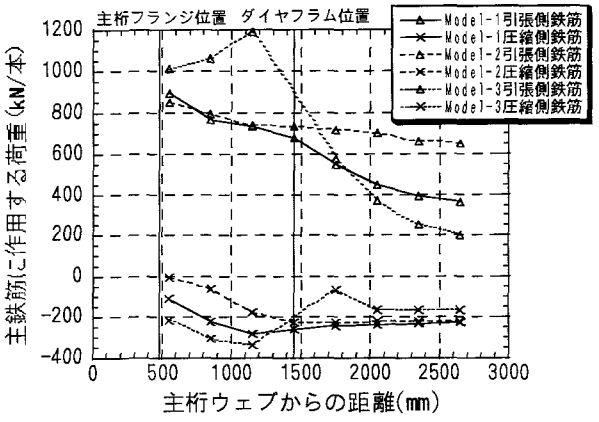

図−7.1　主鉄筋に作用する荷重分布

下フランジによるずれ止め作用によって橋脚コンクリートに荷重を伝達する部材と考えた方がより合理的であると思われる．

7．橋脚の挙動

(1) 橋脚主鉄筋に作用する荷重分布

主鉄筋の 1 本当たりに作用する圧縮，引張応力に鉄筋断面積を乗じ荷重としたものの分布を図−7.1 に示す．

引張側鉄筋では，Model-1，Model-2 では主桁から離れるにつれて徐々に荷重は減少しているが，逆に Model-3 ではダイヤフラム位置にかけて荷重の増加が見られる．しかしダイヤフラムより外側での荷重の減少は他のモデルと比較して著しい．

圧縮側鉄筋では，Model-1，Model-2 では主桁ウェブから 1500mm 付近の位置まで荷重が増加し，その後一様の分布

となる．Model-3 でもダイヤフラム位置にかけて圧縮側，引張側の鉄筋とも荷重が増加し，ダイヤフラム位置より外側では一転して荷重が低下し，やがて一様な分布を示す．

(2) 橋脚コンクリートに作用する荷重分布

橋脚に作用する鉛直荷重を定量的に示すため，接合部から橋脚コンクリートに伝達する鉛直荷重の分布を明らかとした．橋脚コンクリートに作用する鉛直荷重を求める方法として，橋脚中央から圧縮側の範囲にあり接合部コンクリート要素と接する橋脚コンクリート要素の鉛直応力に要素断面積を乗じ荷重とした．次に各断面ごとにそれらを足し合わせたものを断面に作用する鉛直荷重としその分布を図−7．2 に示す．

主桁フランジ内の要素の断面 A，B では Model-1，Model-3 が同様の分布性状を示すが，主桁フランジ外の要素では Model-3 がダイヤフラム近傍の断面において大

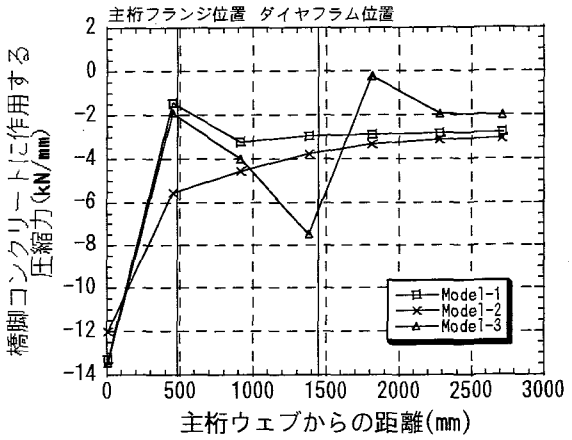

きい値となっている．Model-2 では断面 B における荷重の低下が他のモデルと比較して少なく，それ以降では一様な分布を示すことがわかる．

(3) ダイヤフラムの効果

以上の主鉄筋，橋脚の荷重分布から，ダイヤフラム近傍において橋脚コンクリート，鉄筋とも大きな荷重が作用していることが明らかとなった．したがってダイヤフラムはモーメントを橋脚に伝達するための有効な荷重伝達部材であることが示された．

8．結論

本研究では接合部コンクリート，横桁に着目し FEM 解析によって要素応力から求めた荷重による評価を行なった．

(1) 接合部コンクリート

接合部コンクリートは主桁フランジ内の要素と主桁フランジ外の要素においてそれぞれ別系統の荷重伝達機構を有しており，主桁フランジ内要素は横桁ウェブから作用する圧縮力と橋脚から作用する圧縮力によって圧縮ストラットが形成されこれが主要な荷重伝達機構となる．

主桁フランジ外要素では横桁から伝達するモーメントおよび主桁近傍から伝達されるモーメントに対して，圧縮側で橋脚コンクリートからの支圧力，引張側で接合部内に貫通させた主鉄筋に作用する引張力の2つの力により橋脚に曲げを伝達する機構となる．

接合部コンクリートのモーメント分布は主桁近傍への集中が見られたものの，適切な横桁形状を採用することで各部材への伝達作用を高め Model-2 では横桁に，Model-3 ではダイヤフラムに負担させることで主桁近傍から離れた範囲へ伝達させることが可能となる．

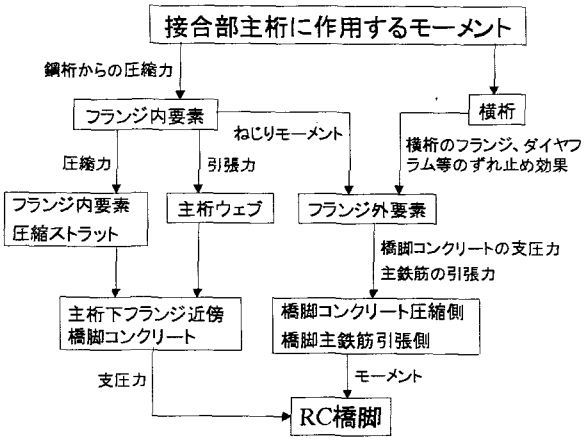

図－8．1 荷重伝達機構

(2) 横桁

横桁は横桁ウェブのスタッドを介して接合部コンクリートに荷重を伝達する部材とするよりも，主に横桁フランジを内向きとしそのずれ止め効果によってコンクリートに荷重を伝達する部材とした方がより合理的である．

またダイヤフラムは曲げに対して有効な荷重伝達部材となりうることが確認された．

(3) 荷重伝達機構

接合部を構成する部材の力学特性によって明らかとなった鋼桁から RC 橋脚への荷重伝達機構を図で示すと図－8．1のようになる．

謝辞：本研究は著者が埼玉大学大学院博士前期課程在籍時に，建設材料研究室にて行った修士論文の内容をまとめたものである．また本研究で使用した実験は研究名称「鋼桁とＲＣ橋脚の剛結構造の応力伝達に関する検討」と題し，日本道路公団試験研究所，（株）宮地鐵工所，（財）高速道路調査会，上下部一体ワーキンググループ（川崎製鉄（株），三井造船（株），片山ストラテック（株））で行なった実験結果を使用しました．実験データを提供していただきました日本道路公団試験研究所の皆様，ならびに実験に携わった各企業の方々にはここに深く感謝いたします．

参考文献

1) 米澤 健次：コンクリート系構造部材の非線形有限要素解析手法の開発とせん断抵抗機構の分析，平成6年度千葉大学博士論文，1995年3月

2) 杉山 孝雄：鋼桁を鉄筋コンクリート橋脚に接合した複合構造の耐荷性能に関する研究，平成8年度埼玉大学修士論文，1996年3月

3) 杉山 孝雄，Mochammad AFIFUDDIN，町田 篤彦，佐藤 徹：鋼－コンクリート複合構造接合部の耐荷機構に関する研究，コンクリート工学年次講演会論文集第 19 巻第 2 号，pp.1449-1454，1997年6月

4) 佐藤 徹，清水 功雄，太田 貞次，町田 篤彦：複合ラーメン橋の接合部設計法に関する一提案，土木学会構造工学論文集，pp.1431-1438，1999年3月

5) 清水 功雄，井ヶ瀬 良則，田中 祐人，長谷 俊彦：鋼桁とRC橋脚剛結部における応力伝達機構，土木学会第 54 回年次学術講演会I-A140，1999年9月

6) 長谷 俊彦，小林 潔，大久保 宣人，安松 敏雄：鋼桁とRC橋脚剛結構造に関する実験的研究，土木学会第 54 回年次学術講演会I-A141，1999年9月

7) 長谷 俊彦，井ヶ瀬 良則，清水 功雄，田中 祐人，小林 潔，大久保 宣人：鋼桁とRC橋脚の剛結部応力伝達機構に関する実験的考察，第4回複合構造の活用に関するシンポジウム講演論文集，pp.207-212，土木学会，1999年11月

STUDY ON MECHANICAL CHARACTERISTIC OF CONNECTION IN STEEL-CONCRETE HYBRID RIGID FRAME BRIDGE

Toru ISHIZAWA and Atsuhiko MACHIDA and Toshihiko NAGATANI and Toru SATO

When we design connection in steel-concrete hybrid rigid frame bridge, we have to adopt rational structure about connection in order to transfer load smoothly from girder to RC column. But load transfer mechanism in connection has not ever been to probed. Therefore in this study, first I examined appropriation of finite element method (FEM) analysis the way which compare result of experiment in connection in steel-concrete hybrid rigid frame bridge with result of FEM analysis. Next I did 3-dimensional FEM analysis subject of real bridge and examined about concrete in connection, cross girder and RC column. In this result, I tried to suggest rational structure in connection and probe load transfer mechanism in connection.

Behavior of Steel Girder-Reinforced Concrete Pier Composite Connection

By

Chakree Bamrungwong

Dissertation submitted in partial fulfillment of the requirements
for the degree of Doctor of Engineering

Saitama University
Graduate School of Science and Engineering

Supervisor	:	**Prof. Atsuhiko Machida**
Examining Committee	:	**Prof. Hiroki Yamaguchi**
		Prof. Hiroshi Mutsuyoshi
		Prof. Yoshiaki Okui

September 2001

CHAPTER 2
Analytical Methodology

2.1 Introduction

Reliable analytical methodology is currently necessary, as there seems to be no generalized and accurate analytical method that can predict the behavior of the composite connection. With the accurate analytical methodology, the designers can quickly simulate the behavior of such a structure under any preferable loading conditions and check the structural performance in every specific aspect. The accurate analytical methodology, certainly, cannot substitute the necessity of the test of prototype specimen which is much more reliable way to investigate the characteristics of the structures. But it helps put off the necessity to run a random experiments that is very costly and time consuming, only to get to know at the end that the particular type of structure is not a potentially applicable in the real works.

2.2 Objectives

Correspondingly to the problem stated above, this phase of research was established. The main objective of this phase is set as to develop the analytical methodology based on finite element method that can accurately simulate the behavior of the structure consisting of the steel girder-reinforced concrete pier composite connection subjected to the external load.

Due to its proven generality and effectiveness, the finite element procedure is chosen to be the main methodology in analyzing this complicated structure. A finite element analysis package, MARC was utilized in computation along with the pre- and post-processing program, MENTAT. The three-dimensional finite element analysis is conducted in this research phase with taking into account the non-linear material properties of concrete, reinforcing bar and steel plate.

The finite element analysis of the structure consisting of steel girder-reinforced concrete pier composite connection composes of 3 main analytical tasks, those are, the modeling of the structure with finite element meshes, the modeling of the material properties that will be assigned to each element, and the execution of the analytical program to determine the responses of the structure. These three analytical tasks are explained separately as follows.

2.3 Modeling of Structure Consisting of Steel Girder-Reinforced Concrete Pier Composite Connection

In this section, the construction of the physical finite element models representing the reinforced concrete pier, steel girders, and the interface between the pier and the girders, applied in this research are described consecutively in the following sub-sections.

2.3.1 Modeling of Reinforced Concrete Pier

In finite element analysis of the reinforced concrete structures, there are 2 physical modeling methodologies that are widely used. The first method is called the discrete meshing. In this method, the concrete and reinforcing bars are discretely simulated by using two different types of element. Instead of rigidly connecting the reinforcing bar nodes to the surrounding concrete nodes, the interface elements are applied to link these two elements together. The stiffness of this interface element is usually determined based on the bond-slip behavior between concrete and reinforcing bar.

The other method of structural modeling for reinforced concrete structures is by constructing the distributed meshes. The concrete and reinforcing bars are not considered to be two different elements with two unique materials properties of concrete and steel as in the first method. But they are considered to be the same element sharing the same geometrical boundaries, and having an averaged steel-concrete material property.

Although the structural model of distributed mesh type is more convenient to construct, it represents a less physical meaning and proved to be not suitable for some structural types. Therefore, in this research the discrete meshing is selected to apply in constructing the finite element model of the structure having steel girder-reinforced

concrete pier composite connection. The types of element used to simulate concrete and reinforcing bars are as follows.

2.3.1.1 Concrete

Element number 7 named as a "three-dimensional arbitrarily distorted cube" provided in MARC analysis package is used to represent the concrete. Element number 7 is an eight-node hexahedral using the trilinear interpolation functions. It posses 3 global translation degrees of freedom per node. Because of the complexity of the full structural model, this type of lower-order element is selected so as to reduce the analytical difficulties as well as to shorten the analytical time. The element shape is as shown in Fig. 2.1.

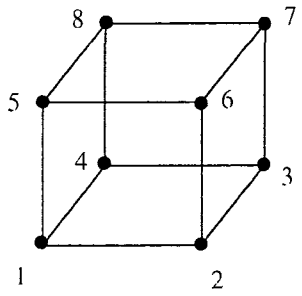

Fig. 2.1 Concrete element

2.3.1.2 Reinforcing Bar

The three-dimensional truss element (MARC element number 9) is used to simulate the reinforcing bars. This 2-node truss element is a simple linear straight truss with constant cross-section and three global translation degrees of freedom. The element shape is as shown in Fig. 2.2.

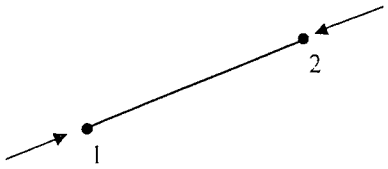

Fig. 2.2 Reinforcing bar truss element

2.3.2 Modeling of Steel Girder

The girder components consist of steel plates, which form the main as well as lateral

girders, and the studs. The structural modeling of these components is as described in the following sub-sections.

2.3.2.1 Steel Plate

The bilinear thick shell element (MARC element number 75) is used to simulate the steel plates on both main and lateral girders. This is a 4-node, thick shell element with global displacements and rotations as degrees of freedom. The bilinear interpolation is used for the coordinates, displacements, and the rotations.

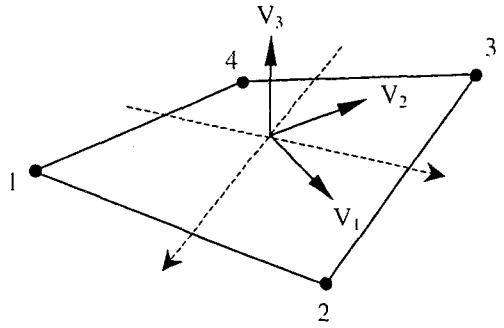

Fig. 2.3 Thick shell element

2.3.2.2 Stud

The studs, which are welded on both main and lateral steel girders, are physically represented by the 2-node beam elements as not only they are considered to be able to transfer the axial forces but also they will resist the bending forces transferred from concrete to steel plate elements.

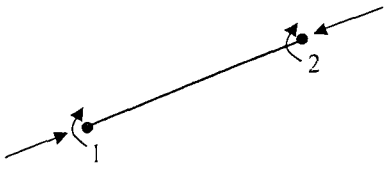

Fig. 2.4 Beam element

2.3.3 Physical Modeling of Interface between Concrete-Reinforcing bars, and Interface between Concrete-Steel Plate

2.3.3.1 Concrete-Reinforcing Bar Interface

As the concrete and reinforcing bar are discretely modeled with different elements, there is a necessity in connecting these two elements together. In this research, the concrete is linked to reinforcing bar element with the spring elements. Force in the spring will stand for the interface force while the displacement of spring will represent the slip on the interface. The constitutive law of this spring element will be discussed later in this chapter.

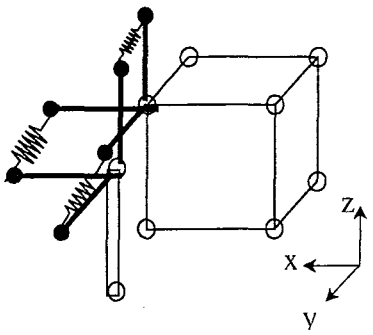

Fig. 2.5 Concrete-reinforcing bar interface springs

2.3.3.2 Concrete-Steel Plate Interface

Spring elements are used to model the interface between these conjoining materials as well. At each particular couple nodes, there are 3 springs linking the steel plate node to the adjacent concrete node. One spring is for transferring the force between concrete and steel plate elements in the direction normal to the interface plane. The other two springs are used to simulate the friction forces on the interface plane.

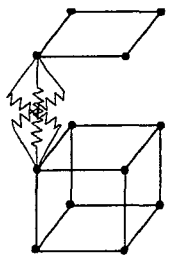

Fig. 2.6 Concrete-steel plate interface element

After decided on the types of element to be used in representing each components of the structure, the full finite element structural model is constructed by carefully combining all of the elements together. However, with only the physical appearance of the structure, the analysis cannot yet be started. The structural elements must be given the material

properties to define how they will behave under the particular stressing circumstances. These material properties are usually assigned to the elements by means of the *constitutive laws or stress-strain relationships. Besides, some element like spring* element requires the properties to be input in terms of force-displacement relationship. The material properties of concrete, reinforcing bar, steel plate, studs, and interface elements will be discussed in details in the following section.

2.4 Material Modeling

To obtain the structural responses from the finite element analysis, it is compulsory that the material properties of each element are provided by means of constitutive laws. So far many researches have been conducted in order to determine the constitutive laws of the construction materials. Some are proven to be more effective than the others under the specific situations. However, there is still no a universal generalized constitutive law that can govern and give out the correct results under any types of stress conditions. Thus it is necessary, especially in the case of the analysis of a relatively new composite structure having steel girder-reinforced concrete pier composite connection, to search for the appropriate constitutive relationship that can accurately describe the behavior of the materials in finite element analysis.

In this section the material modeling of reinforced concrete pier, steel girders, and the modeling of the behavior of interface between concrete-steel plate and concrete-reinforcing bar are described.

2.4.1 *Modeling of Reinforced Concrete*

In the real reinforced concrete structures, concrete and reinforcing bar are acting together as a composite materials. The interaction between concrete and reinforcing bars has been known to play a great role influencing the overall behavior of the reinforced concrete structures. Thus in the finite element analysis where the discretely meshed model is created, the concrete and reinforcing bar elements have to be rationally connected to each other. Generally, there exists two well-known behavioral simulation methods of the concrete, reinforcing bar and their interaction which are, one that is based smeared crack concept, and the other which is done with the application of the interface element between reinforcing bar and concrete. In the first method, the concrete

and reinforcing bar elements are assumed to be perfectly linked to each other and the modifications have to be made in the constitutive laws of both concrete and reinforcing bar elements. In contrast, with the latter method, the constitutive relationships of concrete and reinforcing bar are remained unchanged. But the other interface element with appropriate bond stress-slip relationship is needed to bind these two main elements together.

Both methods have their pros and cons depending on the type of structure being analyzed. Since there is no evidence stating about the appropriate selection of reinforced concrete material modeling for this specific type of composite structure, it is therefore, needed to search for the suitable model. To determine the most appropriate analytical concept for reinforced concrete part in this particular composite structure, both material modeling methods are applied. The preliminary verification would be done by comparing the analytical results to the results obtained from the experiments conducted previously by Japan Highway Corporation and construction companies.

2.4.1.1 Material Modeling of Reinforced Concrete with Application of Smeared Crack Concept

2.4.1.1.1 Introduction

In the real reinforced concrete structures, concrete and reinforcing bar are working together to resist the externally applied loads. Typically, the concrete is designed to resist mainly the compressive stress while the reinforcing bar will help carry the tensile forces. Nevertheless, they, in fact, do work in combination. That means in compression zone not only the concrete will resist the compressive stress but also the reinforcing bars located in the same region. This applies also in tension region, before concrete starts to crack the full composite action does govern. But after cracking, the contribution of the concrete to tensile force becomes less as concrete looses its integrity. This composite behavior can be simulated by applying the smeared crack concept. Smeared crack concept describes how the reinforced concrete responds the applied load after the stress in the concrete element reaches the tensile strength.

With smeared crack concept, the constitutive laws of plain concrete as well as of bare bar are modified to be the averaged values. In addition, the concrete and reinforcing bar elements, which are modeled separately, would be assumed to be perfectly bonded at

the joining nodes. The modified constitutive laws of concrete and reinforcing bar will be described in the following sub sections.

2.4.1.1.2 Material Properties of Concrete and Reinforcing Bar

(a) Concrete

Under Compressive Stress

The stress-strain relationship of plain concrete element under uniaxial compression was derived based on cylindrical compression test data as shown in Fig. 2.7.

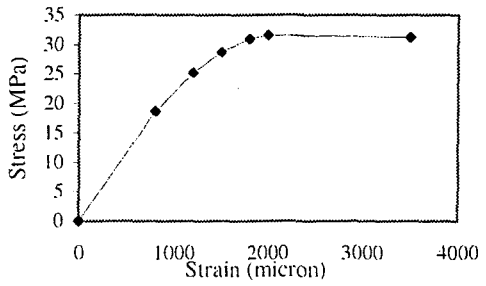

Fig. 2.7 Stress-strain relationship of concrete under compressive stress

Under Tensile Stress

The behavior of the plain concrete can be categorized into 2 successive phases, namely, before reaching tensile strength, and beyond the peak tensile strength. Before the crack initiates in concrete, the concrete is considered to behave elastically with the same modulus of elasticity as in elastic compression. However, after reaching the peak tensile strength, cracks are generated. This causes concrete to behave in totally different way compared to the isotropic material behavior considered in the earlier stage. Concrete starts to exhibit as it is anisotropic material with no resistance to any forces in the direction normal to the crack plane. In reinforced concrete, however, since there exists the reinforcing bar strengthening concrete while it is subjected to tension, the crack concrete will be held in place and the uncracked part can still withstand some tensile force with a gradually reducing stiffness. This phenomenon is called "tension stiffening effect" and can be described by a smeared crack concept.

Due to the tension stiffening effect, based on the smeared-crack concept, concrete is considered to be capable to withstand the tensile load after its tensile strength has been reached with a gradually declining stiffness. In this research, the tension stiffening model proposed by Okamura [56] is adopted to simulate the behavior of the concrete under tension.

In Okamura's model, the cracks are considered not to appear as soon as the magnitude of stress has attained the cracking level, but when the principal tensile strain reaches an upper limit value. The limit strain usually ranges between 0.01% and 0.03%. In other words, it can be said that a certain amount of plastic deformation is allowed to take place after cracking stress is reached. This upper limit is assigned to be twice as much as the tensile strain of concrete at the point where the splitting tensile strength of the concrete is just arrived. The constitutive model of concrete under tensile stress is as shown in Eq.2.1 and Fig. 2.8.

$$\sigma_t = f_t(\varepsilon_{tu} / \varepsilon_t)^c \tag{2.1}$$

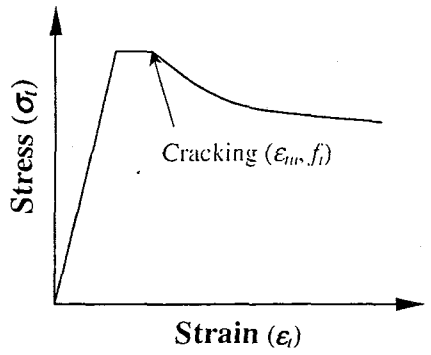

Fig. 2.8 Tension stiffening model

Shear Retention

After the concrete is cracked, it still can withstand the shear force exerted on the plane of crack with gradually reducing shear stiffness. This is mainly contributed by the aggregate interlock and dowel action. To simulate this phenomenon, the shear retention model proposed by Bangash [11] is adopted. Bangash, proposed a linear relationship between shear resistance of cracked concrete and the tensile strain normal to the crack plane which could be expressed as in Eq. 2.2. The shear retention factor β' by Bangash was adopted and multiplied to shear modulus of uncracked concrete, G, for the new shear modulus ($G_{new} = \beta' G$).

$$\tau^* = \beta' G \gamma^* \quad (2.2)$$

where:

τ^* : shear stress

γ^* : shear strain

G : the shear modulus of uncracked concrete

β' : the interlocking factor = $1-(\varepsilon_t/0.005)^{K1}$

ε_t : the tensile strain normal to the crack plane

K1 : parameter ranges from 0.3-1.

Note : K1 was assumed to be equal to 1 so as to simplify the analysis.

(b) Reinforcing Bar

In smeared-crack concept, not only the concrete but also reinforcing bar element is assumed to have an average type of constitutive relationship. This modification is done to compensate for the slip that is neglected in the model in order to ease the analytical complication, with the assumption that the perfect bond condition presents at the interface between concrete and reinforcing bar elements. Neglecting to modify the constitutive law of the reinforcing bar in analysis will finally leads to the over-stiff response of the structure to the applied load.

The modified constitutive law of reinforcing bar crossing the crack which was developed by Shin [69] is adopted in this research. His model was developed by taking into account some factors those are influential to the post-yielding constitutive law. In his works, 140 parametric study cases were conducted. The results showed that the average stress and average strain could be well related to each other in a bilinear fashion having a clear offset point for the initiation of strain hardening (yield stress = f_y as in Eq. 2.3). Beyond yielding point, $\overline{f_y}$, the strain hardening rate is assumed to be held constantly at the modulus E_{sh}.

$$E_{sh} = 100(f_y - \overline{f_y})\, K_p\, K_y\, K_h\, K_a\, K_c\, K_k \quad (2.3)$$

Where;

E_{sh} = strain hardening rate in bilinear stress-strain relationship of reinforcing bar

$\overline{f_y} \geq 0.5 K_{yo} K_{ko} fy$

$K_p = p_x^{0.5px}$

$K_y = (400/f_y)^{0.1(px/py)\text{cosec}\theta}$

$K_h = (p_x/p_y)^{0.067}$,

$K_a = \text{cosec}\theta^{0.2}$

$K_c = (30/f_c')^{0.25}$

K_{k0}= 1 for deformed bar, f_y =yield strength(MPa),

$K_{y0} = (0.1 p_x f_y/f_c')^{0.5} \leq 1$

p_x,p_y = reinforcement ratio in each direction,

f_c':compressive strength of concrete MPa.

Before the first yielding occurred, it was assumed that the bar remained elastic with modulus of elasticity equaled to its actual value. The initial yield stress could be determined by considering the equilibrium of forces in the cracked concrete surrounding reinforcing bar element Eq. 2.4.

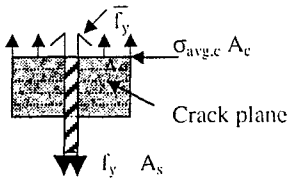

Fig. 2.9 Equilibrium condition of cracked concrete

$$(\sigma_{avg.c})\, A_c \;+\; (\,\bar{f}_y\,)\, A_s \;=\; (f_y)\;\; A_s \qquad (2.4)$$

Where; $\sigma_{avg.c}$ = Average stress in concrete

A_c = Cross-sectional area of concrete area surrounding a particular reinforcing bar element

A_s = cross-sectional area of reinforcing bar

By solving Eq. 2.4, with the assumption of strain compatibility at the individual section, the concrete and reinforcing bar elements have an equaled average strain (ε_{avg}), the initial yield stress of concrete can be calculated as shown in Eq. 2.5.

$$\bar{f}_y \;=\; [A_s f_y \;-\; (\sigma_{avg.c}\,(1\text{-}p_x))] \,/\, (p_x) \qquad (2.5)$$

Where; p_x = reinforcement ratio (area of a reinforcing bar divided by the area of concrete element surrounding this bar*)

*Note : the surrounding concrete area was determined by using the method proposed by An, X., et al. [5]

The modified constitutive relationships of reinforcing bars are as shown in Fig. 2.10.

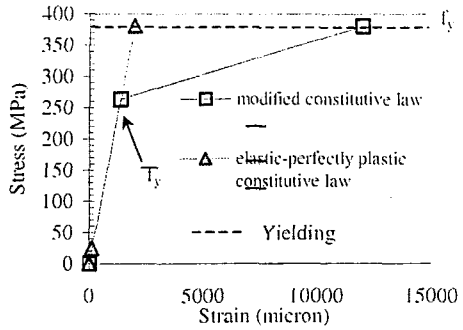

Fig. 2.10 Modified constitutive relationship of reinforcing bar

2.4.1.1.3 Application of Smeared Crack Concept

Without taking into account the reduced stiffness of concrete and reinforcing bar, the slipping phenomenon of reinforcing bar on the surrounding concrete is plainly omitted. After cracks are initiated, the concrete will be held rigidly in place by a non-brittle reinforcing bar element as their node are perfectly bonded to each other. This will cause the reinforced concrete model become very stiff and eventually overestimated the actual behavior. Thus to take the advantage of reduction in number of nodes in the finite element analysis, the smeared crack concept has to be applied.

The analytical procedures with the application of smeared crack concept will be described later in this chapter.

2.4.1.2 Material Modeling of Reinforced Concrete with Application of Reinforcing Bar-Concrete Interface Elements

2.4.1.2.1 Introduction

As an alternative to the material modeling of reinforced concrete structures based on the smeared crack concept, the material modeling of reinforced concrete can also be performed by implementing the reinforcing bar-concrete interface elements. This interface element will simulate the bond stress-slip behavior at the interfacing boundaries of the concrete and reinforcing bar elements. This type of material modeling is physically, closely resembled to the real material behavior. The material modeling of reinforced concrete structure with the application of interface element is described in

this part beginning with the explanations on modeling of concrete, reinforcing bar, and the interface elements. The verification of this method of material modeling with the experimental results, will be shown later along with the comparison to analytical results obtained from the analysis based on the smeared crack concept.

2.4.1.2.2 Material Properties of Concrete and Reinforcing Bar

(a) Concrete

The properties of the plain concrete under the uniaxial compression stress condition, is obtained straightly from the compression tests of the cylindrical concrete specimens. While under tensile stress condition, the concrete is assumed to behave elastically until reaching the tensile strength. Beyond this point, the concrete element would be cracked. Therefore, the tensile resistance of the element in the direction normal to the crack plane is assumed to drop down to zero.

As the nonlinear finite element analysis is of three-dimensional type, the element will be stressed by the forces in all directions. The properties of concrete under multi-axial stress state must be considered. In this research the measurement of yielding of multi-axial state of stress, or the yield condition of concrete, proposed by Buyakozturk [16] is adopted. The yield criterion of Buyukozturk's plasticity model can be expressed in a general form as in Eq.2.6.

$$\sqrt{J_2 + \frac{\beta\sigma_0 J_1}{\sqrt{3}} + \frac{\gamma}{3} J_1^2} - \frac{\sigma_0}{\sqrt{3}} = 0 \qquad (2.6)$$

The parameter σ_0 can be calculated by substituting the uniaxial compressive strain-hardening curve obtained in experiments to the general form of yielding criteria as stated in Eq. 2.7.

$$\sqrt{\frac{\bar{\sigma}^2}{3} + \frac{\beta\sigma_0\bar{\sigma}}{\sqrt{3}} + \frac{\gamma}{3}\bar{\sigma}^2} - \frac{\sigma_0}{\sqrt{3}} = 0 \qquad (2.7)$$

The shear retention factor proposed by Bangash is also adopted in this analytical method to retain the shear resistance of concrete after cracking.

(b) Reinforcing Bar

For reinforcing bar, the material properties is assumed to be explainable by an elastic-perfectly plastic stress-strain relationship (see Fig. 2.11) Yielding of the reinforcing bar is determined by the yield strength value obtained from the tensile strength test in the experiments.

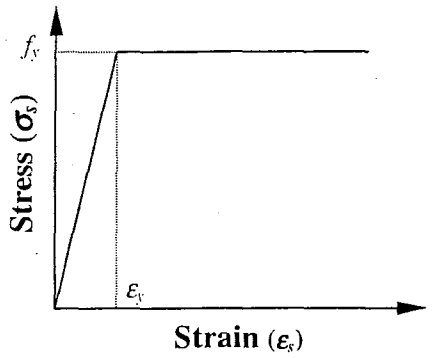

Fig. 2.11 Elastic-perfectly plastic constitutive relationship of reinforcing bar

(c) Development of Reinforcing Bar-Concrete Interface Element

In this phase, to connect the concrete to the reinforcing bar elements in the structural model, the interface element is used as an alternative method to the application of smeared crack concept. The bond stress-slip-strain model proposed by Shima [68] is adopted here because of its generality as well as its accuracy. Shima showed that the bond stress-slip relationship is highly dependent on the boundary conditions of the reinforcing bar in the concrete. He found that with taking into account the strain in the reinforcement, the accurate relationship could be satisfactorily expressed. His bond stress-slip-strain relationship has been verified with the experimental results to be sufficiently generalized and accurate for application in most analytical cases. However, in his research, Shima had not proposed any dedicated element to work with this constitutive law for the analysis with finite element method. Therefore, in order to apply this interface property in finite element analysis an interface element consisting of springs in three directions was developed in this research. In addition, as the bond stress derived by Shima is an average value which is not the stress occurs exactly at the surface of the reinforcing bar, thus in the analysis with the proposed interface elements linking the reinforcing bar to the adjacent concrete element, the location away from reinforcing bar surface where bond stress has an average value needs to be determined and the surface area at this location must be used in computing the average spring force and the stiffness.

Since in this case, the spring is used as the interface element, the bond stress-slip-strain relationship will be first converted to be in the form that can be directly applied as spring's stiffness. Then the further derivation is performed in order to clarify the ambiguity in Shima's expression about the location where the averaged bond stress acts on. The bond stress-slip-strain relationship proposed by Shima can be expressed as in Eq. 2.8.

$$\tau = \frac{0.73 f_c' (\ln(1+5s))^3}{1+\varepsilon \times 10^5} \tag{2.8}$$

Where,

s	= 1000S/D
τ	= average bond stress
f_c'	= concrete strength
S	= slip
D	= bar diameter
ε	= strain

In his research, the slip was defined to be, not the relative displacement between bar and concrete, but the displacement of the bar at the point concerned from the fixed point in concrete. This definition was considered to be quite general because the relative displacement (or slip) between the reinforcing bar and the concrete was independent on the condition of surrounding concrete which was usually deteriorated to some degree as the applied load was increased. The slip can be calculated as,

$$S = \int_{x_0}^{x} \varepsilon dx + S_0 \tag{2.9}$$

Where,

S_0	= free end slip
x_0	= location of free end
x	= location of the point concerned

Furthermore, the local bond stress at any locations along the direction of an embedded bar is proportional to the slope of the strain distribution curve at that point. Thus at any point, the bond stress τ can be expressed as,

$$\tau = \frac{ED}{4} \frac{d\varepsilon}{dx} \tag{2.10}$$

Where,

E = Young's modulus of the bar

D = bar diameter

$\frac{d\varepsilon}{dx}$ = slope of the strain distribution curve

To implement the bond stress-slip-strain relationship proposed by Shima into the interface element, the stress has to be initially converted to force acting on the specific reinforcing bar area. By multiplying the bond effective area to the bond stress, the bond force can be obtained, Eq. 2.11.

$$f(1) = \tau \text{ x Area} \tag{2.11}$$

Where,

f(1) : average bond force

τ : average bond stress

Area : bond effective area

By substituting the bond stress-slip-strain relationship (Eq.2.8) into the bond force equation (Eq.2.11), we can obtain the relationship between the bond force and slip at the interface as shown in Eq.2.12.

$$f(1) = \tau \times \text{Area} = \frac{0.73 f_c' (\ln(1+5s))^3}{1+\varepsilon \times 10^5} \times \text{Area} \tag{2.12}$$

Where,

Area : bond effective area = $k_z \pi D L$

D : bar diameter

L : length of bar element

k_z : bond-effective zone factor

In order to simulate the real mechanism at the interface between concrete and steel bar, the spring element is used to represent this physical link. Therefore, in the analysis, there is a need for formulation of the stiffness of this interface spring. In this research, the stiffness of the interface spring is derived by, firstly, differentiating the bond force-slip-strain relationship shown in Eq. 2.12 with respect to the slip. It is assumed here that strain stays constant at each particular moment.

$$\frac{df(1)}{dS} = \frac{d}{dS}\left[\frac{0.73f_c'(\ln(1+5S/D))^3 \times k_z \pi dL}{1+\varepsilon \times 10^5}\right] \quad (2.13)$$

Where

f(1) : average bond force

By solving Eq. 2.13 the stiffness of interface spring (kN/mm^2) could be obtained as;

$$K_{bs} = \frac{0.73f_c' \times k_z \pi dL}{1+\varepsilon \times 10^5} \times \left(\frac{15}{D+5S}\right) \times \left(\ln(1+5\frac{S}{D})\right)^2 \quad (2.14)$$

Where

K_{bs} : interface spring stiffness

For the springs connecting concrete and bar elements in x and y directions, they are assumed to have the very high stiffness. This assumption is imposed so that the displacement compatibility between concrete and steel bar in transverse direction will be held in the directions normal to the bar surface. In this analysis, the spring stiffness is assumed to be 100 times of stiffness of bare steel bar.

$$K_{xy} = (100)(E_s)(\pi D^2/S) \quad (2.15)$$

Where

K_{xy} : stiffness of the interface springs in directions normal to the reinforcing bar surface

E_s : modulus of elasticity of the reinforcing bar

D : diameter of the bar

S : slip on the reinforcing bar-concrete interface

In the actual application, the interface between the concrete and reinforcing bar is simulated by using the spring element to link reinforcing bar node to the adjacent concrete node. However, the bond stress derived by Shima is an average value that is not the stress occurs exactly at the surface of the reinforcing bar. Thus, in the analysis with the proposed interface element linking the reinforcing bar to the adjacent concrete element, the location away from the reinforcing bar surface where bond stress has an average value needs to be determined and the surface area at this location must be used in computing the average spring force and stiffness.

In order to determine the location where the average bond stress acts upon, it is assumed that at the moment the concrete starts to crack, the reinforcing bar section located on that cracking plane yields immediately. Based on this assumption, the maximum surrounding concrete area (A_{cmax} in Fig.2.13) that initiates this phenomenon can be calculated as,

$$A_{cmax} f_t = A_s f_y$$

$$A_{cmax} = \frac{A_s f_y}{f_t} \tag{2.16}$$

Where

A_s : sectional area of reinforcing bar
f_y : yield stress of reinforcing bar
f_t : tensile strength of concrete

This derivation is similar to the calculation previously introduced by An.,X et al. [5]. Furthermore, if this maximum surrounding concrete area is assumed to be of a circular shape and the bond stress distribution in radial direction from the reinforcing bar axis is assumed to be of triangular shape as shown in Fig.2.13, the surface area that the average bond stress acts upon will be larger than the surface of the reinforcing bar on where the interface element exists by the ratio k_z (bond-effective zone factor) as expressed in Eq.2.17. By substituting the bond-effective zone factor into Eq.2.14, the average stiffness for interface spring that is necessary in the analysis, can be calculated.

$$k_z = R_{avg} / R_{bar} = \frac{1}{3}\sqrt{\frac{f_y}{f_t}} \tag{2.17}$$

Where

R_{avg} : distance from the axis of reinforcing bar to the surface where average bond stress acts upon
R_{bar} : radius of the reinforcing bar.
F_y : yield strength of the reinforcing bar
F_t : tensile strength of concrete

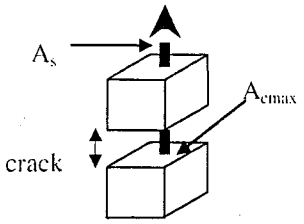

Fig. 2.12 Yielding of reinforcing bar at crack plane

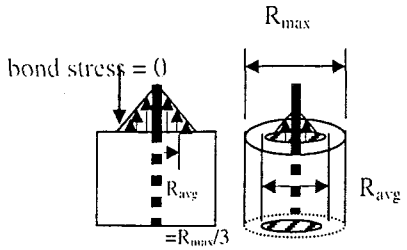

Fig. 2.13 Stress distribution on bond-effective zone

Since the assumption that the steel will yield immediately is applicable only before the cracking of concrete's bond effective area takes place, after cracking, it is, again, necessary to revise the bond effective zone factor (k_z). In this research, the recalculation of the bond effective zone factor is done based on the consideration that when the first crack is initiated in the concrete element, the concrete will loose its integrity to some degree. The stress transferred from reinforcing bar to the cracked concrete element will be spread less widely than the initial bond effective area due to the deterioration of the interface, causing the reduction in the bond effective zone factor. The modified bond effective zone factor is formulated by assuming that after the strain in the reinforcing bar (which is nearly compatible with concrete strain before cracking) reaches the maximum tensile strain of concrete (ε_{cr}), the bond effective zone will be linearly decreased from the original value until the strain in reinforcing bar, which is connected to that concrete element, arrives the yielding limit (ε_y). At this yielding state, the bond effective zone factor is assumed to be equal to 1. It means that the bond stress will concentrate in a smaller region. The bond can hardly be distributed to the remote area as the concrete has lost the integrity due to cracking, Fig 2.14.

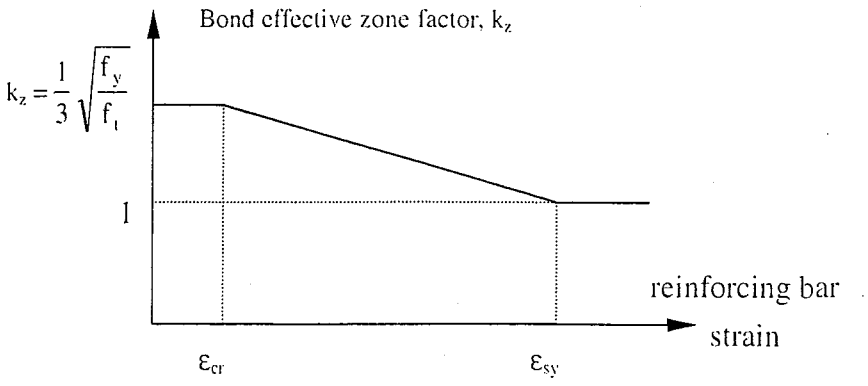

Fig. 2.14 Linear reduction in bond effective zone factor after concrete cracks

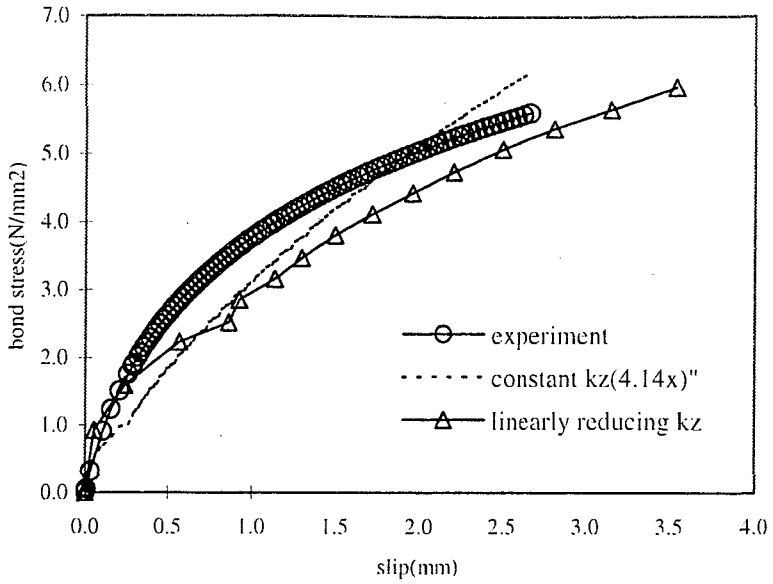

Fig. 2.15 Plot of the bond effective zone factor versus the strain in reinforcing bar

2.4.1.2.3 Verification of Finite Element Analysis with Application of Reinforcing Bar-Concrete Interface Element

Since the reinforcing bar-concrete interface element is newly developed in this research, it is necessary to verify the applicability of this element before putting it in the real use in the full model finite element analysis. The verification of the reinforcing bar-concrete interface element was performed by applying it to simulate the behavior of the reinforced concrete specimen tested by Shima. The experimental data acquired was from the pull-out test series of the reinforced concrete. The specifications of the test specimen are as shown in the Table 2.1 and Fig. 2.16

Table 2.1 Specification of specimen in pull-out test series of Shima [68]

Steel bar	SD 30	SD 50	SD 70
Diameter of bar D, mm	19.5	19.5	19.5
Young's modulus E_s, Gpa	190	190	190
Yield strength f_y, MPa	350	610	820
Initial strain of strain hardening ε_{sh}, %	1.65	1.40	0.60
Tensile strength f_u, MPa	540	800	910

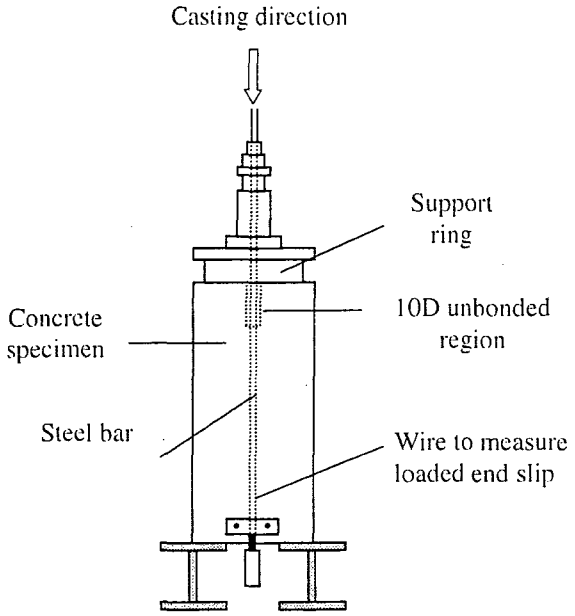

Fig. 2.16 The pull-out specimen tested by Shima

The three-dimensional arbitrary distorted cube (MARC element No.7) was used to represent the concrete, while for the reinforcing bar, the three-dimensional truss element (MARC element No.9) was applied. The fixed-displacement boundary condition was applied at the concrete elements surrounding the reinforcing bar elements on the loading side. Similar material properties of concrete and reinforcing bar as described in this section were assigned to the concrete and reinforcing bar element, respectively. The spring elements were applied to connect the reinforcing bar nodes to the adjacent nodes of concrete elements. Constitutive law of this interface spring was as derived in this section. Then the stepwise monotonic load was applied. The analytical result is shown in Fig. 2.15 in terms of bond stress-slip relationship at the distance 2D from the free end of the specimen.

It could be concluded based on the comparison between analytical and experimental results that, the interface element shows a comparable trend in prediction of the bond stress as well as slip to that obtained in the experiment conducted by Shima. The calculated relationship shows a less stiff behavior after the cracking of concrete is initiated. This might be due to the imperfection of the assumption that the reduction of bond effective zone factor is linearly decreased from the initial value immediately after cracking, to be equal to 1 at the yielding of reinforcing bar. However comparing to the application of constant bond effective zone factor from the beginning throughout the

analysis, the case of using decreasing factor clearly shows better trend in prediction of the bond stress-slip relationship.

2.4.2 Material Modeling of Steel Plate and Stud

So as to reduce the complication in the complicated three-dimensional nonlinear analysis, the steel plate elements are assumed to behave as an elastic-perfectly plastic material. The von Mises yield criteria was used to simulate the yielding surface of these metallic material. The constitutive relationship is as shown in Fig.2.17.

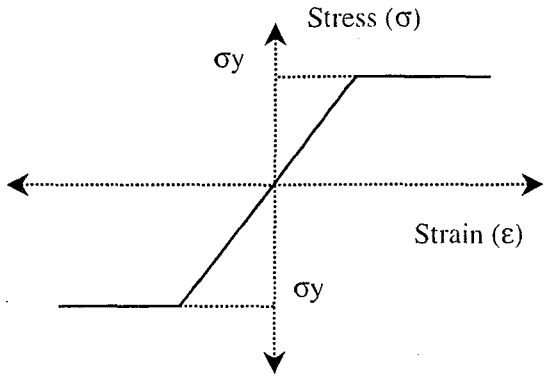

Fig. 2.17 Constitutive relationship of steel plate and stud

After all of the mechanical characteristics of the main construction materials, namely the reinforced concrete and the steel girders, are modeled, the next task is to link this reinforced concrete pier and the steel girders together. The detailed explanation about how to put these two main structural components together in the finite element analysis will be explained in the following section.

2.4.3 Development of Steel Plate-Concrete Interface Element

2.4.3.1 Introduction

At the connection region, the reinforced concrete pier is rigidly cast in the steel girder case (in the case of main with lateral girders added on), or fully covers a simple girder. The composite action between these two primary substructures is usually assumed in the analysis to be of a perfect-bond condition. This analytical assumption might be true if the reinforced concrete pier is perfectly encased by the strong steel girder with lateral girder having studs shear connectors welded on. However, in some cases where these

rigidity enhancing components are not available, like when only a main girder is designed to be embedded in the reinforced concrete pier, the slip between reinforced concrete and steel girder would be too considerable to neglected in the analysis. Thus in order to construct an accurate finite element analytical model that can handle the calculation of both cases, the interface element is developed.

2.4.3.2 Steel Plate-Concrete Interface Property and Development of New Interface Element

In this phase, the steel plate-concrete interface property proposed by Yonezawa [80] was adopted because of its confirmed accuracy and the simplicity in application. Yonezawa derived the concrete-steel plate interface properties based on the results from series of experiments he conducted. His main objective in researching for the interface property is to apply it in the finite element analysis of the structures having the steel plate being in contact with the concrete. Some influential parameters taken into account in the derivation of interface property are, the confining force, the compressive strength of concrete, and the thickness of the interface element. He, eventually, came up with the relationship between bond stress and slip at the interface between concrete and steel plate.

Table 2.2 Detailed formulation of steel plate-concrete interface property [80]

Springs in the direction normal to the interface	**Springs in the direction tangential to the interface**
1.Under compressive normal stress Assuming that under compressive stress, the interface is as rigid as steel plate, thus K_n = (200,000A) per unit length 2. Under tensile normal stress σ_n = $(0.04 F_c / 0.05)\delta h$ $\sigma_n(A)$= $(0.04 F_c / 0.05)A\delta h$ F_n = $(0.04 F_c / 0.05)A\delta w$ Thus the stiffness of spring in this direction is K_n = $(0.04 F_c / 0.05)Ah$ Where σ_n : stress in the direction normal to the interface (N/mm^2), F_c : compressive strength of concrete (N/mm^2), A : effective area (mm^2), F_n : force in the direction normal to the interface (N), δ : slip (the deformation of the spring, mm), K_n : Stiffness of spring in the direction normal to the interface (N/mm), h : virtual thickness of the interface element	1. Under compressive normal stress [when; $\sigma_t \leq 0.65\sigma_n$] F_t = $(\mu_n \sigma_n / 0.02)A\delta h$ K_t = $(\mu_n \sigma_n / 0.02)Ah$ [when; $\sigma_t \geq 0.65\sigma_n$] assuming that the stress keeps constant while slip increases infinitely F_t = $0.65 \sigma_n Ah$ K_t = 0 2. Under tensile normal stress [when: $\sigma_t \leq 0.04\sigma_n$] F_t = $(\mu_n \sigma_n / 0.02)A\delta h$ K_t = $(\mu_n \sigma_n / 0.02)Ah$ [when: $\sigma_t \geq 0.65\sigma_n$] F_t = 0 K_t = ∞ Where F_t : force in the direction tangential to the interface (N), K_t : stiffness in the direction tangential to the interface (N/mm)

The detailed formulations can be divided into 2 parts those are, first, the formulation of interface property in the direction normal to the interface plane, and the other is the formulation of interface property in the direction tangential to the interface plane. The summary of detailed formulation of Yonezawa's interface property is as presented in Table 2.2.

To implement this property into the finite element analysis, Yonezawa had developed the interface element that was of rectangular shape with four corner-nodes. As the thickness of the interface element was unknown, he conducted the parametric study to find the effect of this influential parameter. Finite element program was used in his parametric study. He found that the appropriate values of the thickness that should be used in the analysis, should not be less than 0.001 mm, or else the finite element analysis would be prone to numerical difficulties. However, as this virtual thickness has no physical meaning and no specific value has been clearly suggested, it may cause some difficulties as well as the ambiguities in finite element analysis of steel plate-concrete composite structure. Therefore the new interface element is developed in this research so as to eliminate these problems.

A three-dimensional spring element is used to represent the interface between concrete and steel plate. Since the spring element itself has no dimension, the difficulties in choosing appropriate value of the virtual thickness of the interface element will be removed. All the thickness factors present in formulae derived by Yonezawa are then normalized. Thus the virtual thickness "h" is diminished out from the expression for properties of the three-dimensional interface spring.

The formulation for the concrete-steel plate interface property and the derivation of the stiffness of the interface element, are as illustrated in Table 2.3. Whilst the formulae look essentially similar to those presented by Yonezawa, it should be noticed that the variable representing the virtual thickness has rationally been taken away.

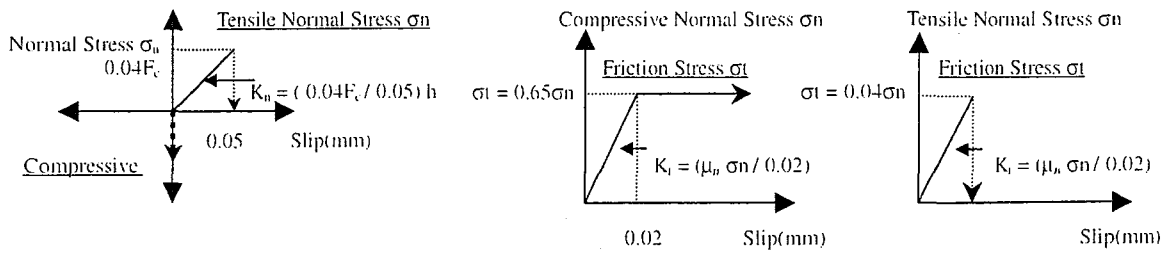

Fig. 2.18 Bond stress-slip relationship of interface element

Table 2.3 Formulation of concrete-steel plate interface property

Springs in the direction normal to the interface	**Springs in the direction tangential to the interface**
1.Under compressive normal stress Assuming that under compressive stress, the interface is as rigid as steel plate, thus K_n = (200,000A) per unit length 2. Under tensile normal stress σ_n = $(0.04 F_c / 0.05)\delta$ σ_n (A)= $(0.04 F_c / 0.05)A\delta$ F_n = $(0.04 F_c / 0.05)A\delta$ Thus the stiffness of spring in this direction is K_n = $(0.04 F_c / 0.05)A$ Where σ_n : stress in the direction normal to the interface (N/mm^2), F_c : compressive strength of concrete (N/mm^2), A : effective area (mm^2), F_n : force in the direction normal to the interface (N), δ : slip (the deformation of the spring, mm), K_n : Stiffness of spring in the direction normal to the interface (N/mm)	1. Under compressive normal stress [when; $\sigma_t \leq 0.65\sigma_n$] F_t = $(\mu_n \sigma_n / 0.02)A\delta$ K_t = $(\mu_n \sigma_n / 0.02)A$ [when; $\sigma_t \geq 0.65\sigma_n$] assuming that the stress keeps constant while slip increases infinitely F_t = $0.65 \sigma_n A$ K_t = 0 2. Under tensile normal stress [when; $\sigma_t \leq 0.04\sigma_n$] F_t = $(\mu_n \sigma_n / 0.02)A\delta$ K_t = $(\mu_n \sigma_n / 0.02)A$ [when; $\sigma_t \geq 0.65\sigma_n$] F_t = 0 K_t = ∞ Where F_t : force in the direction tangential to the interface (N), K_t : stiffness in the direction tangential to the interface (N/mm)

2.4.3.3 Verification of Steel Plate-Concrete Interface Element

The confirmation of the applicability of the interface element developed in this research was done by implementing the interface element into the finite element model of steel plate-concrete composite specimen. The representative specimen was chosen from the series of experiments conducted by Yonezawa [80]. The steel plate-concrete composite specimen is as shown in Fig. 2.19.

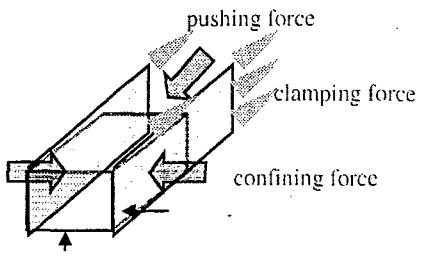

Fig. 2.19 Specification of the specimen tested for the steel plate-concrete interface property by Yonezawa

In the finite element analysis, the concrete and steel plate are simulated by the three-dimensional arbitrary distorted cube (MARC element No.7) and the bilinear thick shell element (MARC element No.9), respectively. The properties of both materials used in this finite element analysis are as described in section 2.4.1.2.2.

The three dimensional springs are used to connect the steel plate nodes to the adjacent concrete nodes. The steel plate nodes are, therefore, retained in all translation directions (x, y, and z) by concrete nodes and vice versa. The derived spring stiffness is input through MARC subroutines (USPRNG and IMPD) into the calculation. It is noted that the area that is used to compute the stiffness of interface element is defined to be the summation of a quarter of the areas of plate elements surrounding that particular plate node as illustrated in Fig. 2.20.

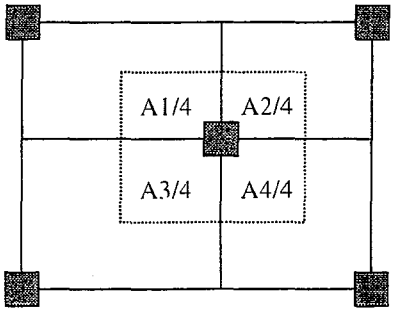

Fig. 2.20 Nodal area for calculating the stiffness of interface

$$Anode = (A1/4) + (A2/4) + (A3/4) + (A4/4) \quad (2.17)$$

Where

Anode : the total steel plate area on which the nodal force is acting

A1, A2, A3 and A4 : the component areas located on plate element number 1,2,3 and 4, respectively

For the boundary condition, the fixed translation conditions are imposed at the end of concrete block. In addition, before the first pulling load step starts, the clamping (or confining) pressure of magnitude 822 MPa is applied onto both plates. Then the stepwise pulling load is applied at nodes located at the end of both plates. This displacement and mechanical boundary conditions are illustrated in Fig.2.19.

The analysis is verified by comparing the analytical results to the experimental results obtained by Yonezawa. By means of the relationship between the interface bond stress

and slip, it can be deduced that the analytical simulation with the application of newly developed interface element can predict the interface behavior very closely to the real behavior. Therefore, it is concluded here that without having to assume the virtual thickness of the interface element as in Yonezawa's analysis, by using the proposed steel plate- concrete interface element, the behavior of the interface can be accurately predicted.

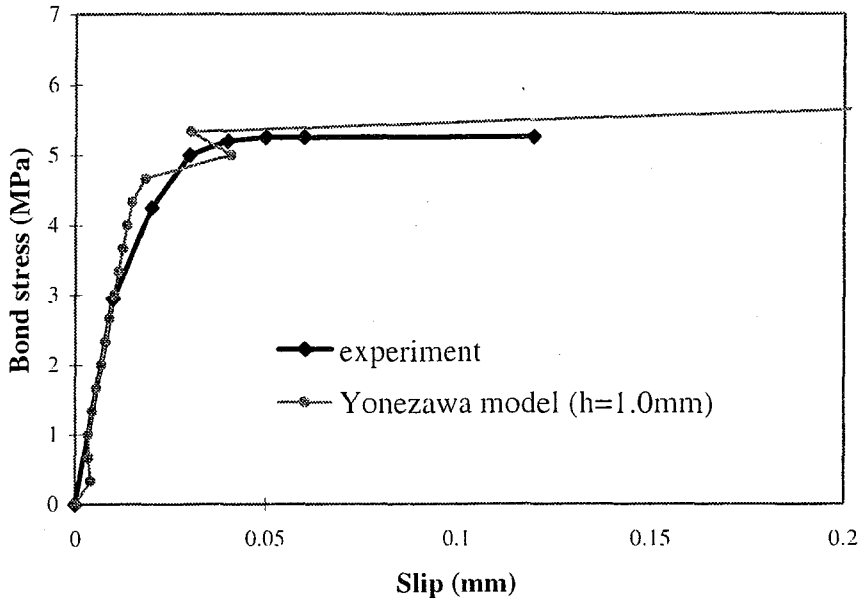

Fig. 2.21 Verification of application of interface spring element

2.5 Finite Element Analytical Procedures

After having made the structural model, determined the properties of all materials, and assigned the properties in terms of constitutive law to all elements, the next step is to conduct the analysis based on the finite element method. The analytical program utilized throughout this research is MARC analysis package. In this analysis package, the input information is divided in to 3 main parts, those are the input of the analysis parameters, the input of model definition, and the input of loading history.

In the first part, input of analysis parameters, the sizing of workspace is specified. Then the key information such as the element type (element number), numbers of applied loads, and the numbers of defined sets of nodes and elements, are specified.

The connectivity among elements and coordinates of every nodes are registered in the second part, model definition. In addition to these geometrical data of the structure, the fundamental material properties along with the boundary conditions also have to be listed in this part.

Up to this stage, MARC acknowledges the physical layout and mechanical properties the elements. The program is now ready to accept the input of apply loads and proceed the analysis. Further modification to the basic input in the main input card can be performed by accessing the source program through the particular subroutines. The finite element analytical procedures adopted in MARC can be illustrated by the flowchart in Fig. 2.22.

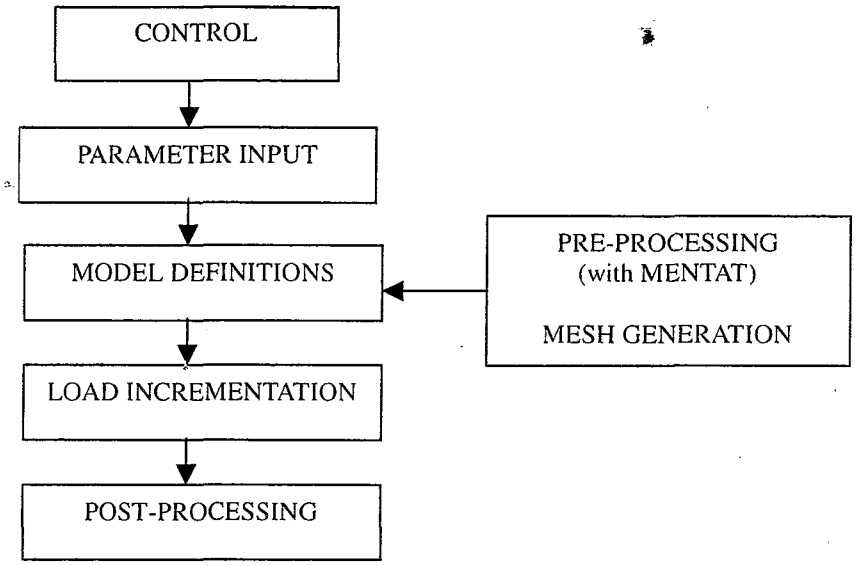

Fig.2.22 Flowchart of finite analytical procedures in MARC analysis package

In this research, some nonlinear properties of materials are input through and calculated in the subroutines, namely, USPRNG, USHRET, and IMPD. The functions of these user subroutines provided in MARC are;

USPRNG : for defining the user preferable stiffness of the springs. The stiffness of the reinforcing bar-concrete as well as steel plate-concrete interface element are defined in this subroutine.

USHRET : for defining the shear retention factor of the concrete element

IMPD : this subroutine is used not as directly to input the material properties like USPRNG and USHRET subroutines. It is used to store the resultant strains and stresses coming out at the end of the current loading increment to be used at

the beginning of the next loading increment. This is to solve the numerical difficulties in the nonlinear finite element analysis of the complicated structures like the ones analyzed in this research. The works done by the IMPD subroutine are :

1) Storing the final displacement data at the end of the current loading increment. This displacement data will be converted to be the strain in reinforcing bar that will be used in the calculation of the stiffness of reinforcing bar-concrete interface element. It is because the stiffness of this element is dependent on the strain in reinforcing bar in addition to the dependency on the slip as defined by Shima. (Eq.2.8)

2) Storing the slips of the reinforcing bar nodes located at the interface between reinforcing bar and concrete elements in terms of nodal displacements. This value will be used again at the beginning of the next loading step.

3) Storing the normal and frictional forces acting on the nodes of steel plates. These forces will be used in the consecutive loading increment to determine the stiffness of steel plate-concrete interface element.

Some nodal data which cannot be directly acquired by IMPD subroutine, such as the normal and frictional forces acting on steel plate nodes, will be transferred from the subroutine USPRNG via the common blocks to IMPD. This is to assure that the data to be reused in the next increment are the final values obtained at the end of the current loading increment.

2.6 Preliminary Verification of Analytical Methodology and Selection of Suitable Reinforced Concrete Material Model

After constructing the structural model, the material properties that also have already been derived, are assigned to all elements in the model. Then we can now start to conduct the analysis based on the finite element procedures. To check whether the proposed analytical methodology is valid, at the primary stage, the method is applied to simulate the response of the structure consisting of steel girder-reinforced concrete pier composite connection subjected to the external load. The structure selected to be analyzed is one of the composite connection specimens tested by Japan Highway Corporation and construction companies [41]. The design specification of this specimen is as shown in Fig. 2.23.

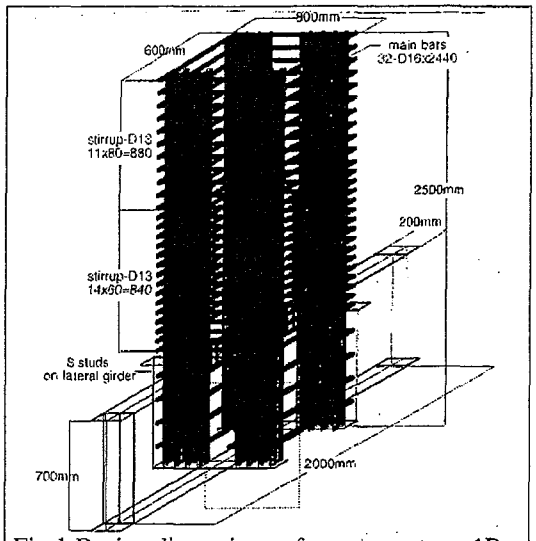

Fig.1 Design dimensions of specimen type-1B

Fig. 2.23 Design specifications structure consisting of steel girder-reinforced concrete pier composite connection

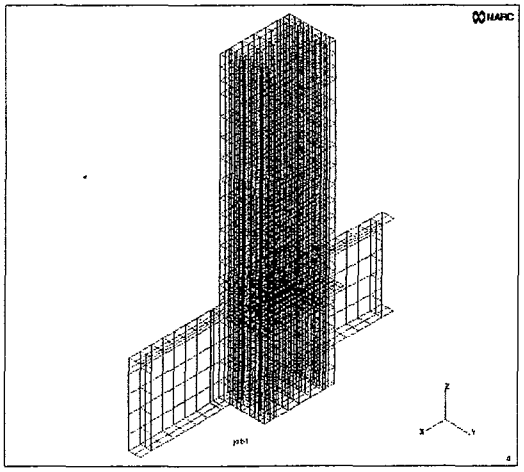

Fig.2.24 Finite element meshes of steel girder-reinforced concrete pier composite connection specimen

The finite element structural model of this test specimen is illustrated in Fig2.24. In order to separately account for the effect of each structural component, the structural model was discretely meshed. The structural components those are, concrete, reinforcing bar and stirrup, steel plate, and stud, are represented individually by the different types of element. The 8-node three-dimensional arbitrarily distorted cube element (MARC element No.7) is used to simulate the concrete material. The

reinforcing bars including both stirrup and longitudinal one are represented by 2-node three-dimensional truss element (MARC element No.9) while the 4-node thick shell elements (MARC element No.75) are used to simulate the steel plate. The 2-node beam element (MARC element No.14) is used to represent the stud.

Due to the symmetry of the structure along the middle plane (in this case, on the plane normal to y-axis), a half physical finite element model was constructed. The boundary conditions consist of displacement as well as mechanical boundary conditions. Those condition imposed before the beginning of the calculation to the structural model are,

1) Displacement boundary conditions : the fixed displacements on the half plane (the plane having normal vector along y-axis). Nodes located on this plane was considered not be able to translate in y-direction and not able to rotate about x-and z-directions. At the support, the translations in all directions, namely, along x-, y-, and z- directions are essentially prohibited.

2) Mechanical boundary conditions : these boundary conditions are used to simulate the loading applied to the structure. The distributed load is initially applied on the surface of the top elements by using "dist load" function. Then this load is kept constant while the horizontal load is incrementally applied via "point load" function throughout the analysis.

As this preliminary analysis is also conducted to aid the selection of the more appropriate material model of reinforced concrete between the smeared crack concept and the analysis with the application of the reinforcing bar-concrete interface element explained in section 4.1.1 and 4.1.2, orderly, both material models of reinforced concrete are applied in two separated analytical cases. The study case 1 and 2 are conducted to verify the results from the finite element analysis with application of smeared crack concept and from the finite element analysis with application of reinforcing bar-concrete interface element, respectively. The way that the reinforced concrete material property is formulated, is as discussed priory in section 4.1.1 and 4.1.2 and it will not be restated here. Only the results from the analyses with both concepts are explained and based on the results, the more appropriate modeling of reinforced concrete in the structure consisting of steel girder-reinforced concrete pier composite connection is determined.

Having finished constructing structural model as well as assigning the material properties to the elements, the distributed load is then applied. It is kept constant until

the end of analysis. The horizontal load is applied to the structure monotonically with the maximum load assumed beforehand to be 150 kN. However, this value may not be reached in some cases due to the failure of material prior to arriving this pre-specified ultimate load. For the convergence testing, the displacement criteria (No.1, in MARC control card) was used. The maximum allowable value of the change in displacement increment divided by the displacement increment default was set to be not greater than 15 percents. The stepwise increment of this horizontal applied load is programmed via the "auto increment" function. The analytical package will automatically choose the amount of load increment accordingly to the control parameter registered by the user. It should be noted here that, all of the mechanical loads are applied in the increment next to increment zero as it is required by the package that at the initial increment, the analysis must be within an elastic stage, both geometrical and material nonlinearities are not allowed to occur in this initial stage.

The results from the analysis case 1 (smeared-crack concept based) and case 2 (with interface element) are shown in terms of the load-displacement relationship, and load-reinforcing bar strain relationship in Fig.2.25 and 2.26, respectively.

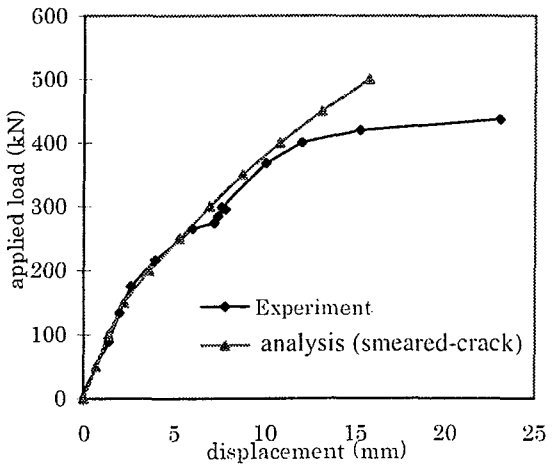

Fig. 2.25 Load-deflection relationship

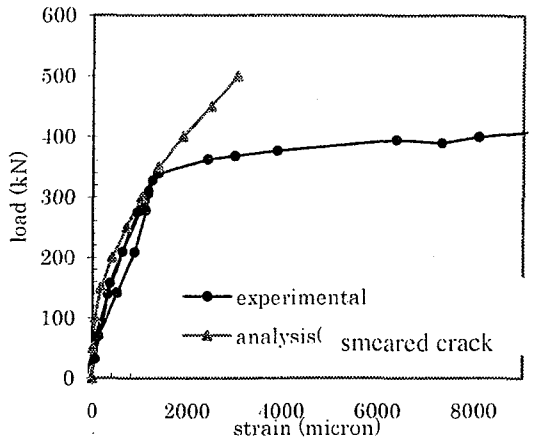

Fig. 2.26 Load-reinforcing bar strain relationship

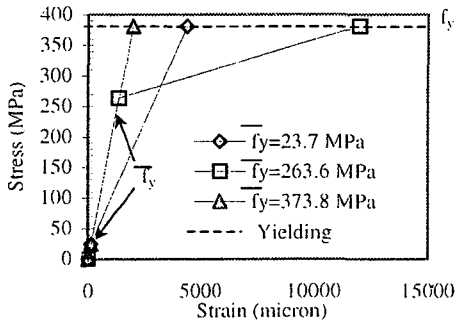

Fig. 2.27 Modified constitutive law of reinforcing bar

It can be seen that before concrete cracks the analysis can predict the behavior of structure quite accurately. However, some discrepancies can be observed beyond this cracking point. The behavior predicted by analysis based on smeared crack concept and with the application of the reinforcing bar-concrete interface element show a good agreement with the experimental results. Nevertheless, the smeared crack based analysis cannot simulate the behavior of structure correctly after the yielding of reinforcing bar takes place. This is expected to be due to the imperfection of the modified constitutive law of the reinforcing bar. To check if this speculation is correct, the additional three comparative analytical cases having different constitutive laws are conducted. In these three cases, the initial yielding stress is modified to be different from those calculated by Shin's method. The modified constitutive laws of reinforcing bar in all study cases are as shown in Fig2.27. The initial yield stress is alternated to be $\bar{f}_y$ = 263.6, 380.7 (same as the actual yielding stress of the reinforcing bar), and 23.7 MPa in case 1, 2,

and 3, respectively. The stiffness of the reinforcing bar after passing through the initial yielding point ($\bar{E}_{sh}$) is calculated by using the equation proposed by Shin (Eq.2.3). The same analytical procedures were followed and the results of these 3 cases are shown in Fig. 2.28 and Fig. 2.29.

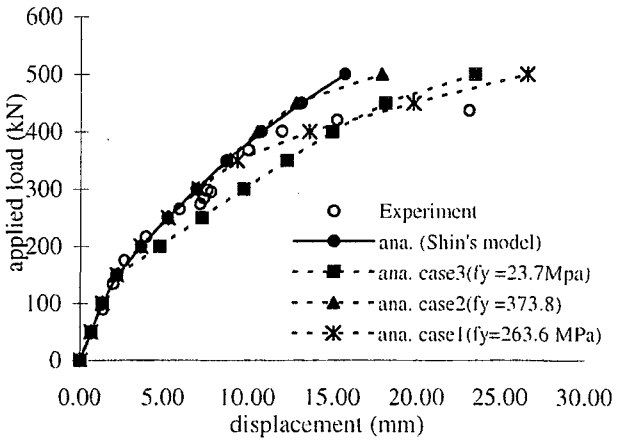

Fig. 2.28 Load-displacement at loading point relationship

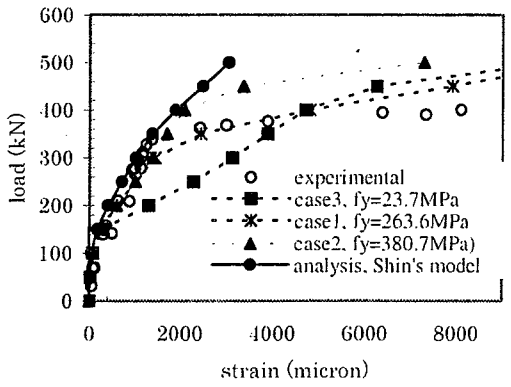

Fig. 2.29 Load-reinforcing bar strain relationship

It can be clearly seen that by using the constitutive law of reinforcing bar proposed by Shin, the structure behaves more stiffly compared to the experimental result which is nearly similar to the results from comparative case 2, where the actual elastic-perfectly plastic model with actual yield point is applied. However, when the yield stress of reinforcing bar is assumed to be 263.6 MPa in comparative case 1 (obtained by trial and error), the analytical prediction shows quite comparable result to the experimental data

both in the elastic and inelastic ranges. For case 3, where the minimum initial yield stress (defined in Eq.2.3, $\bar{fy}$ = 23.7 MPa) was used, the stiffness of the entire structure as well as the rate of change of strain in reinforcing bar becomes obviously lower. Therefore it can be concluded that the modification of initial yield stress and the post-yielding stiffness can greatly affect the predicted behavior of the structure. In addition, it can be deduced that the constitutive relationship proposed by Shin is not regarded as the generalized model.

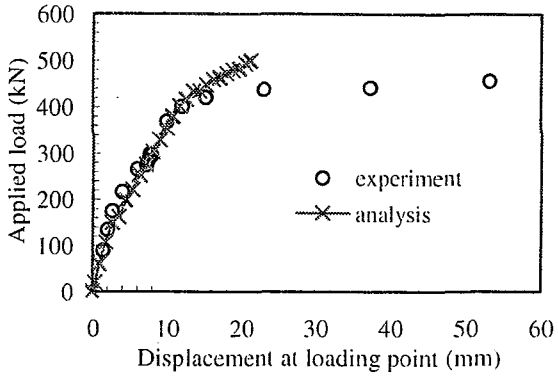

Fig.2.30 Load-deflection relationship from finite element analysis with application of reinforcing bar-concrete interface element

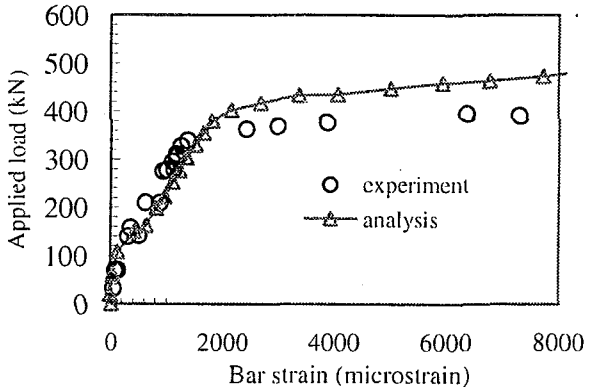

Fig.2.31 Load-bar strain relationship from finite element analysis with application of reinforcing bar-concrete interface element

In contrast, with the application of reinforcing bar-concrete interface element, the analysis gives out a closer behavioral prediction than the one which is based on the smeared crack concept, Fig.2.30 and 2.31, especially in the load-reinforcing bar strain relationship after yielding of reinforcing bar occurred. The real constitutive law of the reinforcing bar and concrete can be used straightly without having to be modified.

However it should be noted that the calculation time is noticeably increased when the reinforcing bar-concrete interface element is implemented into the model as the degree of nonlinearity is greatly increased.

Based on this comparisons, it is suggested that the analysis with the application of the proposed reinforcing bar-concrete interface element should be used in analyzing the structure consisting of steel girder-reinforced concrete pier composite connection, as it is proved to be more generalized than the analysis based on smeared crack concept in where the accurate modified constitutive law of reinforcing is still not available. Therefore, hereafter in this research, the finite element analysis with the application of reinforcing bar-concrete interface element is used for simulating the behavior of reinforced concrete part in the structure.

Regarding the performance of the steel plate-concrete interface element, according to the comparison between analytical and experimental results, it is obvious that the application of this interface element improves the accuracy of the prediction. The plot between load and the principal strain, Fig.2.32, illustrates that with the application of the steel plate-concrete interface element, the change in strain due to the slip occurring at the interface between the concrete and the steel girder could be predicted more accurately.

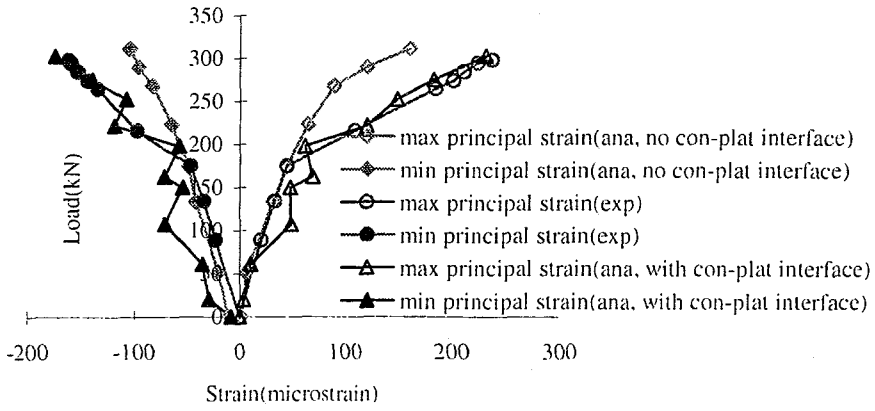

Fig. 2.32 Relationship between load and principal strain
at center of main girder web

2.7 Behavior of Structure Consisting of Steel Girder-Reinforced Concrete Pier Composite Connection

By using the proposed analytical method, the behavior of the connection is visualized. Some important parameters, which can hardly be obtained in experiments, can be obtained in the analysis. From the preliminary analysis, the distributions of forces within the connection are simulated. This is done in order to get a rough idea on how the forces are transferred from one connection components to the others.

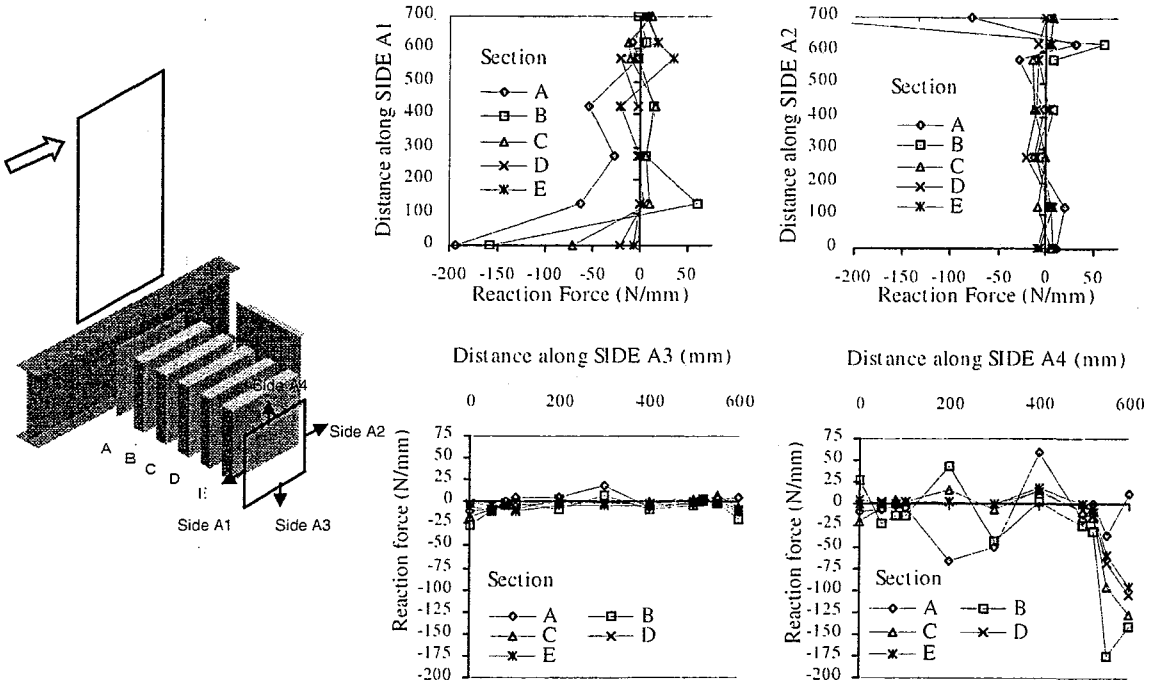

Fig. 2.33 Distribution of normal reaction force on concrete sections located within connection

Fig.2.33 shows the normal reaction forces on concrete elements located at the faces named SIDE A1, A2, A3, and A4 (the reaction forces that equilibrate the forces exerted on concrete element by the surrounding elements adjacent to the faces being considered). It points up that compared to the sections located farther from the main girder (C, D, and E), the stresses on the sections located at the vicinity of the main girder's flange (A, and B) are more intensive. Therefore, it can be deduced that, in this type of specimen, the force transferred from the girder is not well spread throughout the reinforced concrete part in the connection.

In the real construction, the width of the concrete pier is usually designed to be much wider than the width of the main girder's flange. Therefore, in the case that the magnitude of forces applied to the girder is excessively high, while this load is being transferred to the reinforced concrete pier through the connection, it might caused the stress concentration to occur at the vicinity of the main girder's flanges. The stress concentration may eventually originate the local deterioration to the concrete situated near the flange of the main girder. Since this concrete encased by many structural components such as the girder's flanges, lateral girders, and the slabs, it will be difficult to repair if the localized destruction is occurred.

2.8 Conclusions

In this chapter the analytical methodology was developed. It was then preliminarily verified with the results from experiments conducted by Japan Highway Corp. and construction companies. A good agreement could be observed in the comparisons when reinforced concrete was modeled with the application of reinforcing bar-concrete interface elements. Therefore, it is deduced that this method is more generalized than the modeling with smeared crack concept which still lacks of the accurate constitutive relationship of reinforcing bar. Moreover, by implementing the steel plate-concrete interface element into the finite element model, the slip between concrete and steel plate can be correctly simulated. Nevertheless, a further verifications with some other experimental results are still needed to assure the generality of this analytical method.

The results from the preliminary analysis suggested that due to the stress concentration observed at the vicinity of the main steel girder, the local deterioration, which is difficult to be repaired, may occur. This rises up the other point of consideration in design that how to effectively distribute the load transferred from the main girder passing through the connection to the reinforced concrete pier without initiating any local deterioration in concrete located within the connection. As well it questionable to the existing structures that have already been constructed using this method that how safe and how difficult to repair if the local deterioration does accidentally happen.

CHAPTER 5

Verification of Analytical Methodology

5.1 Introduction

As stated earlier, the demerits in application of this type of composite structure is the difficulty in design and analysis. Though to the time many analytical procedures have been proposed in order to analyze this kind of structure, none of them is guaranteed to be sufficiently generalized. Another alternative analytical method proposed in this research, in chapter 2, as well, needs a verification of its generality and accuracy. Thus, in addition to the preliminary simulation of the composite connection specimen tested by Japan Highway Corp. and construction companies, the experiment was carried out in this research course with one of the objective set as to verifying the proposed analytical method.

In this chapter, the behavior of composite connection specimens simulated by the proposed analytical procedures, are verified by comparing to the experimental results. The verification is presented in terms of the overall structural behavior namely, the load-deflection relationship, and the relationship between reinforcing bar strain and the applied load. The load-reinforcing bar strain relationship will also show the analytical trend how, compared to the experimental results, loads from pier are being distributed to the connection.

5.2 Relationship between Applied Load and Deflection

The comparisons between analytical and experimental load-deflection relationships of specimen C-1, C-2, C-3, and C-4 are as shown in Fig5.1 to 5.4, respectively. The deflection is measured at 1500 mm above the top of the composite connection.

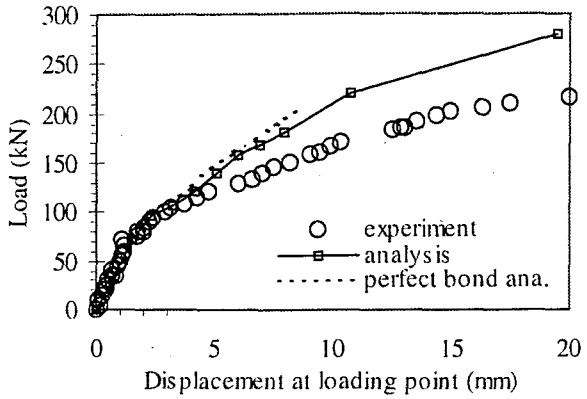

Fig.5.1 Load-deflection relationship of specimen C-1

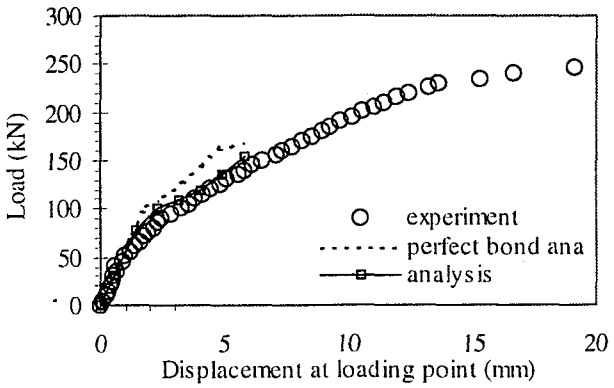

Fig.5.2 Load-deflection relationship of specimen C-2

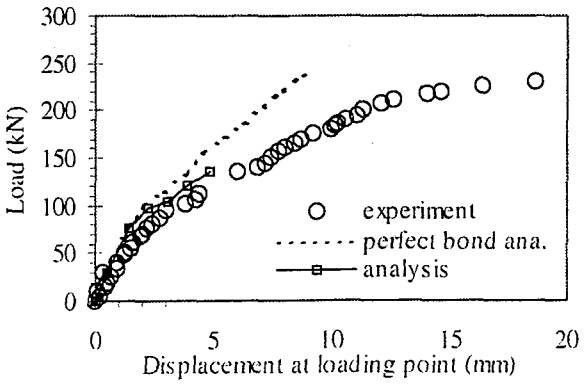

Fig.5.3 Load-deflection relationship of specimen C-3

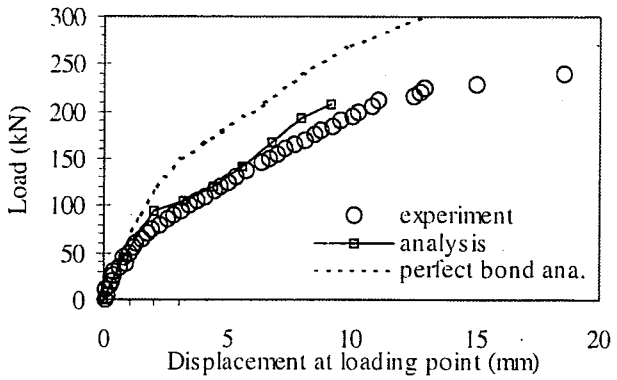

Fig.5.4 Load-deflection relationship of specimen C-4

From the Fig.5.1 to 5.4, it can be seen that the behavior of all specimens can be simulated fairly accurately within the elastic range. The point at which the structure first looses the stiffness (cracking of concrete begins) can be predicted correlatively to that observed in experiments. However, beyond this point the simulated behavior seems to be stiffer than the experimental one, particularly for specimen C-1. For this specimen, the simulation could not follow the real behavior when the second reduction in stiffness occurs. In the test, this point was occurred at the load step where the separation between concrete and the main girder initiated. At this point, a very high degree of discontinuity does occur at a wide crack on tension side as well as the distributed cracks in the connection's concrete. At this stage, the bond might have fully lost at some large openings allowing the slip to occur quite freely. The simulation with the assumption of linearly reducing bond effective zone factor having minimum value equal to 1, might not be able to handle this situation. Therefore further study is needed in this area to modify the function of bond effective zone factor. For specimens C-3, due to a high degree of nonlinearity, the analysis fails to converge beyond 50 percent of the real applied load. Therefore, the convergence testing must be readjusted carefully when apply this method of analysis. In these four figures, the relationship between load and deflection predicted by the proposed analytical methodology is also compared to the result of analysis with an assumption of perfect bond between concrete and reinforcing bar node. It is obvious that the improvement in the results can be achieved when the proposed method is applied.

5.3 Load-Reinforcing Bar Strain Relationship

The relationships between applied load and the strain on reinforcing bars measured at 50 mm above the connection on tension side are shown in Fig. 5.5 to 5.8.

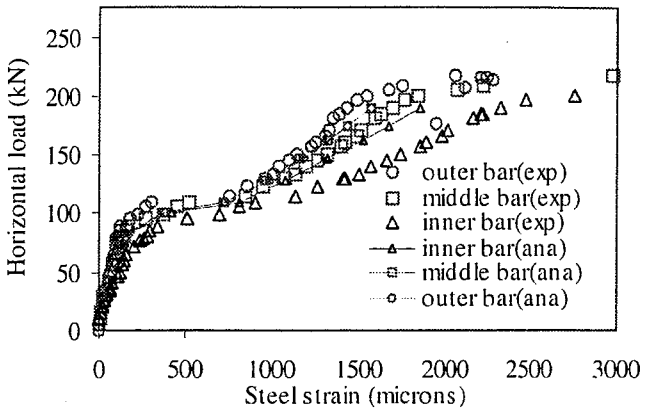

Fig.5.5 Load-reinforcing bar strain relationship of specimen C-1

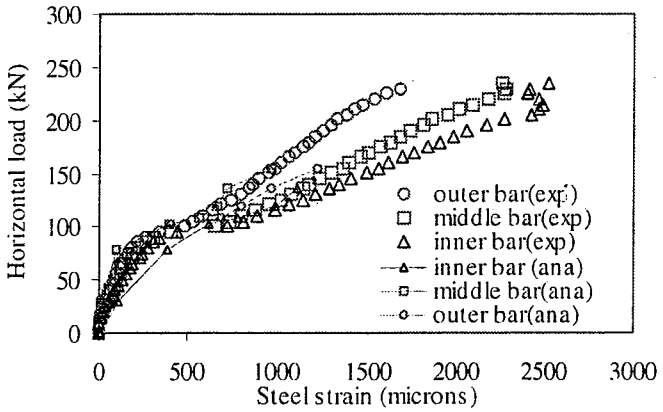

Fig.5.6 Load-reinforcing bar strain relationship of specimen C-2

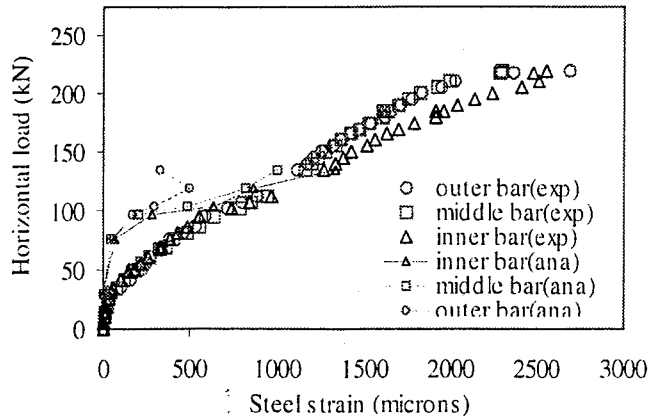

Fig.5.7 Load-reinforcing bar strain relationship of specimen C-3

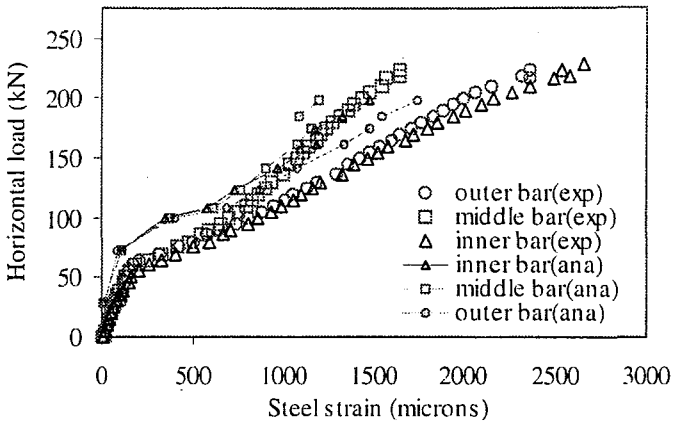

Fig.5.8 Load-reinforcing bar strain relationship of specimen C-4

In this aspect, the analytical predictions show a correlative trend with the experimental results in the comparisons. Quantitatively, the analytical behaviors of reinforcing bars on tension side of specimen C-3 and C-4 seem to be stiffer than the real behavior observed in the tests. This might be due to the fact that, in the test, as some cracks were pre-generated during transporting the specimen onto the testing base, the first drop in structural stiffness occurs rather early compared to the analytical results. Another reason might be because the mismatching between the young modulus provided by the steel manufacturer and the real value that might be lower. In specimen C-3, due to the divergence occurred in analysis, the simulation has stopped just at the middle of the entire process. However, it still shows the correlative trends with the experimental results. According to these curves, it can be interpreted that, although the analysis could not proceed until reaching the ultimate state, the predicted distributions of steel strains in the lateral direction have more or less the same trend as in experimental results, especially in the elastic range.

5.4 Conclusions

Based on the comparisons between analytical and experimental results it could be deduced that the fair agreement between the analytical and experimental results is evidenced in an elastic range. Nevertheless, the analysis is quite prone to the divergence problem due to the high degree of nonlinearity in material models. Therefore this method should be applied with a careful adjustment of convergence test. In addition, not

only the overall behavior which can be fairly predicted, the distribution of forces in the lateral direction simulated with the analytical procedures also shows a correlative trend with that observed in the test.

CHAPTER 6

Force Transfer Mechanisms

6.1 Introduction

Unlike a normal reinforced concrete beam-column joint in the typical reinforced concrete structure, the structure consisting of steel girder-reinforced concrete pier composite connection is rather more complicated. Various influential connection components are usually arranged in a three-dimensional space, thus make it difficult to visualize the interactions among them.

In the ordinary reinforced concrete beam-column joint, the system is comparatively unsophisticated. Within the connection, there exist only some few basic elements such as the reinforcing bars and concrete. In practice, these elements are laid on the symmetrical layers and can be easily designed. Various two-dimensional design methods have been developed since the early 1900. Those design methodologies are, for instance, a two-dimensional strut-and-tie model, arch model, stress fan model, etc. Such designs have been proved to be acceptably accurate and some have even been implemented into the regional design code for concrete structure, CEB-FIB 1990 [19].

However, in the structure being considered in this research in which the composite connection between the steel girder and the reinforced concrete pier presents, although the symmetrical layout does exist, it is not collapsible into one representative plane. The aforementioned two-dimensional methods are, therefore, inappropriate to be applied. This leads to the immediate necessity of an alternative model capable to describe the interactions among the components in the composite connection.

Having briefly explained in Chapter 4 about the behaviors of the connection components observed in the experiment, in this chapter, the conclusive explanations on the interactions among those components will be given. The validity of the force transfer mechanisms explained in this chapter will be qualitatively confirmed against

the experimental as well as analytical results (Chapter 7). Based on the mechanisms to be explained hereafter, the alternative model for predicting the behavior of composite connections will then be proposed in the consecutive chapter.

6.2 Force Transfer Mechanisms

In this research, the structure of interest consists of the reinforced concrete pier, steel girder, and the composite connection. In the experiment, to simulate the behavior under static loads, the vertical as well as the horizontal forces were applied on to the reinforced concrete pier. These externally applied forces were transferred through the pier, connection, main girder, and eventually, they were balanced by the reactions from the supports located on the main girder preventing the structure from being displaced.

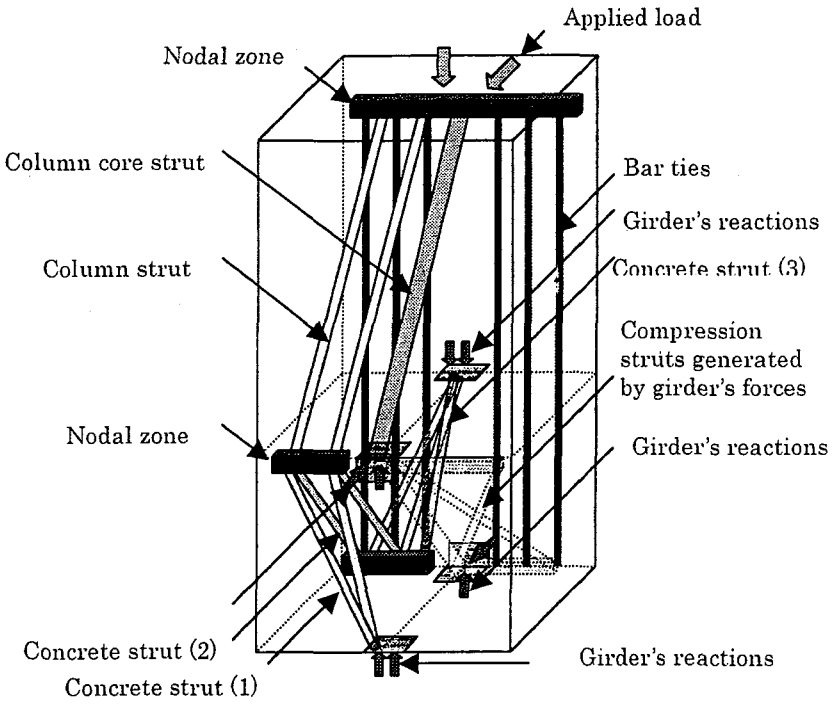

Fig.6.1 Flow paths of forces inside the structure.

Since the main purpose of this research phase is to investigate the force transfer mechanism within the connection, the connection, henceforth, will be considered as the main system. The system is stressed by sets of external forces those are exerted by the reinforced concrete pier and by the main girder. In the following sections, the transfer of applied forces and reactions through the reinforced concrete pier and the main girder

will be described. Then, taking into account the pier and main girder forces as the external loads to the system, the mechanisms formed within the connection to balance these loads will be consecutively explained. Fig.6.1 briefly illustrates the flow paths of forces inside the structure.

6.3 Force Transfer in Reinforced Concrete Pier

When the specimen is vertically and horizontally loaded at the top of the pier, the applied forces generate both flexure as well as shear in the pier section. The shear force is assumed to be uniformly distributed over the entire length of the pier down to the top of the connection. At this position, shear force is equilibrated by the horizontal reaction from the connection. The reaction is partly contributed by the studs on the top flange of the main girder and partly by the intact reinforced concrete in the compressive zone. At the ultimate state, as the uncracked concrete area becomes smaller, the contribution of concrete is greatly reduced. However, on the flange of the main girder, since there is a group of studs holding the pier's concrete and the main girder together, even though the crack has deeply propagated through the depth of the section, the contribution of this portion in resisting shear will be relatively less decreased. From this phenomenon, we can deduce that the distribution of shear force from the pier to the top of the connection is not uniform in the lateral direction.

The flexure, in another way, will produce a couple of compressive and tensile forces on the pier's section. The couple generated in the pier is balanced by the reactions from the connection. In the compression zone, the compressive force in the pier is responded by the top flange of the main girder as well as by the concrete within the connection. In the opposite direction, the tensile force in the pier is also kept balanced by the bond force on reinforcing bars embedded in the connection concrete. Then the surrounding concrete will convey the force to the bottom side of the main girder's top flange (details of this action will be explained in section 6.4, force transfer in composite connection.

Based on the stress field concept, A. Muttoni, J. Schwartz, and B. Thurlimann[1] stated that the distribution pattern of forces within the concrete element is directly dependent to the dimension of supports at both ends of the compressive strut, the larger the difference in support size between both ends is, the more distributed stress will induced in the strut. Correspondingly to this concept, the distribution of pier's force on the top of

connection into the lateral direction can be determined. It should be noted, although, that in the experiment, the forces applied onto the reinforced concrete pier are those from the actuators and on the other end by the reaction from the connection. Since the widths of actuator heads are not much different from the width of the pier, therefore, the forces from actuator heads are nearly uniformly distributed in the lateral direction onto the top of the connection.

6.4 Force Transfer in Main Steel Girder

In forms of couple and shear, the forces from the reinforced concrete pier are transferred via the connection to the main girder. Similarly to the ordinary reinforced concrete beam-column joint, the couples are generated by rotation of the connection. The connection will push and pull the section of steel girder in the compression and tension regions, respectively, and cause the bending moment in the main girder. Along with this moment, the vertical shear will be shifted from the connection to the main girder. Then these forces will be resisted by the reactions from the supports positioned at both ends of the main girder. By the set of forces mentioned, the structure is brought into equilibrium without any rigid body movement. Fig. 6.2 shows the forces transferred from the connection passing through the main girder and locked in place at the supports.

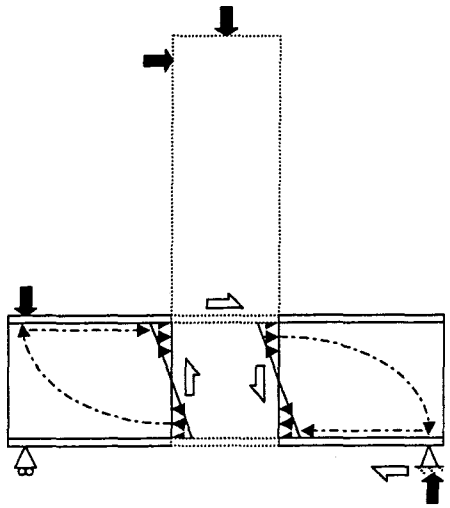

Fig.6.2 Force transfer in main girder and reactions on connection faces

The particular point that makes the force transfer from the composite connection to the main girder different from that in the ordinary reinforced concrete beam-column joint is

that, on the surface where the girder begins to emerge into the connection, force from the main girder is decreasingly distributed away from the center of the girder. The forces in the web and flange of the main girder start to laterally distribute not only onto the main girder deposited inside the connection itself, but also to the concrete within the connection, whereas, in the ordinary beam-column joint, as the section is not changed in shape, the forces form the beam would rather be more uniformly distributed across the width of the beam and joint. The main girder's force will be distributed in the direction away from the center of the girder with reducing magnitude to the outer connection concrete as shown in Fig.6.3.

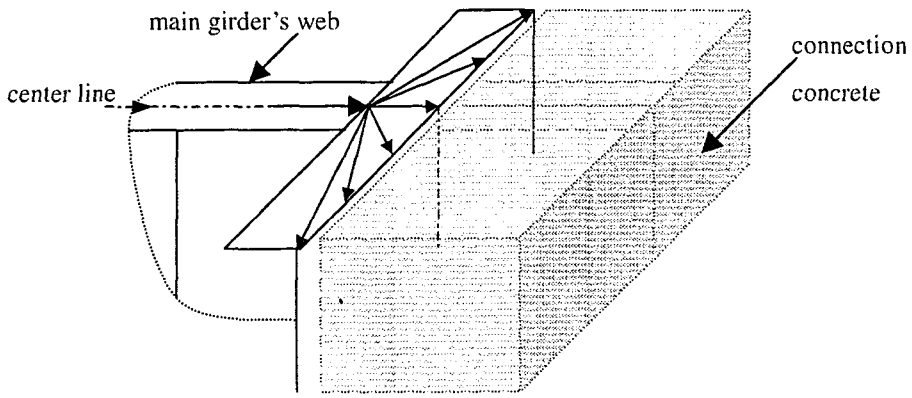

Fig.6.3 Distribution of main girder's force onto the connection.

6.5 Force Transfer Mechanisms in Composite Connections

In this section, the composite connection is considered as the system and all of the forces exerted by the other structural members to the connection, are thought of as the externally applied loads. The mechanisms are established within the connection to react to the external forces. The external forces can be, more specifically, classified into 2 types according to the source of the forces. One is a group of forces applied to the system by the reinforced concrete pier and the other is that coming from the main girder. The pier's forces compose of compressive and tensile forces generated by the flexure, and the horizontal shear force acting on the top plane of the connection. Identically, the main girder also induces a couple of compressive and tensile forces as well as shear onto left- and right-hand sides of the system. These externally applied forces are as illustrated in Fig.6.4.

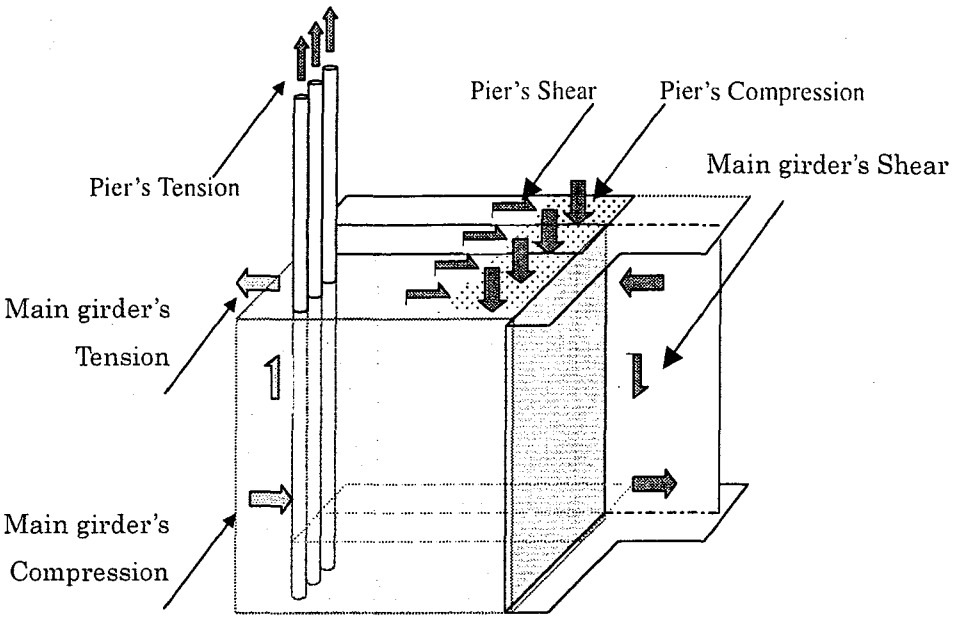

Fig.6.4 Forces externally applied to the system

To reduce the complexity, the mechanisms formed inside the composite connection are classified into two parts namely; those are the mechanisms reacting to the forces from pier and to the forces from the main girder. The force transfer mechanisms within the composite connection of specimen C-1, C-2, C-3, and C-4, are described on this basis in the following sub-sections. It is noted that, to express the total system, these two separated mechanisms must be combined to each other.

6.5.1 Specimen C-1

In this sub-section, the explanations regarding the mechanisms established within the connection to resist the pier's forces will be given in the first place. Then the mechanisms originated by the main girder's forces will be successively explained.

Above the connection, other than the pier's compression force that is directly applied onto the top flange of the main girder (Fig.6.7), there is the other portion of compression forces which is transferred straightforward to the concrete within the connection (Fig.6.5). Since, on the compression side, the connection concrete is not supported firmly by any dedicated connection components at the portion laterally away

from the main girder, therefore the external compression force from pier will be redirected to the place where there is the upward force to balance it (via Strut 1 and Strut 2, in Fig. 6.5). This vertical force will be addressed partly to the lower left corner of the connection block in where the ends of the tension reinforcing bars are located (Strut 2) as well as partly declining to the bottom flange of the main girder (Strut 1). On the tension side, by the bond forces of reinforcing bars, the pier will be held in equilibrium. The reinforcing bars' bond forces will be transferred to the top-left corner of the connection via Strut 3. These inclined forces will be balanced by the reaction from the main girder's top flange, Fig.6.5.

For the mechanisms established to respond the forces from the main girder, they are graphically shown in Fig.6.6 and 6.7. While the structure is being loaded, the main girder will generate flexures as well as shear to the connection. The effects of flexures applied to the connection can be represented by the couples of compressive and tensile forces exerted on both left and right faces of the connection. Partially, these horizontal forces will be transferred through the connection by the main girder itself, whereas the rest will be laterally distributed and carried by to the connection concrete. The girder forces that are transferred in the connection via the girder itself are as shown in Fig.6.7. The girder's compressive and tensile forces will try to rotate the connection girder in a counterclockwise direction. To prevent the free rotation of the connection girder, the other couple generated by pier's forces, described previously, will counteract these forces. In addition, this down-and-upward forces will help balance the shear forces from the main girder being applied on the left and right faces of the connection girder.

At the same time, another mechanism ruling the transfer of the main girder's forces, is also formed in the connection concrete, Fig.6.6. Fig.6.6(a) shows the main mechanism which assists carry the major part of the main girder's forces. This concrete strut is formed within the boundary of the top and bottom flanges, and left and right stiffeners. Due to the change in section (from girder's section only to the girder's plus concrete's section), the horizontal forces from the main girder are also spread in the direction away from the main girder to the outer connection concrete. The compressive force applied at the bottom-left face of the connection will be laterally distributed and ended up being held at the compressive zone on the top-right position, Fig.6.6(b). On the other side, the compressive forces coming from the top-right face will be directed to location where there is the force that can balance it, and this location is at the bond-effective zone of the reinforcing bars, Fig.6.6(c).

All of the mechanisms described here are additive to each other in establishing the principal force transfer mechanisms within the connection of specimen C-1. This proposed mechanism can reasonably describe the actual behaviors of the composite connection in specimen C-1 observed during the loading test, for example, the excessive rotation of the connection at the ultimate state. This phenomenon is occurred due to crushing of concrete located on the limited bearing areas under the top flange of the main girder (Fig.6.5, bottom and top ends of strut 1, and 2, respectively). At the ultimate state the external forces applied to the pier is remarkably increased, while the bearing area is remained unchanged, therefore, the stress concentration occurs in these regions and finally causes a crushing of concrete. After the concrete is softened, the connection concrete looses its integrity with the main girder, and results in the excessive rotation. The crack pattern recorded on the surface of connection concrete is another example that proves the validity of the proposed mechanism. The crack patterns of the test specimens are given in Appendix A1. For specimen C-1, it can be seen that the cracks propagate into nearly the same directions as those of strut 1, 2, and 3 in Fig.6.5. Since these struts represent the flow directions of the principal compressive forces thus the cracks can be expected to occur parallel to the axis of the struts.

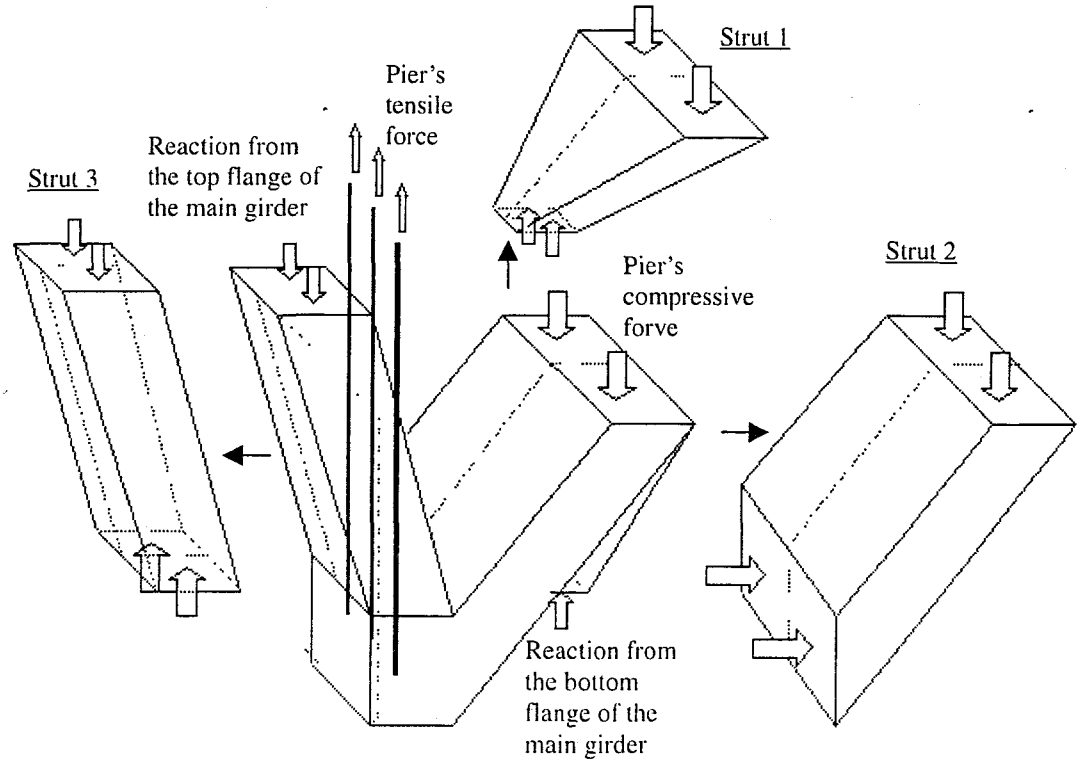

Fig.6.5 Force transfer mechanisms inside connection concrete of specimen C-1.
(established to resist pier's forces)

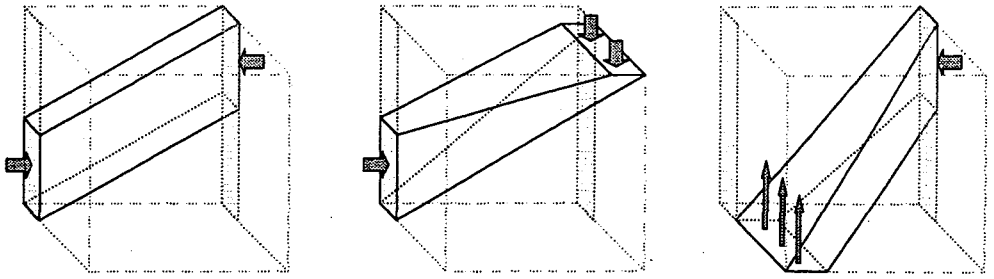

(a) Distributions of the main girder's compressions (left & right) to the connection concrete bounded by flanges and stiffeners

(b) Distributions of the main girder's compression (left) to the connection concrete

(c) Distributions of the main girder's compression (right) to the connection concrete

Fig.6.6 Force transfer mechanisms inside connection concrete of specimen C-1. (established to resist main girder's forces)

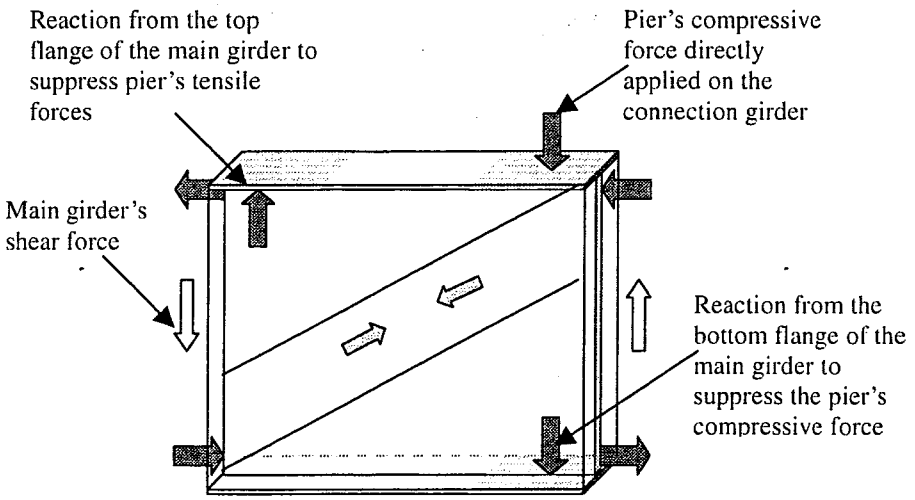

Fig.6.7 Force transfer mechanism in portion of main girder inside connection (C-1)

6.5.2 Specimen C-2

Fig.6.8 shows the force transfer mechanism in the connection of the specimen C-2 in which there are the lateral girders encasing the connection concrete. The mechanism of force transfer in this type of connection is essentially identical to that of specimen C-1 except that on concrete strut 1 and 3, there are the strut-shaped plates attached. Since there exist the studs joining connection concrete and lateral girders together, it is assumed that these two components behave in a fully composite manner and the same strut-shaped forces transfer path is formed in both components.

The flexure from the reinforced concrete pier (composed of the compression force acting on the top flange of the main girder and the tensile force through the reinforcing bars pulling concrete under main girder's flange on tension side up) is mainly balanced by the reaction couple from the top flange of the main girder and still causing the stress concentration at the vicinity of the main girder similarly to that in specimen C-1. However, due to the composite action between concrete strut 1 and 3 and the lateral girders' strut 1 and 2, the concrete at the bottom of strut 1 and at the top of strut 2 will be less stressed against the bottom and top flanges of the main girder, respectively. It is because fractions of pier forces will be transferred via the lateral girders' struts directly to the main girder. The availability of the lateral girders will also prevent the rotation of the connection causing by the deterioration of concrete struts as they are subjected to the less concentrated stresses.

The mechanisms established to react the forces from the main girder are as illustrated in Fig.6.9. Mechanisms (a), (b), and (c) are identical to those in specimen C-1, while mechanism (d) is the additional one. As demonstrated by Fig.6.3, the force in the main girder is spread laterally through the lateral girder to the connection concrete. It is assumed that the magnitude of this distributed force becomes smaller as the location it is carried to, becomes farther. That means the connection concrete positioned away from the main girder will gain less effect from this distributed force. This assumption is also imposed on mechanism (b), and (c).

For the force transfer in the main girder located inside the connection, Fig.6.10, the vertical forces from the lateral girders are added. As explained earlier, these forces will lessen the forces in concrete strut 1 and 3, and be considered as a positive effect. Via the proposed force transfer mechanism within the connection, the forces from pier are carried to the main girder where they are eventually balanced by the support reactions. By installing the lateral girders to encase the connection concrete, the excessive rotation could effectively be avoided since the stress concentration problem is relieved. This non-existence of disintegration between connection concrete and the main girder is also confirmed in the experiment of specimen C-2.

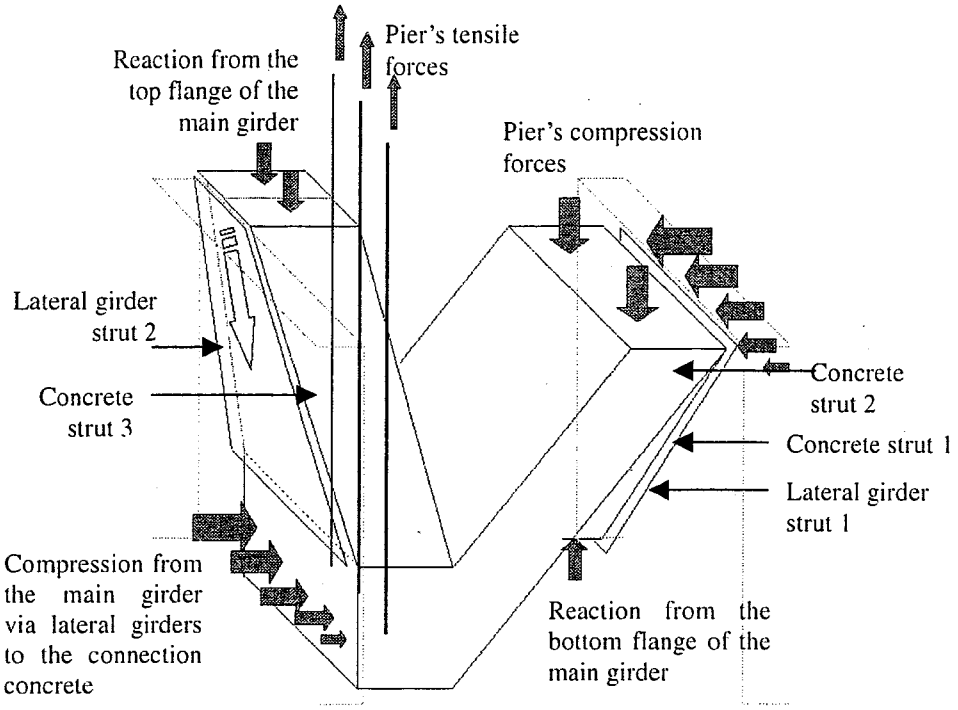

Fig.6.8 Force transfer mechanisms inside connection concrete of specimen C-2.
(established to resist pier's forces)

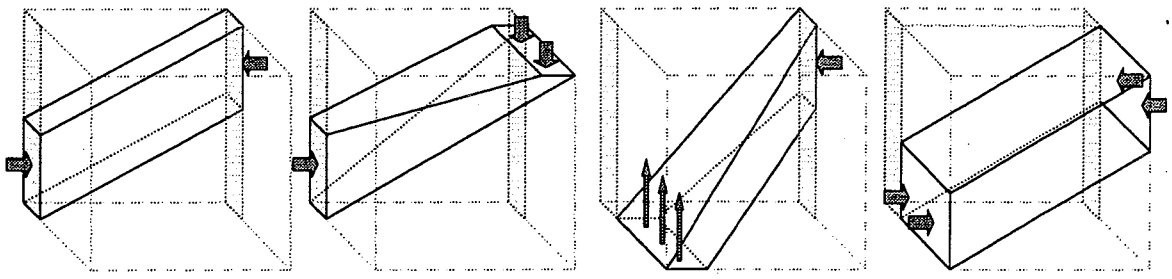

(a) Distributions of the main girder's compressions (left & right) to the connection concrete bounded by flanges and stiffeners

(b) Distributions of the main girder's compression (left) to the connection concrete

(c) Distributions of the main girder's compression (right) to the connection

(d) Distributions of the main girder's via lateral girders to the connection concrete

Fig.6.9 Force transfer mechanisms inside connection concrete of specimen C-1.
(established to resist main girder's forces)

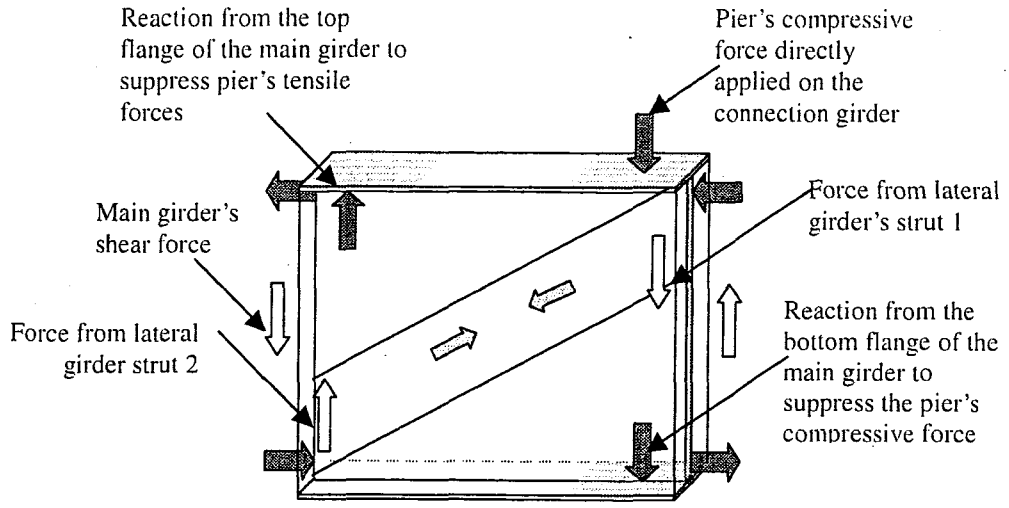

Fig.6.10 Force transfer mechanism in portion of main girder inside connection (C-2)

6.5.3 Specimen C-3

In specimen C-3 of which connection concrete is encased by the lateral girders like in specimen C-2 but with diaphragms connecting lateral girders on both sides together, the fundamental force transfer mechanism is similar to that works in specimen C-2. The flexure from the pier is still carried foremost by the reaction couple exerted by the top flange of the main girder. Nevertheless, as the lateral girders are strengthened by using diaphragms to link them together, they becomes stronger in resisting the portion of the pier's flexural couple which is distributed outward form the main girder. Hence, the outmost portion of concrete, strut 4, in Fig.6.11, would help transfer more force, via the strengthened lateral girder, straightforward to the main girder. It should be noted, although, that the connection concrete strut 1 and 3 are not extended up to the outmost concrete portion like in specimen C-1 and C-2, as it is blocked by the diaphragm.

The role of diaphragms is to hold the lateral girders on right and left side together. Therefore, when the specimen is loaded, the downward and upward movements of right and left lateral girders will be counteracted by the plate-shearing action of diaphragm. As a result of the less movements of lateral girders, the concrete at the location away from the main girder will contribute more in carrying pier's force. In addition, since the pier's force applied to the outmost concrete will be carried only by the lateral girder to

the main girder (lateral girder strut 2), thus, this contribution of lateral girder will reduce the stress concentration which might crush the concrete at the bottom of strut 1, and at the top of strut 3.

Fig.6.12 illustrates the mechanisms established in the connection concrete to resist the forces from the main girder. The directions of these concrete struts are almost the same as those of specimen C-2, with the exception that the struts shown in Fig.6.12(b) and (c) are not extended beyond the diaphragm. Another effect of diaphragm is that, the compressive stress in the inclined concrete struts adjacent to the diaphragm, Fig.6.12(d) and strut 1 and 4 in Fig.6.11, will be lessened as the diaphragm will help carry some part. For the force transfer in the main girder located inside the connection, its pattern is just similar to that presents in specimen C-2.

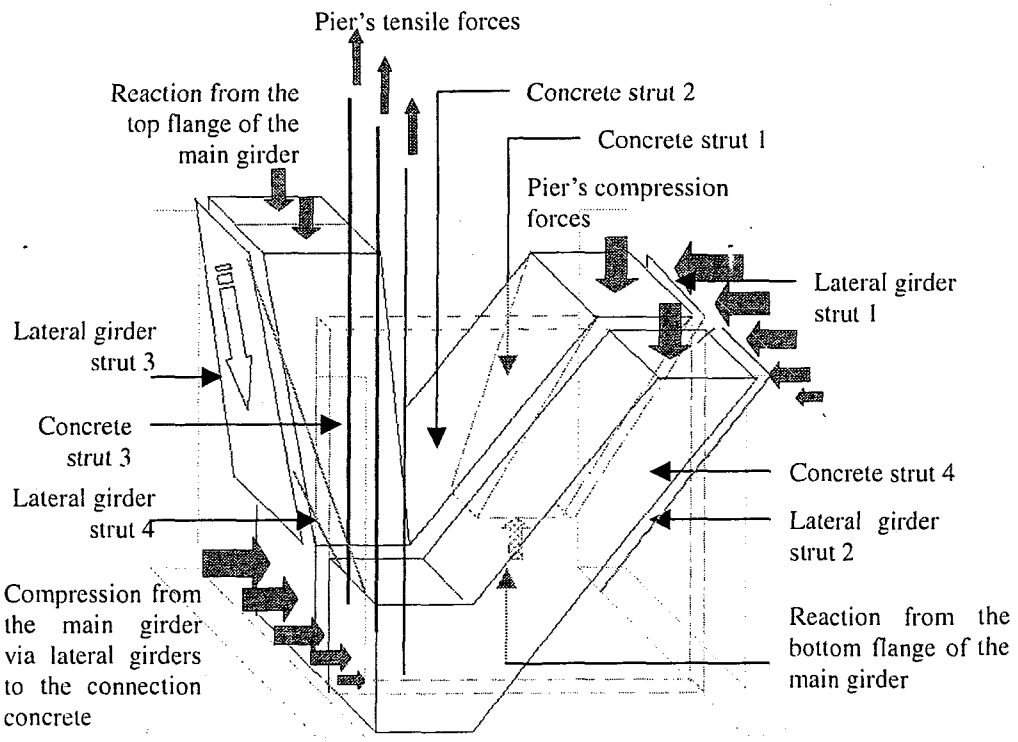

Fig.6.11 Force transfer mechanisms inside connection concrete of specimen C-3. (established to resist pier's forces)

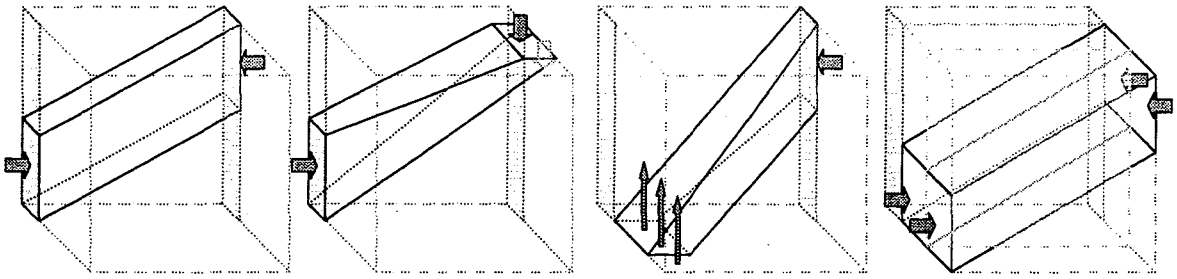

(a) Distributions of the main girder's compressions (left & right) to the connection concrete bounded by flanges and stiffeners

(b) Distributions of the main girder's compression (left) to the connection concrete

(c) Distributions of the main girder's compression (right) to the connection

(d) Distributions of the main girder's forces via lateral girders to the connection concrete

Fig.6.12 Force transfer mechanisms inside connection concrete of specimen C-3. (established to resist main girder's forces)

6.5.4 Specimen C-4

Fig.6.13 shows the force transfer mechanism within the connection of specimen C-4. The mechanism is different from those of specimen C-1, C-2, and C-3 in such a way that, as the top flange is removed from the main girder, the flexure from the pier is transferred to the connection by exerting the compression force on the top flange of the diaphragms, and pulling this flange on tension side up by the bond forces of reinforcing bars. Furthermore, since there is no stud installed on the lateral girders in specimen C-4, so unlike specimen C-2 and C-3, concrete strut 1, 3, and 5, will work independently without the composite action.

In specimen C-2 and C-3, the pier compression and tension will be distributed out laterally and carried by the concrete struts inside the connection. Along with the concrete struts, these forces will also be transferred partly via the lateral girders' struts to the main girder. In specimen C-4, however, rather than being concentrated on the main girder, only some part of pier's forces (concrete strut 1 in Fig.6.11) will be directly conveyed to the bottom flange of the main girder. Another part of the pier's forces will act on the top flange of the diaphragm situated laterally away from the main girder (concrete strut 3 and 5, and the pier's compression exerted on the top flange of diaphragm). Then these forces are transferred forth to the main girder via the lateral girders' strut 1 and 2 alone (it is noted that in this specimen there is no stud provided on the lateral girder so it is assumed to have no composite action with concrete). By this mechanism, the lateral girders will be put to the relatively full usage comparing to the

partial use of the lateral girders in specimen C-2 and C-3 of which lateral girders carry only the minor portion of pier's forces. In addition, the pier's compression will be effectively resisted by the connection concrete located away from the main girder. Similarly, on tension side, due to the steeper inclination of concrete strut 3 and 5, the bars located laterally away from the main girder will also be more fully utilized (comparing to the more inclined concrete strut 3, in specimen C-2).

Comparing to specimen C-3, the diaphragms in specimen C-4 behave in such a same manner as to strengthen the lateral girders. Therefore, the compressive and tensile forces from the pier will be carried more by the lateral girder. The major different between the force transfer mechanisms of these two specimens is that, in specimen C-3, the compressive force from the pier will be exerted on the top flange of the main girder and on the lateral girder via the studs, Fig.6.14. As well, on the tension side, the tensile force will be carried by the hold-down reaction from the top flange of the main girder and by the lateral girder via studs. Contrarily, in specimen C-4, as there is no stud on the lateral girder, the compressive force from the pier will be carried by the bearing area on the top flange of the diaphragms and partially by the bearing on the bottom flange of the main girder. On tension side, by the inclined concrete strut 3 and 5, the tensile force from pier will be transferred to the bottom face of the diaphragm's flange. In practice since the length of lateral girder's stud is relatively short compared to the width of the pier, thus the effective bearing area formed by studs to hold the pier's compressive and tensile forces will be small. This may eventually cause the stress to be rather concentrated at the vicinity of the main girder instead of spreading out laterally as in specimen C-4. Besides, at the topmost studs the force will become intense on the limited area, therefore the local deterioration could be potentially be generated. In specimen C-4, as the pier's compression is exerted on the diaphragm's top flange which has larger bearing area, therefore, the problem of stress concentration at the main girder as well as the local deterioration at the vicinity of the topmost studs can be eased.

The mechanisms established to resist the forces from the main girder are similar to those of specimen C-3 in where the diaphragms are installed, Fig.6.12. As well the force transfer mechanism in the main girder portion embedded inside the connection is the same as that exists in specimen C-2 and C-3, Fig.6.11.

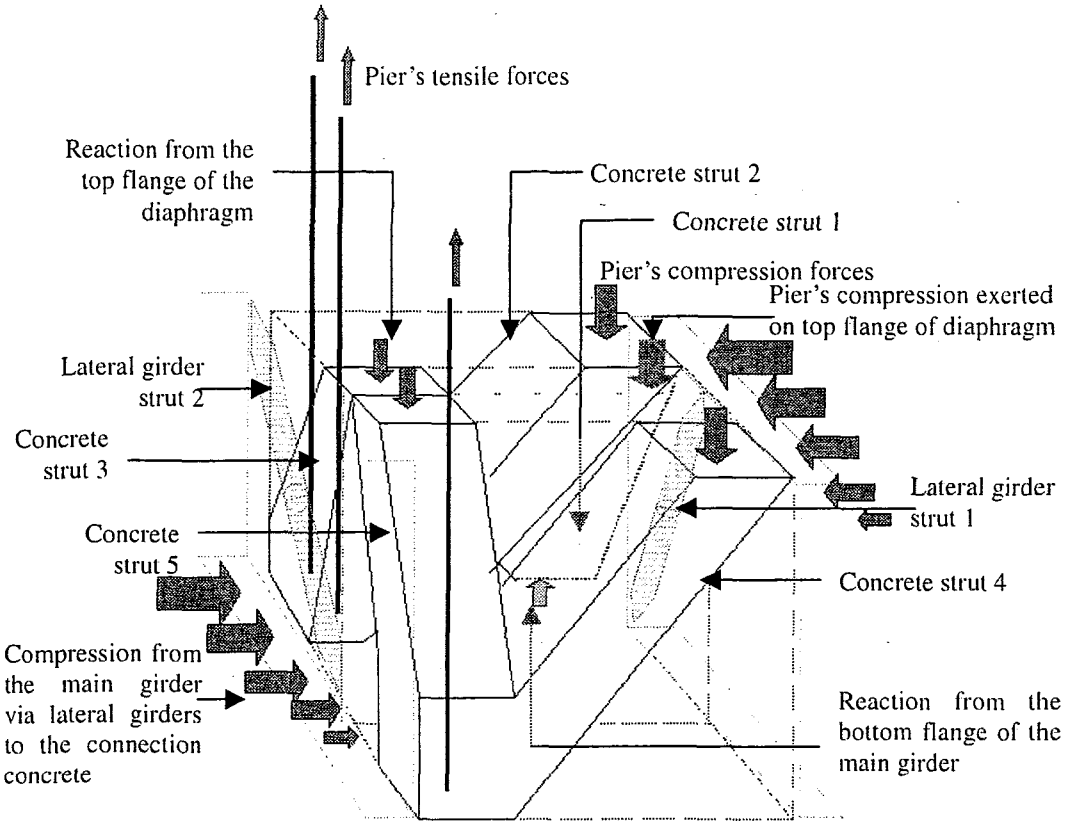

Fig.6.13 Force transfer mechanisms inside the connection concrete of specimen C-4. (established to resist the pier's forces)

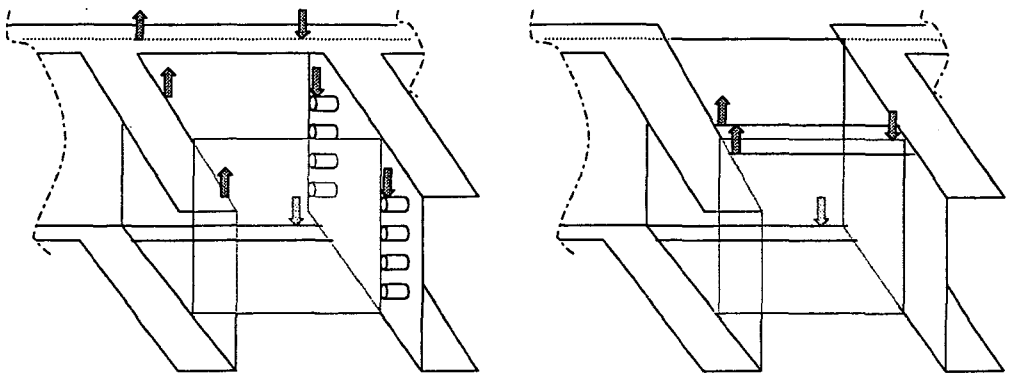

Fig.6.14 Difference between the paths of force transfer from pier to connection in specimen C-3 and C-4

6.6 Conclusions

With the information obtained from the analytical (to be explained in the next chapter) as well as from the experimental investigations, the force transfer mechanisms within the composite connections can be clarified. The accurate path of the force flow should rather be simulated in three-dimensional space than in two-dimensional as conventionally done in the behavioral simulation of the ordinary reinforced concrete beam-column joint.

The mechanisms of the force transfer within the composite connection is organized similarly to the strut-and-tie model, in where the compressive force is carried along the compressive strut and the tensile force is transferred via the tie. The mechanism inside the composite connection plays the important role in conveying the externally applied forces from pier to the main girder that will finally, equilibrated by the support reactions. In this chapter, the composite connection is considered as the main system, where forces applied by the pier and the main girder are thought of as the external forces. From the pier, the vertical compressive and tensile forces are transferred to the top of the connection, while from the main girder, the horizontal couple is conveyed to the side faces of the connection. The simulation of the force transfer mechanism is simplified by taking into account the mechanisms established by these two types of external forces separately. Then the mechanism is drawn out based on the results from both experimental and analytical investigations. The qualitative comparison between the mechanisms proposed for specimen C-1, C-2, C-3, and C-4, and the flow patterns of compressive strains inside the connections from finite element analysis will be given in the following chapter.

By the proposed force transfer mechanisms, the behavior of the specimens observed in the loading tests could be rationally explained. For instances, among all of the specimens tested, the control specimen, C-1, responded the load in the least stiff manner with the smallest ultimate load resisting capacity, the cause of this phenomenon is the disintegration of the connection part. The disintegration between connection concrete and the main girder is occurred potentially due to crushing of concrete located at the highly stressed zones like, at the bottom of strut 1 and at the top of strut 3 in Fig.6.5. The direction of crack propagations recorded during the test (Appendix A), are also correlated with the direction of compressive struts 1, 2, and 3 in the same figure.

By adding in the lateral girders (specimen C-2), this excessive connection rotation could be overcome. The connection could withstand the load until the yielding of reinforcing bar took place. This is due to that the lateral girders strut 1 and 2, share the load from concrete strut 1, and 3, Fig.6.8. The use-to-be highly stressed zones of concrete in specimen C-1 are relaxed, therefore preventing the concrete from crushing. Furthermore, the lateral girder can more effectively distribute the main girder forces to the outer concrete. This, again, helps reduce the stress concentration problem.

When the lateral girders on compression and tension sides were connected to each other with diaphragms (specimen C-3), the better-distributed force transfer from the pier into lateral direction to the connection could be achieved. It was because the strengthened lateral girders increased the rotational stiffness of the connection (Fig.6.11), The pier's forces which is applied on the top of the connect, will be encountered not only by additional lateral girder's strut 1, 2, 3, and 4, but also it will be reacted by the plate-shearing behavior of the diaphragms. In chapter 4, Fig.4.9, the plot of vertical strains on the diaphragm of specimen C-3 obtained from the experiment are shown, the shearing behavior of the diaphragm could be seen in the plots. The plate has the compressive strain coming down form top-right to bottom-left corner. While along the opposite diagonal direction, the plate exhibits the vertical tensile strain. These two observations, in combination, can be interpreted as the shearing behavior of the diaphragm.

With the additional diaphragms' flanges and partially removed main girder's flange, specimen C-4 could also distribute the pier force more uniformly into the lateral direction. Especially on compression side, the relocation of the compression baring area caused the force from pier well distributed onto the connection, thus, reduced the concentration of stress at the vicinity of the main girder and the potential local deterioration that might occur around the studs.

From the research in this phase, it could be concluded that the proposed force transfer mechanisms of the composite connection help improve the understanding about the behavior of the composite connections. In addition, they also suggest the alternative way the designer could think about the force flows within the composite connection, it will, therefore, leads to a more liberated and effective design.

CHAPTER 7

Strut-and-Tie Model for Composite Connection

7.1 Introduction

In case of slender reinforced concrete structure, the flow of compressive stresses is uniformed throughout the entire length and it is referred to as the "Beam" region [7]. To predict the behavior of the beam region, it is simple and sufficiently accurate to apply the sectional method. However, for the connection region, it regularly carries several forces exerted by the conjoining members. The sophisticated combination of forces make the stresses within this region non-uniform, therefore, the accustom sectional method is not applicable. This region is called "Disturbed" region [7].

To predict the behavior of or to design the disturb regions, so far there have been many methods proposed, for example, the strut-and-tie model and the linear or nonlinear finite element method. Even though the FEM recently is widely applied for these purposes, it is still cost and time consuming. According to these disadvantageous, the simpler design and analytical method is being called for, and most of the time the strut-and-tie model is selected as the capable alternative.

In this chapter, the three-dimensional strut-and-tie model is adopted to simulate the behavior of the composite connections. The force transfer mechanisms proposed in Chapter 6 is utilized in parallel to determine the geometry of the struts and ties in the connection. The results of the calculations are then checked against the experimental results and used to verify the applicability of the force transfer mechanism. The basic concept of the strut-and-tie model will be given in the following section. Then the specific application of strut-and-tie model for composite connection will be described in section 7.3. Section 7.4 will show the examples of application of strut-and-tie model for predicting behavior of four composite connection specimens tested in this research course following by the verification of strut-and-tie analysis in section 7.5. Consequently, some design considerations and suggestions are given section 7.6. Finally,

the conclusions along with the recommendations for further development of the model will be provided in section 7.7.

7.2 Strut-and-Tie Model

One of the important advantages of using strut-and-tie model to predict the behavior of such a disturbed region like the composite connection is the flow of forces can be easily visualized. Another advantage of using this kind of model to idealize the flow of forces is that the influences of both shear and moment are accounted for simultaneously and directly in the design. However, along with these advantages, there also exist some disadvantages in utilizing such a method as stated by the Joint ASCE-ACI Committee 445, in the Structural Forum, "Recent Approaches to Shear Design of Structural Concrete" [7] that, "the visualization of the flow of compressive stresses in the concrete allows the development of a truss idealization consisting of compressive struts and the tension ties necessary for equilibrium. It takes experience to determine the most efficient strut-and-tie models for different situation. For any given situation, many strut-and-tie models are possible and no unique solution exists". Their statement about strut-and-tie model has pointed out that there's still no fixed general guideline for designing the structural components in the disturbed region with this method. The inappropriate design with this method will finally price in the large amount of reinforcement or the extra weight due to the excessive size of concrete member.

Dated back to 1984, some researchers had tried to setup the standard for the design of disturbed region with strut-and-tie model. Schlaich and Shafer [65] and Schlaich et al. (1987) [66] have suggested that a strut-and-tie model be chosen after carrying out an elastic analysis. They suggested choosing the geometry of the truss model such that the angles of the compression diagonals are within ± 15° of the angle of the resultant of the compressive stresses obtained form an elastic analysis. Although this approach can give some guidance in choosing the geometry of the strut-and-tie model, it must be recognized that considerable redistribution of stresses takes place after cracking if the member is ductile.

It is obvious that the most important and difficult task in using strut-and-tie model is to conceive the reasonably effective strut-and-tie system within the member. After getting the idealized model, the next step is to dimension the concrete struts and reinforcing bar

ties. Then the system must be solved for the internal forces of each strut and tie. Eventually, it has to be ensured by the designer that concrete strut will not be crushed or the brittle diagonal crack will not be occurred. It is because these are the dangerous mode of failure.

In Chapter 6, force transfer mechanisms inside the composite connection, the directions of the flow of forces are determined. The layouts of those mechanisms are drawn correspondingly to the experimental results; for example, the crack pattern and the strains measured on the connection components. To make sure that the flow paths suggested in Chapter 6 are suitable, following in this section, the proposed mechanisms will be qualitatively compared with the directions of the principal compressive stresses in concrete which are obtained from the finite element analyses. Fig.7.1 (a), (b), (c), and (d) summarize the major force transfer mechanisms in specimen C-1, C-2, C-3, and C-4, respectively.

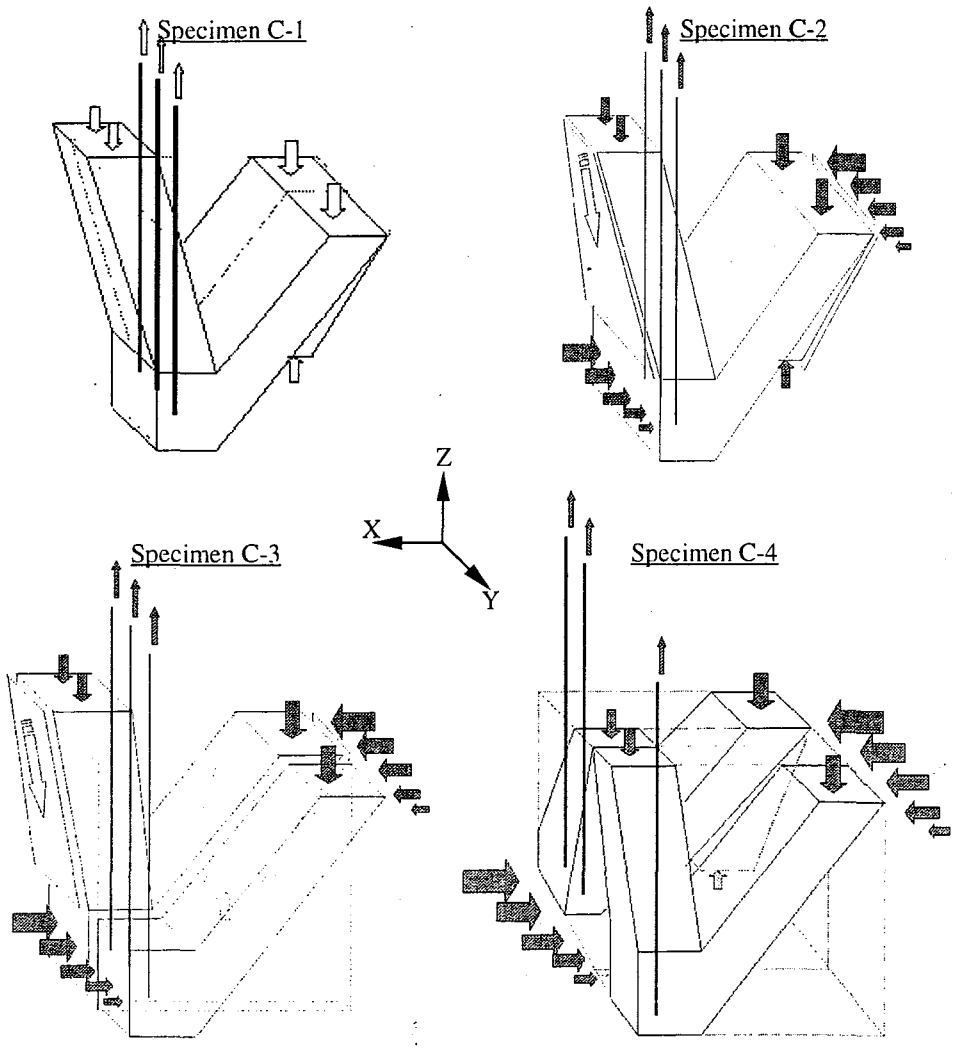

Fig.7.1 Force transfer mechanisms in specimen C-1, C-2, C-3, and C-4

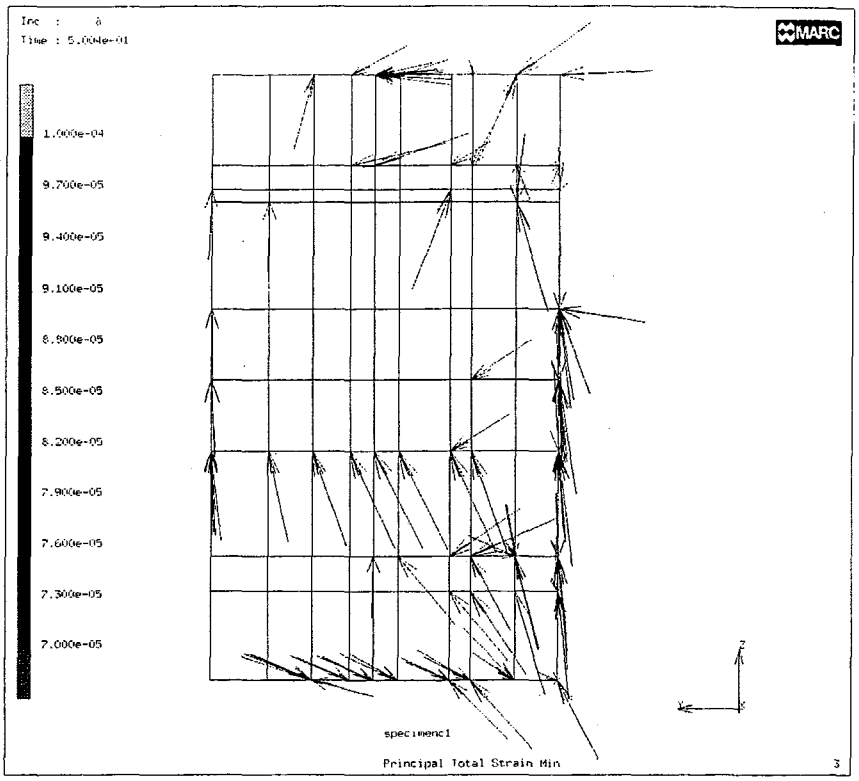

Fig.7.2 (a) Principal compressive stresses in concrete (on compression face, C-1)

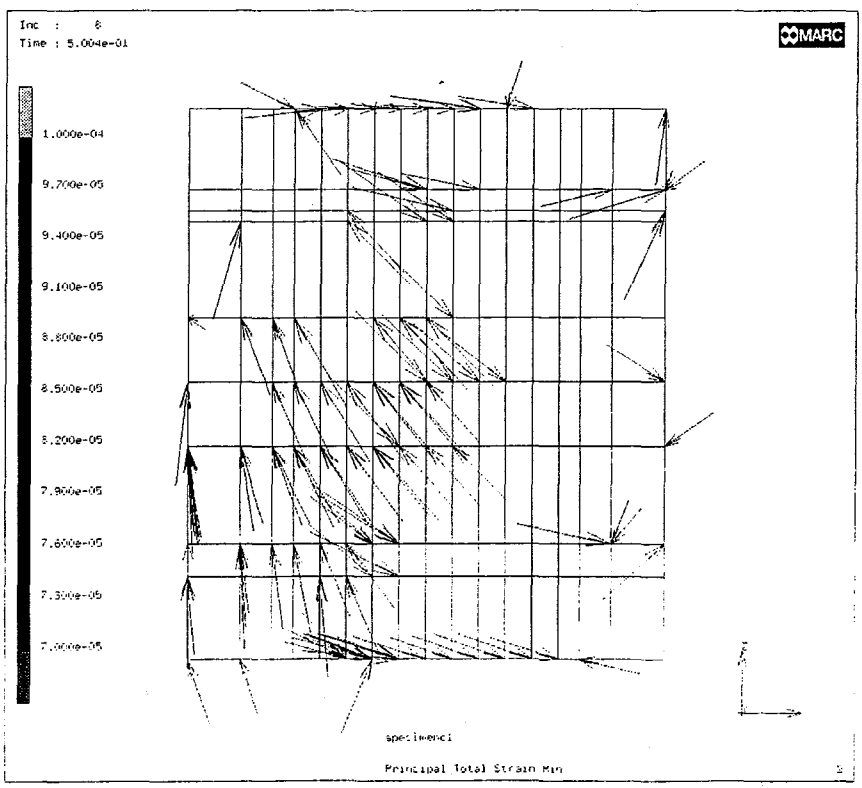

Fig.7.2 (b) Principal compressive stresses in concrete (on middle face, C-1)

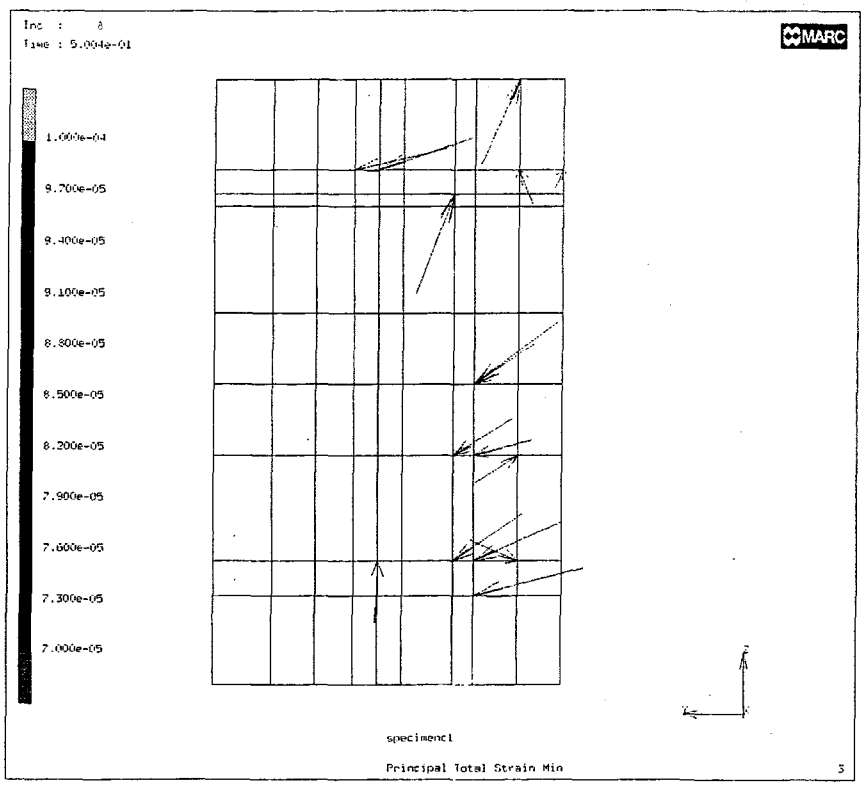

Fig.7.2 (c) Principal compressive stresses in concrete (on tension face, C-1)

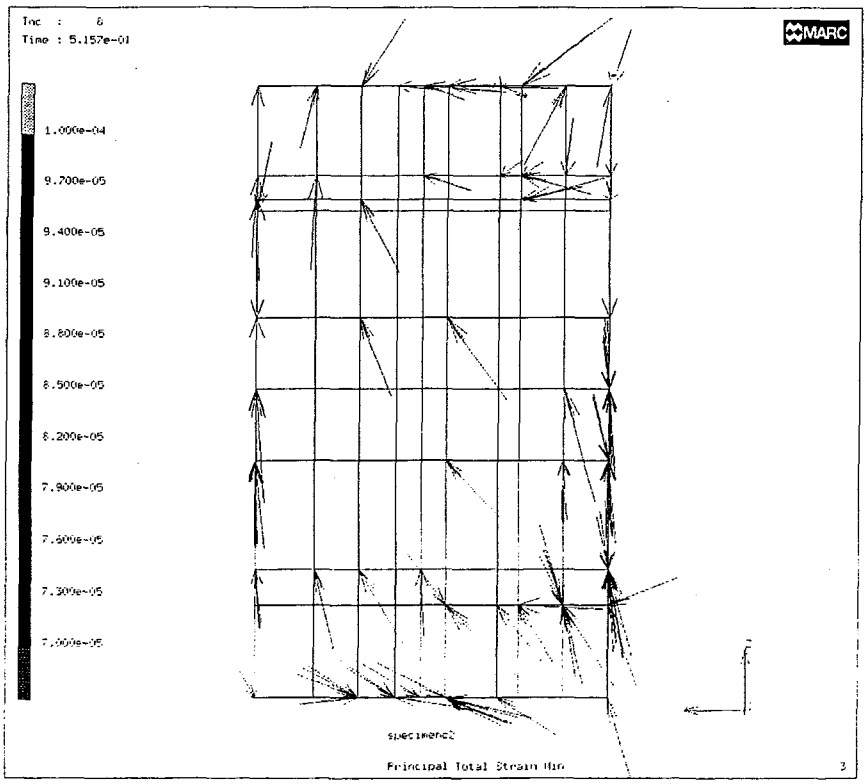

Fig.7.3 (a) Principal compressive stresses in concrete (on compression face, C-2)

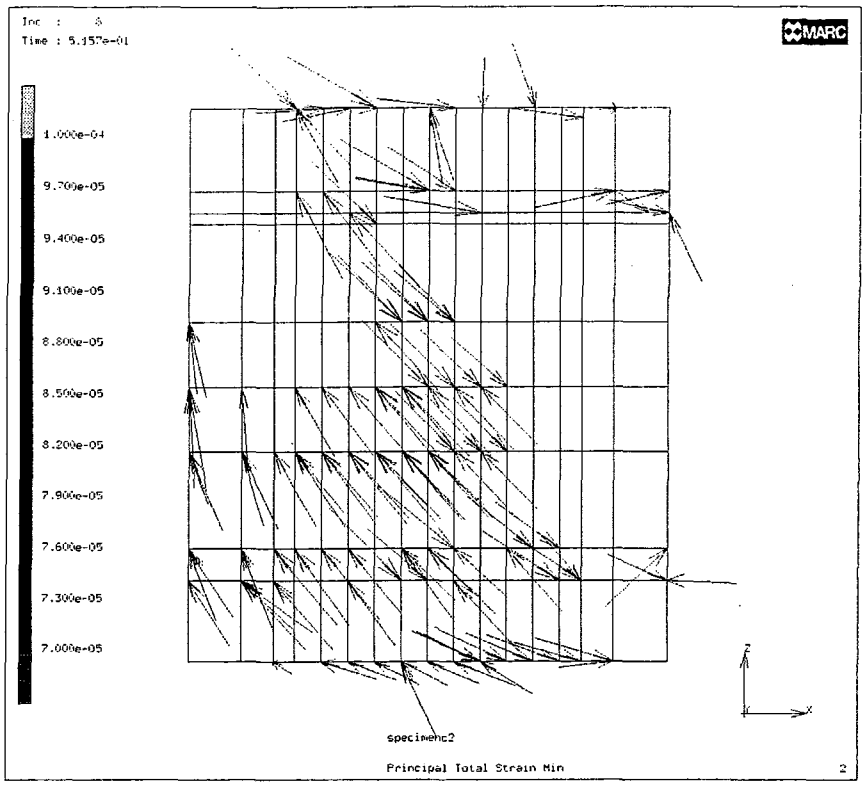

Fig.7.3 (b) Principal compressive stresses in concrete (on middle face, C-2)

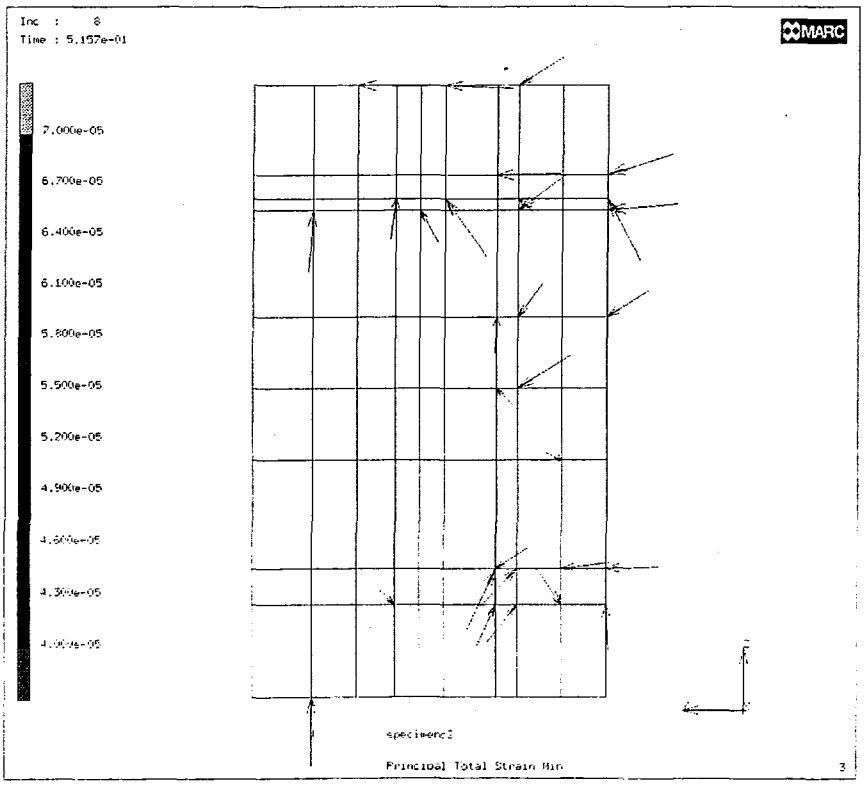

Fig.7.3 (c) Principal compressive stresses in concrete (on tension face, C-2)

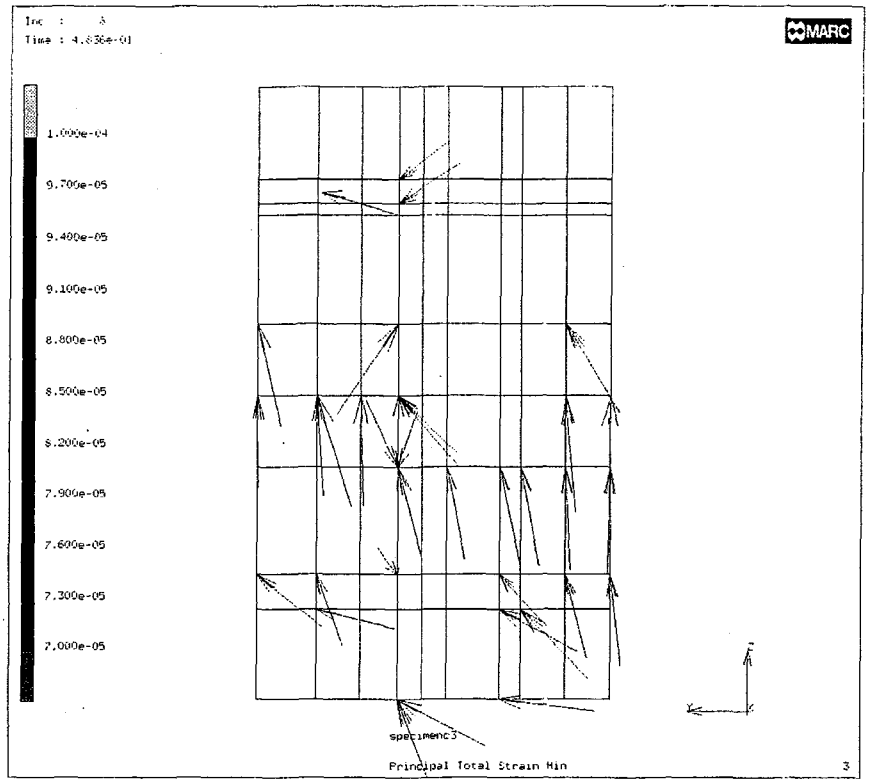

Fig.7.4 (a) Principal compressive stresses in concrete (on compression face, C-3)

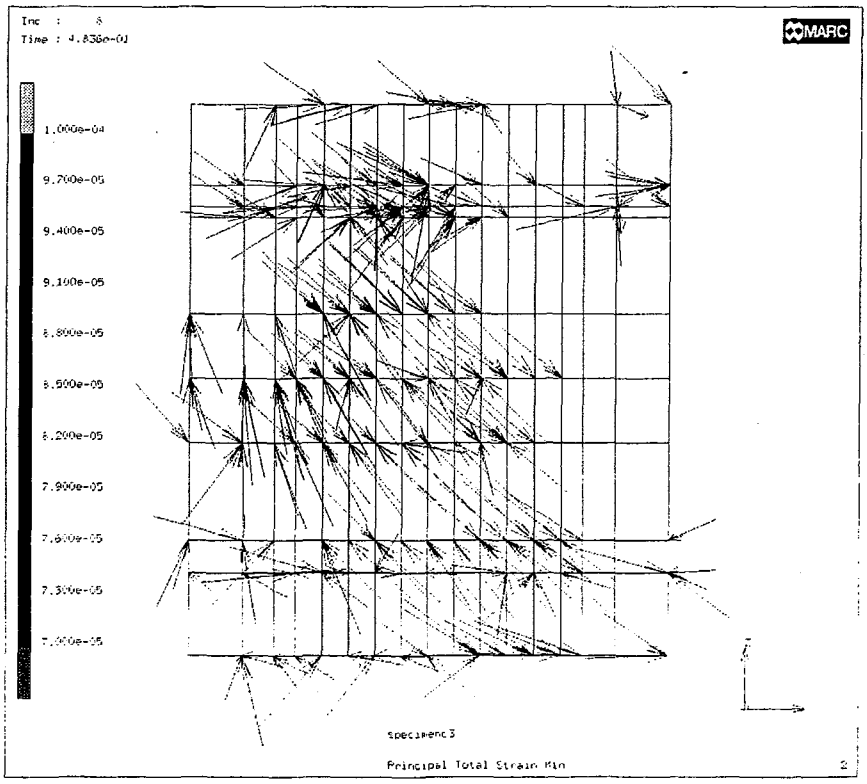

Fig.7.4 (b) Principal compressive stresses in concrete (on middle face, C-3)

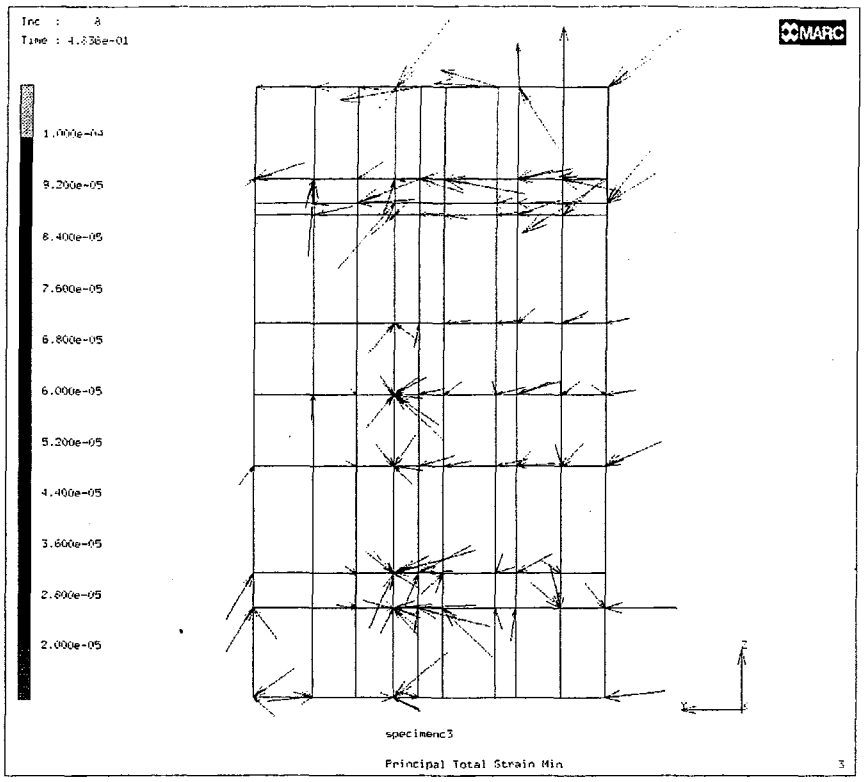

Fig.7.4 (c) Principal compressive stresses in concrete (on tension face, C-3)

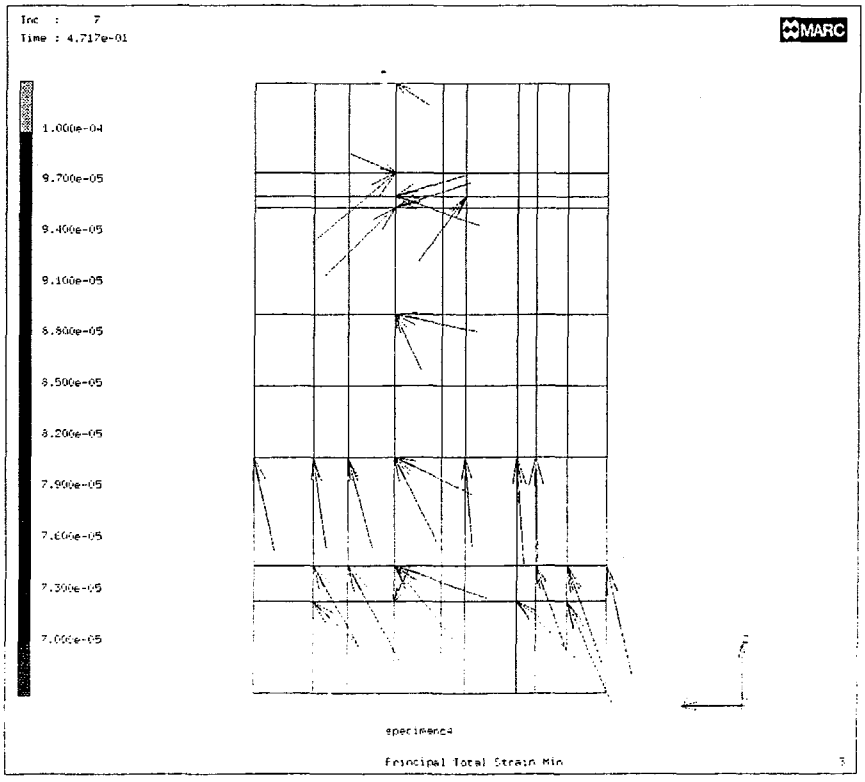

Fig.7.5 (a) Principal compressive stresses in concrete (on compression face, C-4)

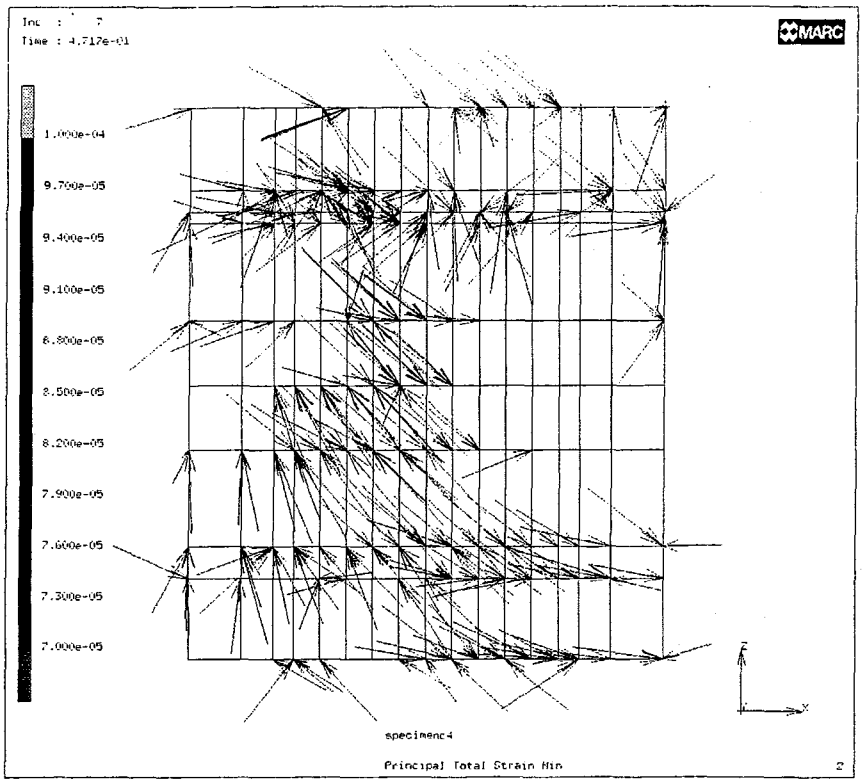

Fig.7.5 (a) Principal compressive stresses in concrete (on middle face, C-4)

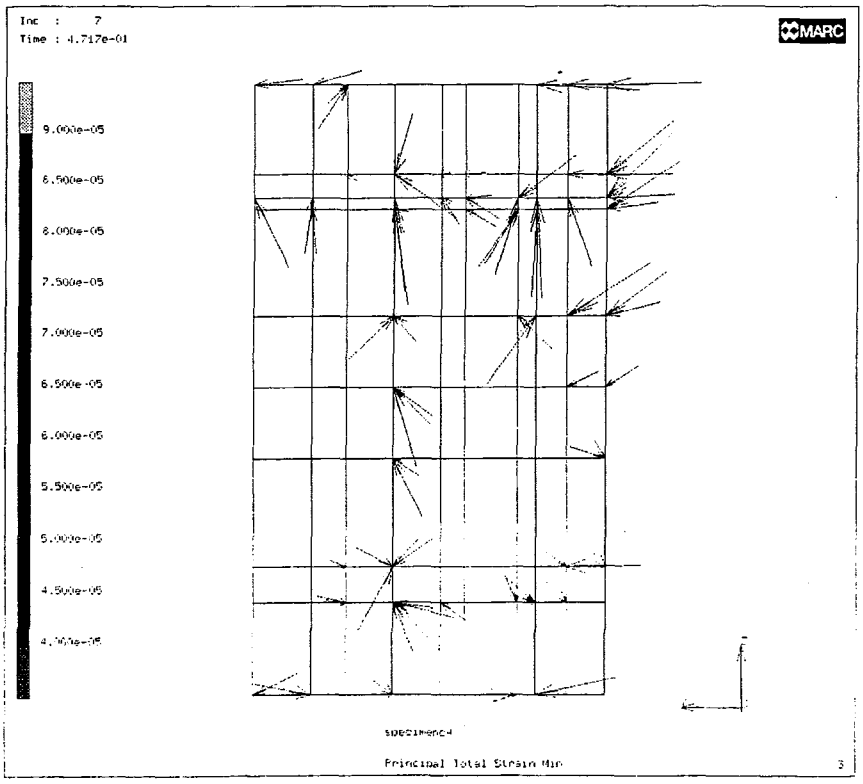

Fig.7.5 (a) Principal compressive stresses in concrete (on tension face, C-4)

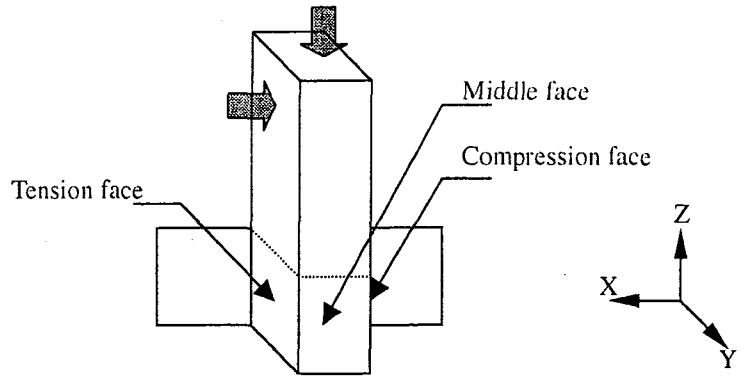

Fig.7.6 Definition of compression, middle, and tension face of the model

Shown in Fig.7.2 (a) (b) (c), 7.3 (a) (b) (c), 7.4 (a) (b) (c), and 7.5 (a) (b) (c) are the principal compressive strains of concrete on compression face, middle face, and tension face of specimen C-1, C-2, C-3, and C-4, respectively. The definitions of compression, middle, and tension faces are referenced in Fig.7.6.

On the compression face of specimen C-1 and C-2, it can be seen that the principal compressive strains originate from the bottom flange of the main girder and flow in the direction pointing to the top-left corner. This is similar to the direction of concrete strut 1 in the proposed mechanisms. For specimen C-3 and C-4, the principal strains seem to be originated at the bottom flange of the main girder as well, but they rather point up more vertically than those in specimen C-1 and C-2. These struts are not extended beyond the position of the diaphragm. In the proposed mechanisms, beyond the position of diaphragm, there presents only a lateral girder's strut in specimen C-3 and none in specimen C-4.

For the principal compressive strain on middle face of all specimens, it could be observed that the strain flows in the direction from bottom-right corner on tension side to the top–left corner on compression side. These analytical observations prove the validity of inclined strut 2 in specimen C-1 and C-2, as well as strut 2 and 4 in specimen C-3 and C-4.

On the tension face, the principal compressive strains are less prominent than on the other faces. However, they still show the trend that is correlative with the direction of strut in the proposed mechanisms. In specimen C-1 and C-2, the principal compressive stresses flow in the direction from top-right corner (under the flange of the main girder) pointing down to the bottom left corner. This flow path is identical to the direction of

concrete strut 3 in both specimens. In specimen C-3, although the flow path is more horizontal, the approximated direction of these principal compressive strains is from the top-right corner (main girder's flange) aiming to the lower part of the diaphragm. In the mechanism proposed for this specimen, concrete strut 3 represents the direction of this flow. Beyond the position of the diaphragm, nearly vertical stresses can be observed. This is because the bond force of reinforcing bar is held straightforwardly by the lateral girder via studs. In the mechanism this force is resisted by the lateral girder's strut 2. For specimen C-4, on the tension face, it can be seen that the principal strains of concrete located adjacent to the diaphragm are flowing from the bottom to both faces of the diaphragm, this phenomenon can be well simulated by concrete strut 3 and 5 in the connection of this specimen.

From this qualitative comparison, it could be deduced that the proposed force transfer mechanisms in all specimens can simulate the flow paths of force within the composite connection with a fair accuracy. Having proved the validity of the mechanisms, in the next step, the dimensions of all struts and ties in the model will be determined. Then the internal forces of struts and ties will be calculated. The calculation procedures are explained in the following section.

7.3 Calculation Procedures

In order to analyze the behavior of the steel girder-reinforced concrete pier composite connection with the strut-and-tie model, the calculation procedures are proposed in this research phase. The calculation steps are described as follows.

7.3.1 Sketch the flow of forces within the composite connection and locate the nodal zones which are the regions bounded by struts, ties, or bearing areas. The rough idea about the force transfer paths can be obtained by deducing from the experimental observations or from the results of elastic analysis as explained earlier.

In this study, the system being considered is the composite connection consisting of reinforced concrete and steel girder components. The compressive struts and tension ties are formed within this part of structure to represent the compression and tension flow paths, respectively. The loads applied onto the connection by the pier and the reactions exerted by the steel girders to the system are considered as the external forces.

The distribution of forces from the pier to onto the connection is computed by assuming that these forces are transferred via the inclined strut system in the pier. With this assumption the non-uniform distribution of pier's compression and shear can be determined.

For the forces exerted by the main girder onto the system, it can be computed based on the sectional method. This group of main girder's forces is composed of flexural forces (compressive and tensile forces) and shear forces. In case of the composite connection having lateral girders, the distribution of forces from the main girder through the lateral girder to the composite connection is simulated by the same method as for the distribution of pier's forces, Fig.6.3. The flexural components are applied to the side faces of the connection and formed the mechanism within the connection, whereas, the shear is assumed to be transferred via the main girder itself into the connection, and this component will be balanced by the vertical forces in the mechanism established by the pier load.

A group of strut and tie elements formed to resist the pier loads is additive to the group of strut and tie elements formed to resist the external forces exerted by the steel girder. The combination will represent the total effect of the external forces to the system.

7.3.2 Determine the geometry of the truss members and nodal zones.

In the calculation of internal forces within the connection, the struts and ties elements are simulated by the truss elements joining each other at the nodal zones. To solve for the internal forces in these truss members, the location of nodes must be determined. In case that the entire truss system is statically indeterminate, the dimension and stiffness of the truss member must also be presumably defined.

The positions of nodal zones are actually pre-determined while the mechanisms are formed. For the dimensions of the truss members, they are dependent on the sizes of the compressive bearing zones (the area on the connection which bear the pier's and main girder's forces), and the anchorage details of the tension ties. The sizes of the compression bearing zones are determined when the external forces from pier and main girder are calculated. For the internal nodal zone which is consisted of reinforcement ties and the connection concrete struts, the width of this zone is assumed as follows,

Internal nodal zone width = 2 x (Ravg) + (space between 2 lines of longitudinal

reinforcements) (7.1)

where,

Ravg = radius of the bond effective area, determined in Chapter 3

$$= \frac{1}{3}\sqrt{\frac{fy}{ft}} \text{ x (radius of reinforcing bar)}$$

7.3.3 Determine the forces in the truss members.

Since the truss systems for composite connections are usually statically indeterminate, the stiffness of the truss members has to be presumably given in order to solve for the unknown forces (forces in reinforcing bars and unknown reactions) and the internal forces of the truss members. Concrete compressive struts are assumed to have a linear modulus of elasticity as well as the reinforcing bar ties. Since the truss system in composite connection has quite complicated layout, to calculate the magnitude of unknown forces in the system finite element analysis program is applied.

7.3.4 Check for the failure that might have occurred in the truss member.

After solving for all of the unknown forces, for the design purpose, the failure of members should be checked. Those potential failure modes which should be cautious of are, the yielding of reinforcing bar, diagonal cracking in the concrete strut, and the crushing of the concrete strut. Yielding of the reinforcing bar and crushing of concrete could be checked by comparing the calculated stresses in members with the actual material properties. For the diagonal failure in concrete strut, the method proposed by Siao [70] is adopted. In his calculation, a single compressive force is replaced by two equivalent struts, Fc, radiating at dispersion angle 2:1 from the original direction of strut, Fig.7.7. These two struts are held together at midheight of the beam by tension force, Ft. Thus the tensile force within the strut can be calculated. The stress generated by this tension component in the strut can be calculated by dividing the tensile force with the area normal to the direction of force.

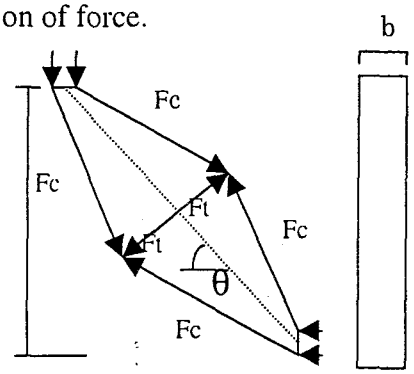

Fig.7.7 Distribution of forces in strut-and-tie model proposed by Siao [70]

With the calculation procedures proposed in this section, the behaviors of composite connection specimen C-1, C-2, C-3, and C-4 are simulated. The method of application and the results of prediction by strut-and-tie model will be shown in the following section.

7.4 Application of Strut-and-Tie Model for Predicting Behavior of Composite Connections

The behavior at the ultimate state of the composite connection specimen C-1, C-2, C-3, and C-4 are simulated by using the proposed strut-and-tie model in this section. The calculations are preformed to check the validity of the force transfer mechanisms whether they are capable in representing the real flow paths of forces. Also, this calculation will prove the applicability of the strut-and-tie calculation procedures, as the solution will be compared with the results obtained in the experiments.

7.4.1 Specimen C-1

In Fig.7.8 (a) and (b), the force transfer mechanism in the connection of specimen C-1 is represented by the combination of strut and tie components.

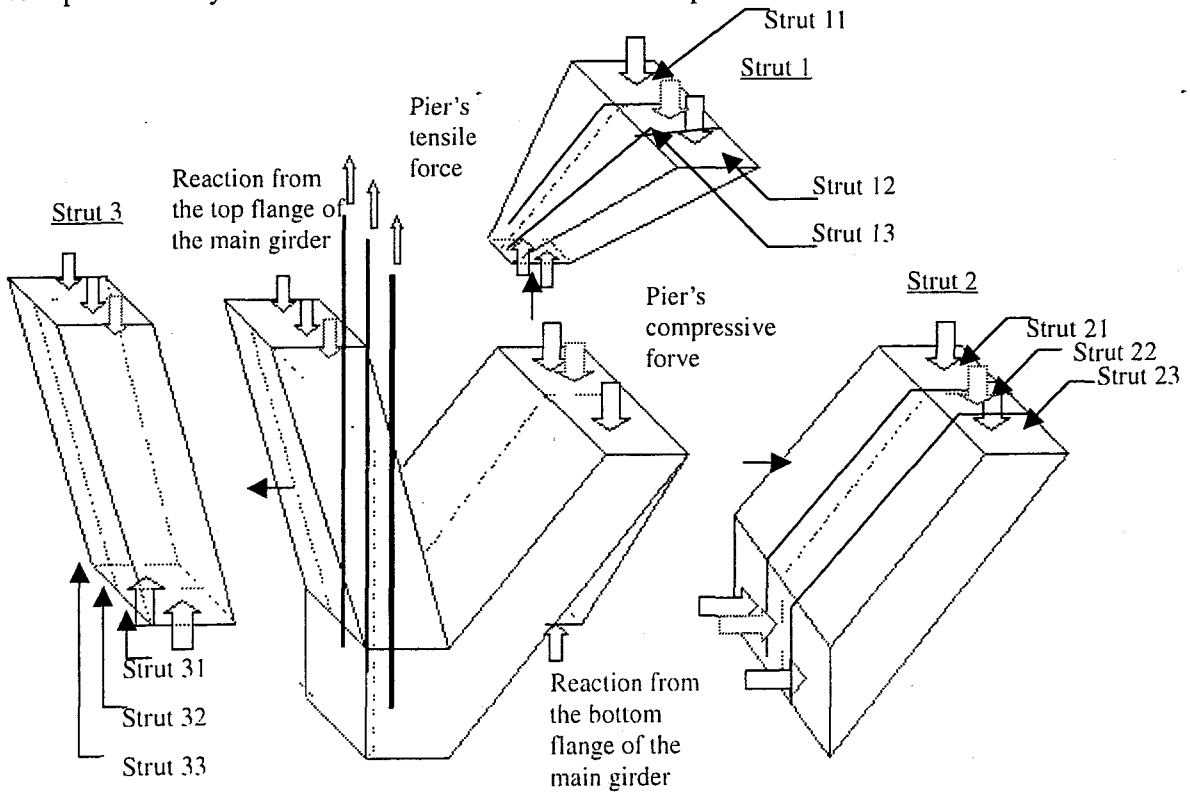

(a) Force transfer mechanisms inside the connection concrete of specimen C-1. (established to resist the pier's forces)

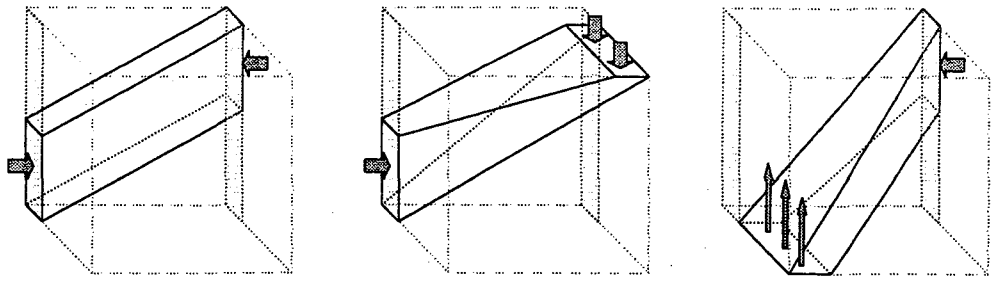

(a) Distributions of the main girder's compressions (left & right) to the connection concrete bounded by flanges and stiffeners (Strut 4)

(b) Distributions of the main girder's compression (left) to the connection concrete (Strut 5)

(c) Distributions of the main girder's compression (right) to the connection concrete (Strut 6)

(b) Force transfer mechanisms inside the connection concrete of specimen C-1. (established to resist the main girder's forces)

Fig.7.8 Force transfer mechanisms in the composite connection of specimen C-1

Onto the system, there are pier's and main girder's forces applied. Those forces are represented by thick arrows in Fig.7.8 (a) and (b). By the sectional method the total flexural forces and shear of the pier and the main girder could simply be determined. The distribution of these forces on particular strut could be calculated as suggested in section 7.1. The distribution pattern is shown in Fig.7.9. In the calculation, it is assumed that all struts that carry these forces to the connection have the same stiffness. The sectional areas of all struts are similar, except that of the middle strut which has the relatively larger area. These compression areas can be obtained from the sectional computation. The larger area of the middle strut reflects the effect of studs on the top flange of the main girder which help hold the concrete tighter and make the compression bearing area in this zone become larger. With the known inclination of the strut from the geometry of specimen, the forces transferred via each strut can then be calculated. From the calculation it is found that the amount of compressive forces conveyed from the loading jack to the top of the connection, are almost identical in all struts. This is due to the inclinations of struts which are very small (the most inclined one forms only 6.28° angle to the vertical axis). Shear force distribution on the top of the connection can also be calculated by the same method. The external forces applied to the system are as illustrated in Fig.7.10 (a)

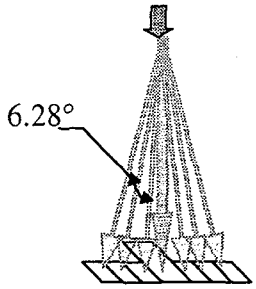

Fig.7.9 Distribution pattern of compressive pier's force on the top surface of connection

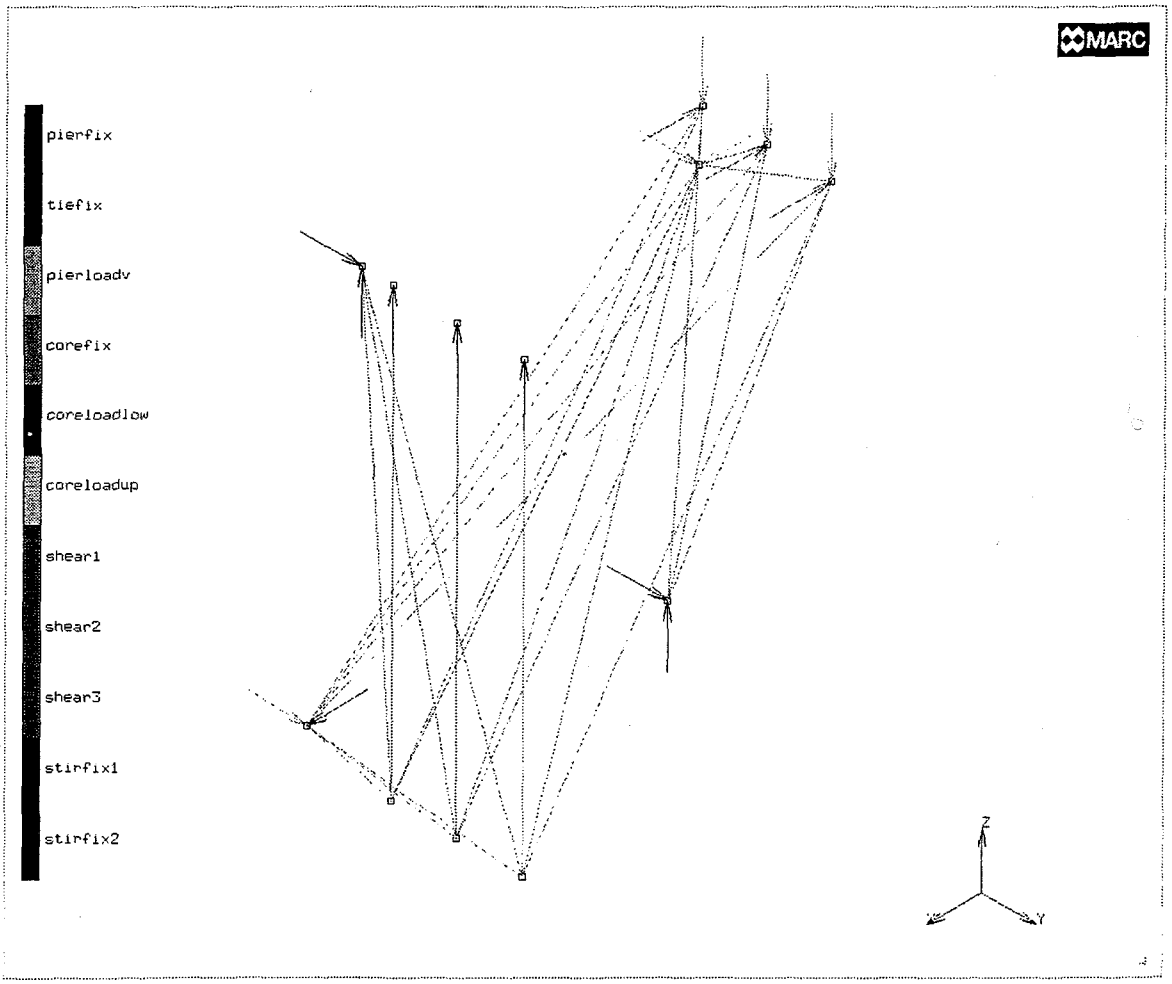

Fig.7.10 (a) Truss analogy representing force transfer mechanism in specimen C-1 (with indications of externally applied forces)

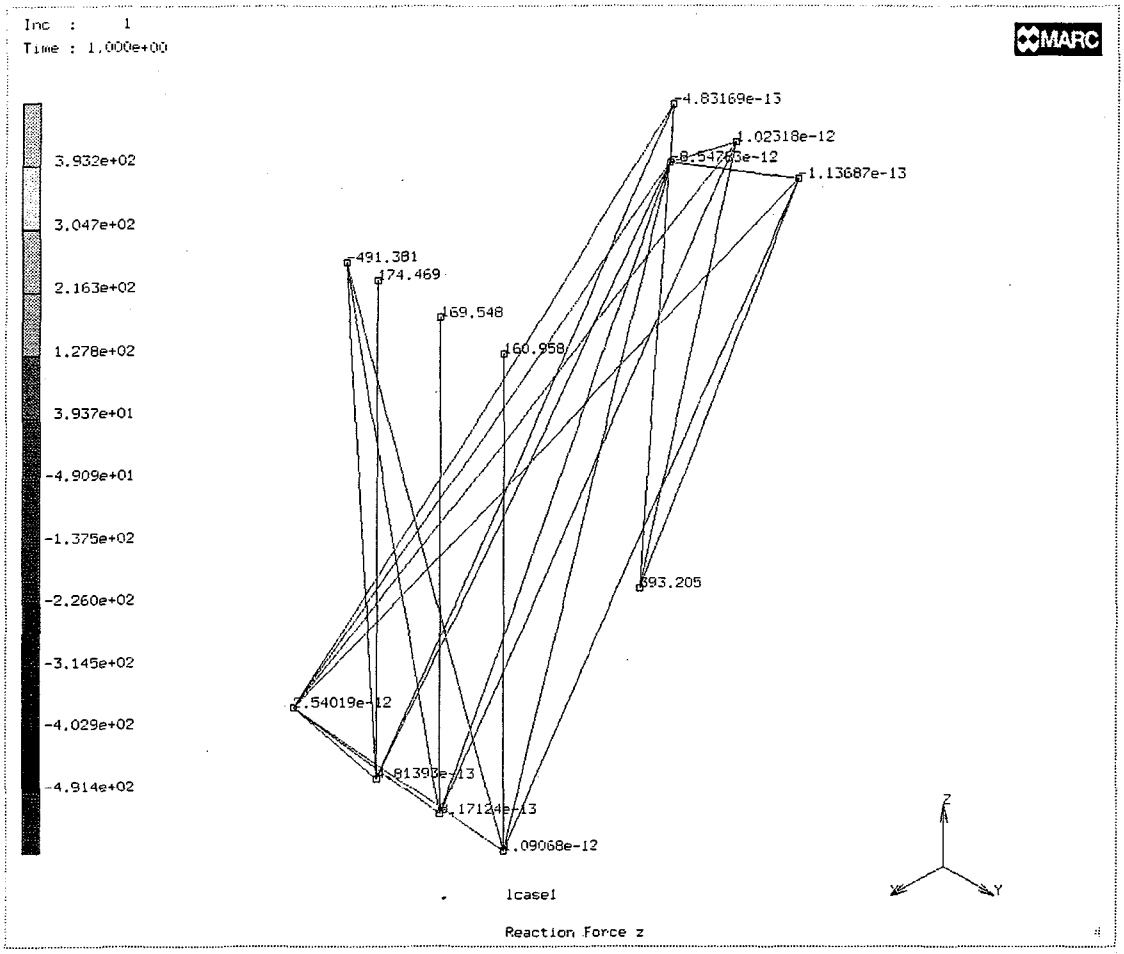

Fig.7.10 (b) Truss analogy representing force transfer mechanism in specimen C-1 (with reaction forces at nodes)

After getting to know the force transfer mechanism or the flow paths of forces, based on the mechanism, the truss system is constructed for analyzing the connection (as suggested in 7.2). In the system, the truss elements are used to represent both of the concrete struts and reinforcing bar ties as shown in Fig.7.10. The directions of trusses in this figure are conformed to the axis of the struts and ties in the mechanism. Strut 1 to 6 in Fig.7.8 are subdivided into three equal portions, for example, strut 1 is equally separated to be strut 11, 12, and 13. This is to simplify the analysis, as the external forces applied on these particular sub-portions are not uniformed such as the pier's shear of which magnitudes are decreased in the direction away from the main girder. Dividing the strut into 3 parts will also make the placement of reinforcing bars which are arranged in three lateral layer convenient, although they are still in the approximated

positions. Then the cross-sectional area of each strut is determined. Since the cross-sectional area of almost all struts are not uniform (struts are not prismatic), the average cross-sectional area of the strut which is calculated by taking the average value of the areas at both ends of struts, is used. The dimensions of struts 1 to 6 in this specimen are as shown in Fig.7.11. It should be noted that the area to be used must be the area of the plane that is perpendicular to the force axis or the axis of strut.

In addition, some other assumptions used in modeling the struts are (see Fig.7.11), for concrete strut series 1 (strut11, 12, and 13), its width at both top and bottom end is assumed to be equal to the depth of compression area in the pier. In the same manner, the width of the concrete strut series 3 (31, 32, and 33) is assumed to be equal to the width of the bond-effective zone constantly from the bottom to the top ends. For the concrete strut series 2, the top end is assumed to be of the same width as the compressive bearing area in the pier above the connection, while at the bottom end, it presumably has the bond-effective zone's width. The bearing areas of strut 4 on the left and right-hand sides are assumed to be equal to the depth of the compressive zone in the main girder. For strut 5, the top end is of the same width as the compression area in the pier, while the bottom end has the same depth as of the compression zone in the main girder. Lastly, strut 6, its depth at the top end is assumed to be equal to the depth of compression zone in the main girder and at the bottom end, this strut is assumed to have the same width similar to the width of bond-effective area. In addition to the major struts mentioned, in the truss analogy, to realistically simulate the effect external forces (Fig.7.10), at the bottom-left and top-right portions of the system the compressive forces from the main girder are assumed to be spread out to the nearby bearing areas, namely, lower end nodes of ties for the bottom-left force, and concrete bearing area node for the top-right force. The dimensions of these struts are determined by averaging the areas at both ends.

It is noted that, in order to determine the size of compressive area in the pier section, in this calculation, the depth of compression area at the ultimate state is used (horizontal load = 210 kN, vertical load = 135 kN).

Then following the procedure in section 7.3.4, this truss system of specimen C-1 is analyzed. In the study, the finite element analysis program, MARC, was used to carry out the analytical work since the system was statically indeterminate to the high degree and it would take time to solve by hand.

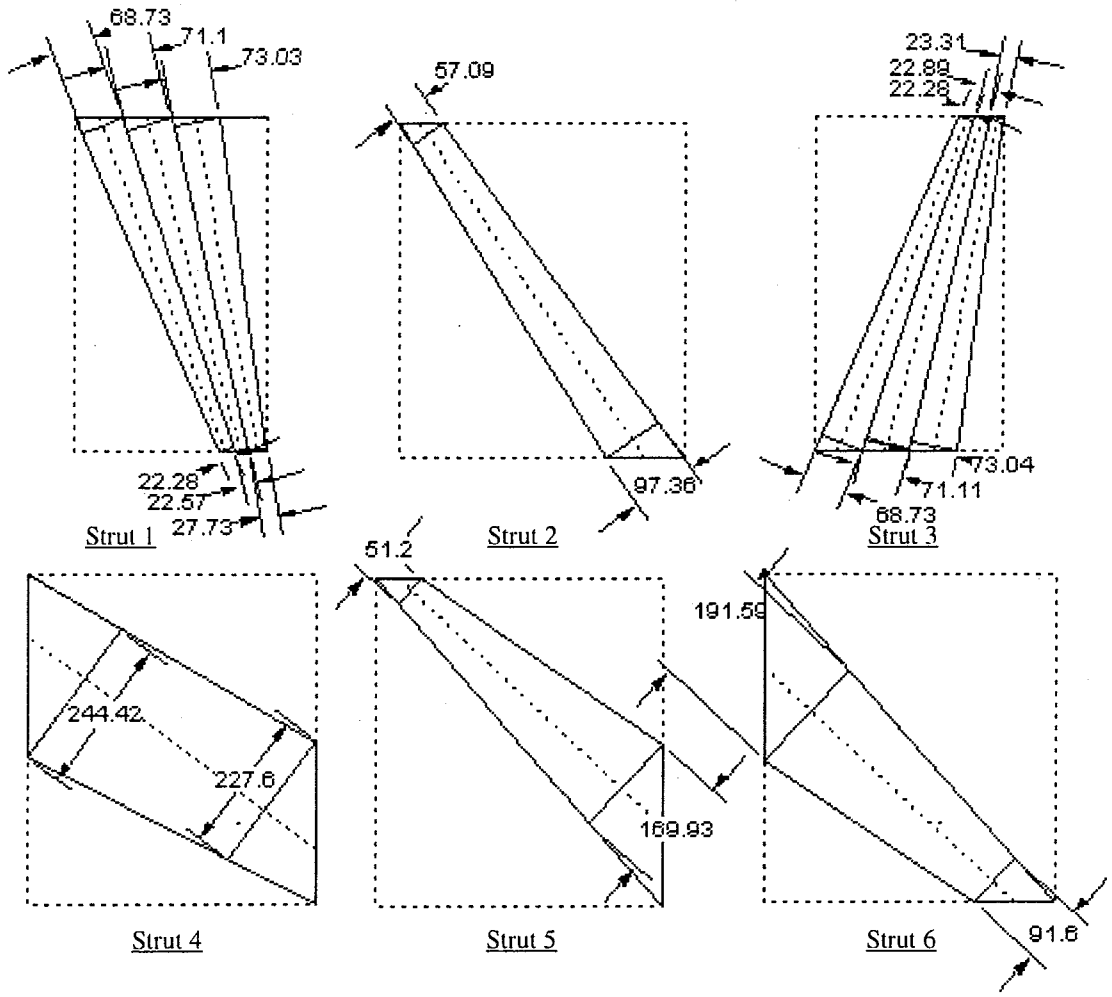

Fig.7.11 Dimensions of the struts used for calculating the cross-sectional areas.

7.4.2 Specimen C-2

In the analysis of specimen C-2, the calculation procedures described in section 7.1 to 7.3 are also followed. The major difference between this specimen and specimen C-1 is that in this specimen, the lateral girders were added to encase the connection concrete. The force transfer mechanisms previously derived for this specimen in Chapter 6 is as shown in Fig.7.12.

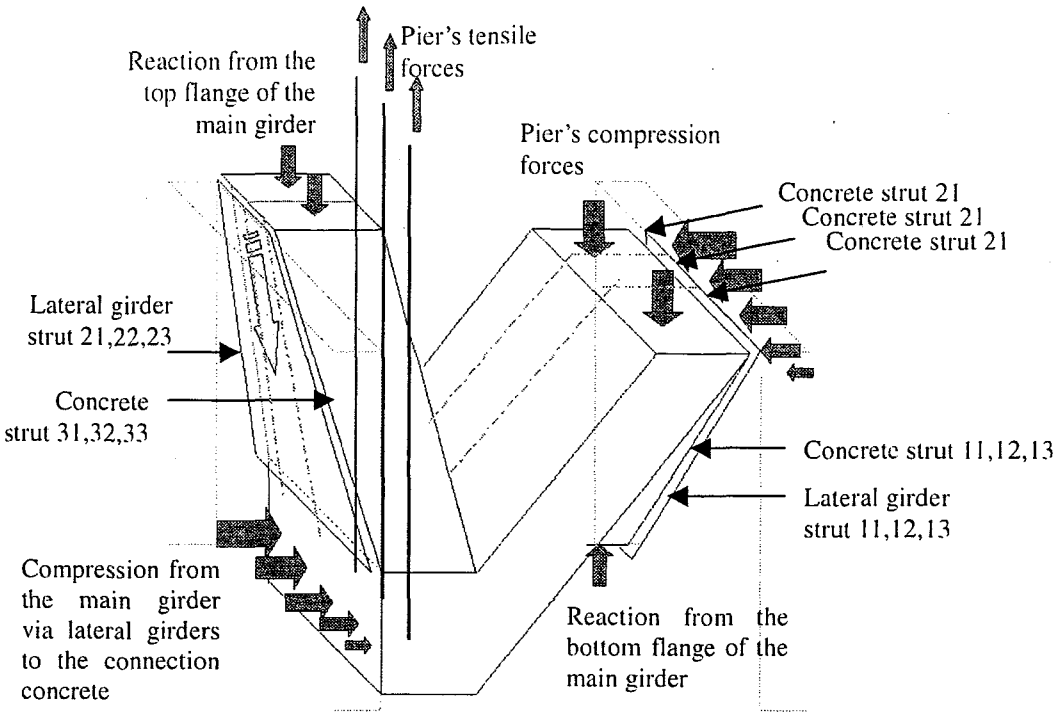

Fig.7.12(a) Force transfer mechanisms in connection concrete of specimen C-2.
(established to resist pier's forces)

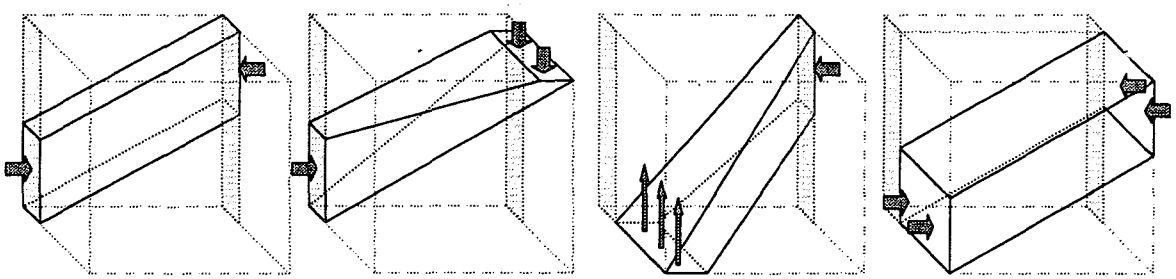

(a) Distributions of the main girder's compressions (left & right) to the connection concrete bounded by flanges and stiffeners

(b) Distributions of the main girder's compression (left) to the connection concrete

(c) Distributions of the main girder's compression (right) to the connection

(d) Distributions of the main girder's via lateral girders to the connection concrete

Fig.7.12 (b) Force transfer mechanisms inside connection concrete of specimen C-2.
(established to resist main girder's forces)

Again, to simplify the analysis with strut-and-tie model, all of struts are divided into 3 portions where portion no.1 in every strut stands for the strut located nearest to the main girder (e.g., 11, 21, 31), and portion no.3 is for the outmost strut (e.g., 13, 23, 33). Moreover, to further reduce the complexity of the model, it is assumed that the studs on

the lateral girder will rigidly hold the concrete with the lateral girder and the full composite action will be resulted. Based on this assumption, the transformed section method is applied to determine the cross-sectional areas of the lateral girder strut series 1 and 2 (11, 12, 13, 21, 22, and 23). These transformed areas of steel are then added to the cross-sectional areas of concrete struts in series 1 and 3, respectively.

The other dimensions of struts are determined by imposing the same assumptions as used for specimen C-1. Another change that makes this model different from the strut-and-tie model of specimen C-1 is the addition of compressive forces distributed from the flanges of the main girder. In specimen C-1, the compressive forces in the flanges are transferred straightforwardly to the portion of flanges located inside the connection without any distribution to the surrounding concrete, only the compressive forces from the web will be spread out laterally to the connection concrete. The externally applied forces in this system are illustrated in Fig.7.13 (a).

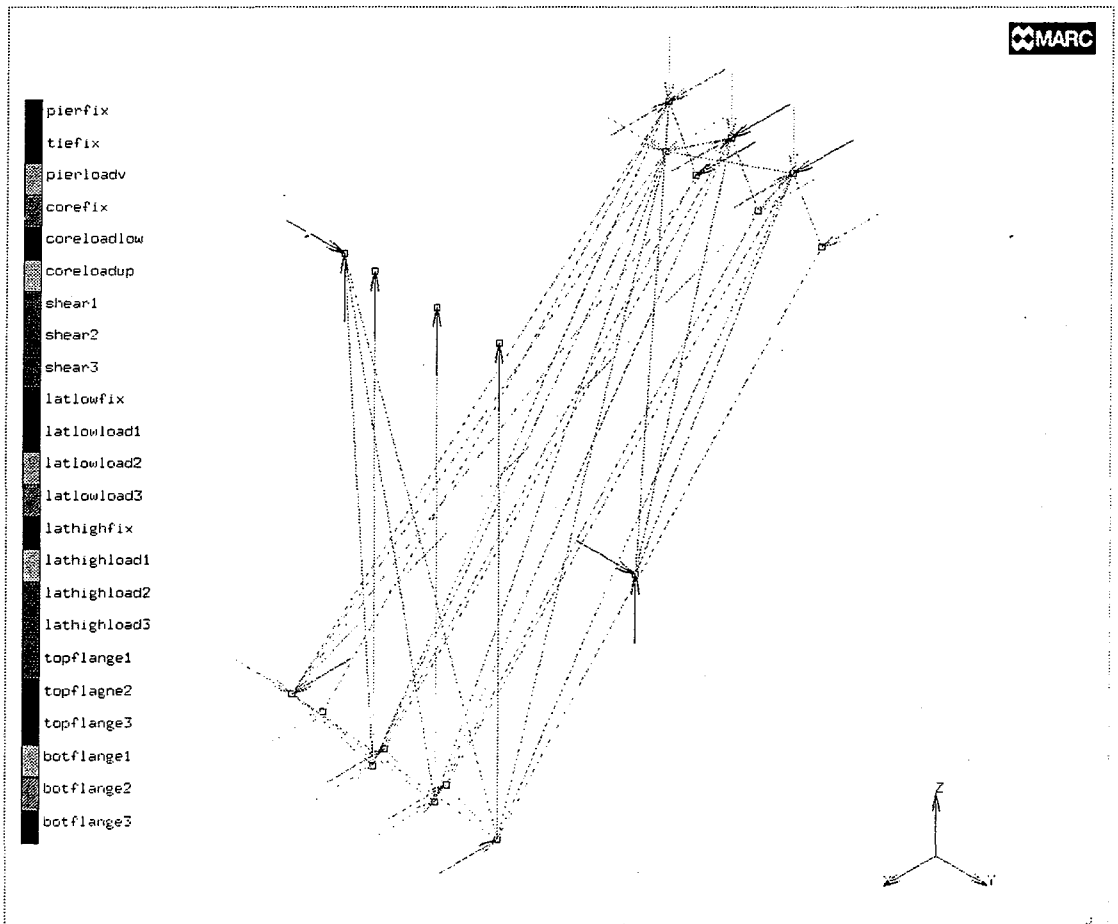

Fig.7.13 (a) Truss analogy representing the force transfer mechanism in specimen C-2 (with the indications of externally applied forces)

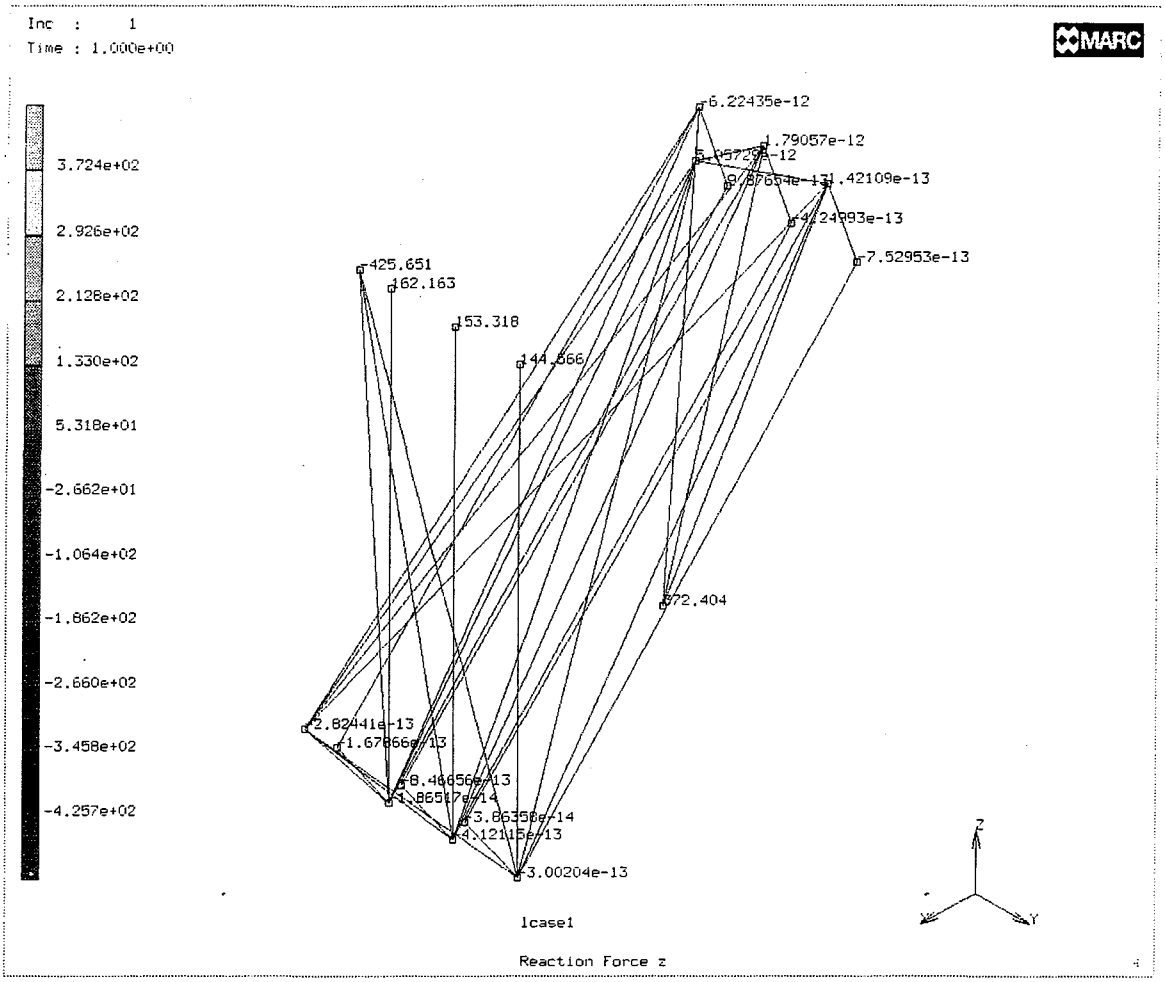

Fig.7.13 (b) Truss analogy representing force transfer mechanism in specimen C-2 (with reaction forces at nodes)

Fig.7.13(b) shows the complete truss analogy of composite connection type C-2. The analysis of the truss system is carried out by using finite element analysis program. This analysis is the one-step type that is to find the equilibrium of the system only at the ultimate state (horizontal load = 210 kN). After reaching the equilibrium, the forces in all strut and tie members are be determined.

7.4.3 Specimen C-3

By following the same calculation procedures as those for specimen C-1, and C-2, the strut-and-tie model for specimen C-3 is analyzed. All of the external forces applied to the system are calculated at the ultimate state. As the ultimate load is given, all bearing

areas in the connection where the compressive forces are transferred to/from can be predetermined. The strut-and-tie model of this specimen is shown in Fig.7.14. This system of strut-and-tie is different from that of specimen C-2 in such a way that there is an additional group of trusses formed in a rectangular shape with the diagonal components joining the corner nodes together. This group of trusses represents the diaphragm that links the lateral girder on tension and compression side together. One of the diagonal trusses running from top-right to bottom-left behaves like a compression strut. It helps the surrounding concrete strut (concrete strut 22 and 23) carry the compressive force from the top-right to the bottom-left corners of the connection. The other will resist the tensile forces, thus, behaves like the tie member. The dimensions of the diaphragm struts and ties are determined based on the assumption that if the failure occurs in the diaphragm, all of the struts and ties representing this plate will be yielded simultaneously. The contribution of diaphragm in resisting force, to the surrounding concrete is taken into account by providing the diaphragm's truss system overlapping on the concrete strut 23 and 33. The behavior of this plate can be confirmed by the strain distribution on the diaphragm measured in the experiment. The other point that should be noted here is that the lateral distribution of compressive force from the web of the main girder will not arrive the concrete located beyond the diaphragm. It is because the diaphragm will block this effect out, Fig. 7.14 (bb), and (bc).

After the flow directions of forces within the connection have been made clear, the next step is to determine the dimensions of the struts and ties. The cross-sectional areas of struts and ties can be computed in a normal way as done previously for specimen C-1 and C-2. Similar to the specimen C-2, the cross-sectional areas of concrete strut series 1 and 3 will be combined with the cross-sectional areas of the lateral girder strut 1 and 3 by the transformed section method. As well, the inclined concrete strut 22, and 23 will take the strengthening effect from the diaphragm. Therefore, the cross-sectional area of these concrete struts will be increased by the transformed area of the diaphragm's compressive strut.

Having defined the external forces (identical to the external forces applied to specimen C-2), represented all struts and ties with the truss members with the predetermined cross-sectional dimensions, and joined them to be a system, the consecutive step is to conduct the truss analysis. Finite element analysis program is used in the computation. Eventually, all unknown forces in the system are solved.

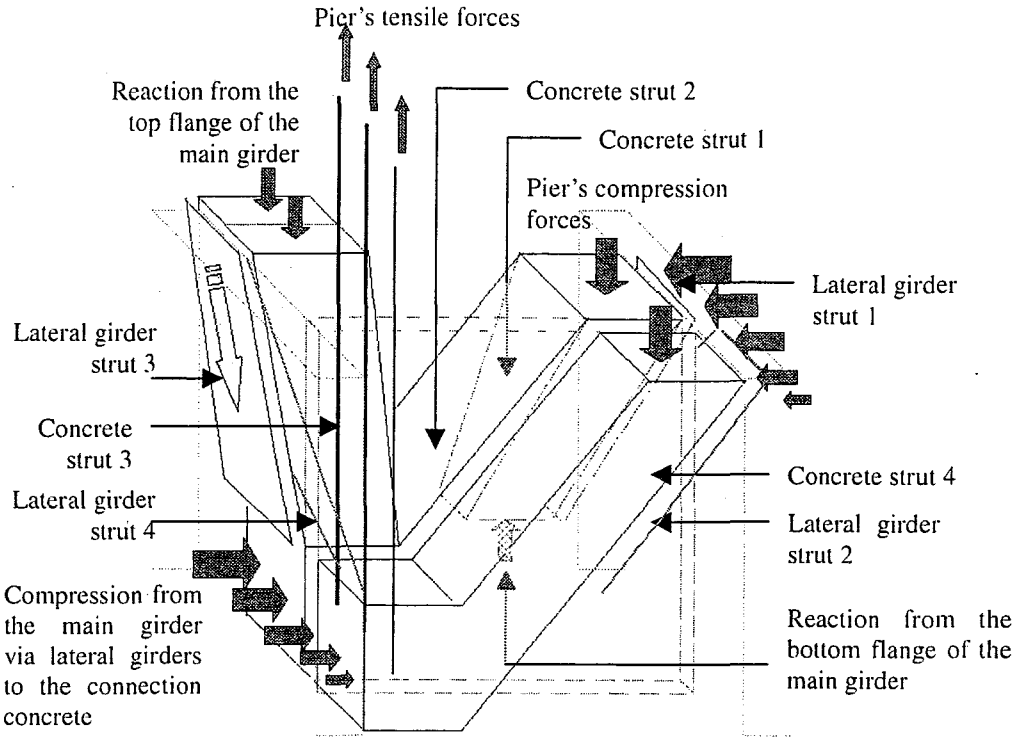

Fig.7.14 (a) Force transfer mechanisms inside the connection concrete of specimen C-3. (established to resist the pier's forces)

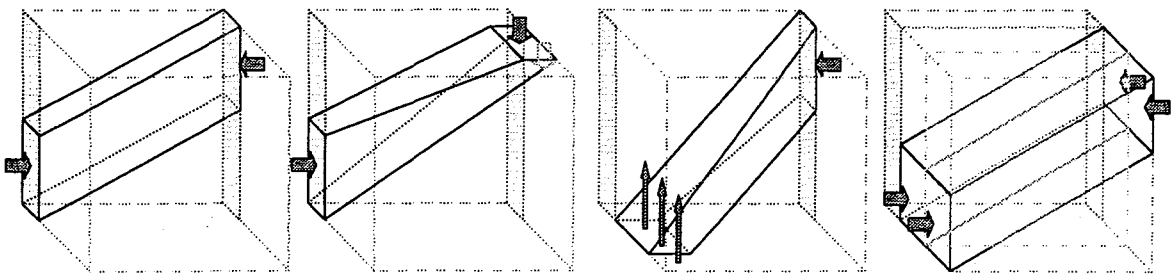

(a) Distributions of the main girder's compressions (left & right) to the connection concrete bounded by flanges and stiffeners

(b) Distributions of the main girder's compression (left) to the connection concrete

(c) Distributions of the main girder's compression (right) to the connection

(d) Distributions of the main girder's forces via lateral girders to the connection concrete

Fig7.14 (b) Force transfer mechanisms inside the connection concrete of specimen C-3. (established to resist the main girder's forces)

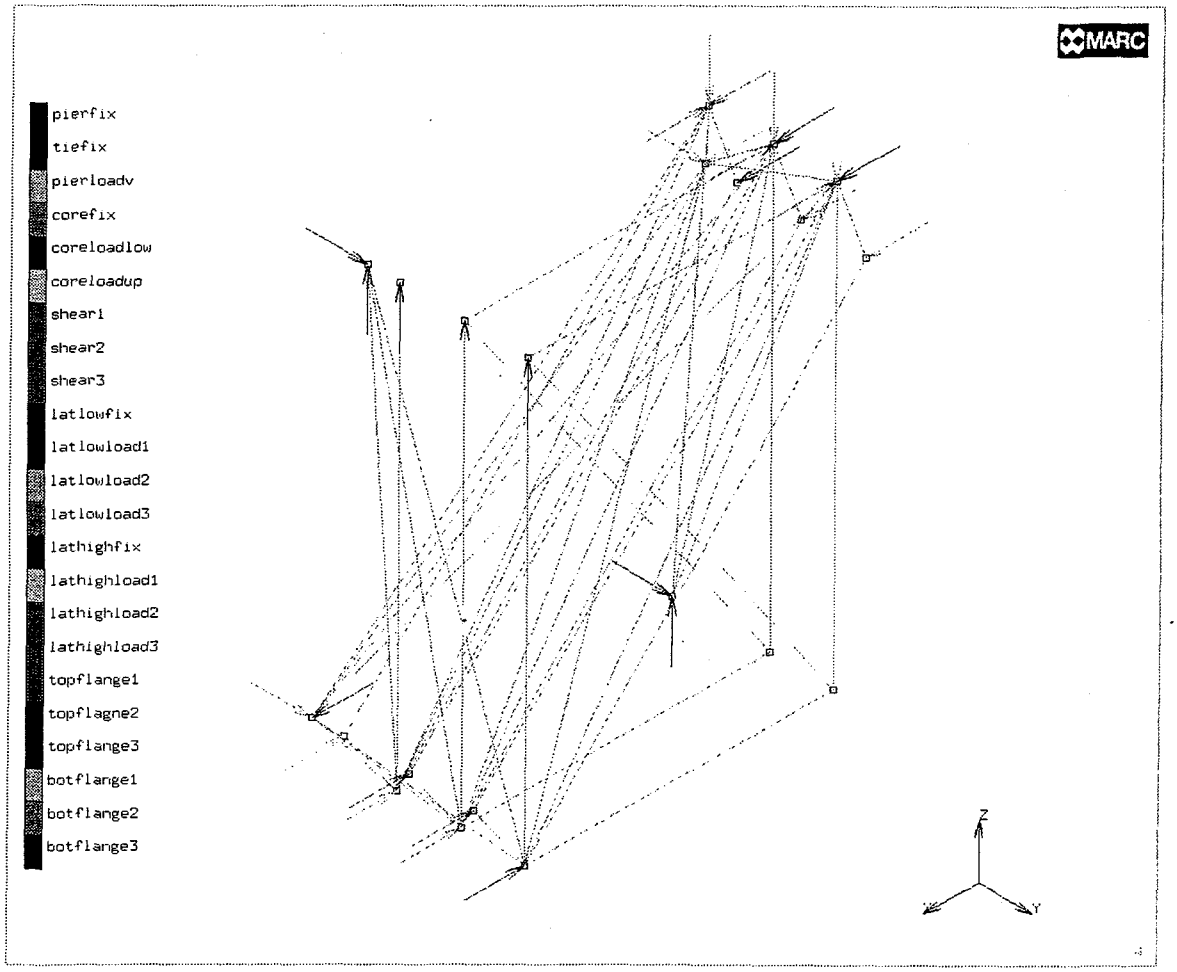

Fig.7.15 (a) Truss analogy representing the force transfer mechanism in specimen C-3 (with the indications of externally applied forces)

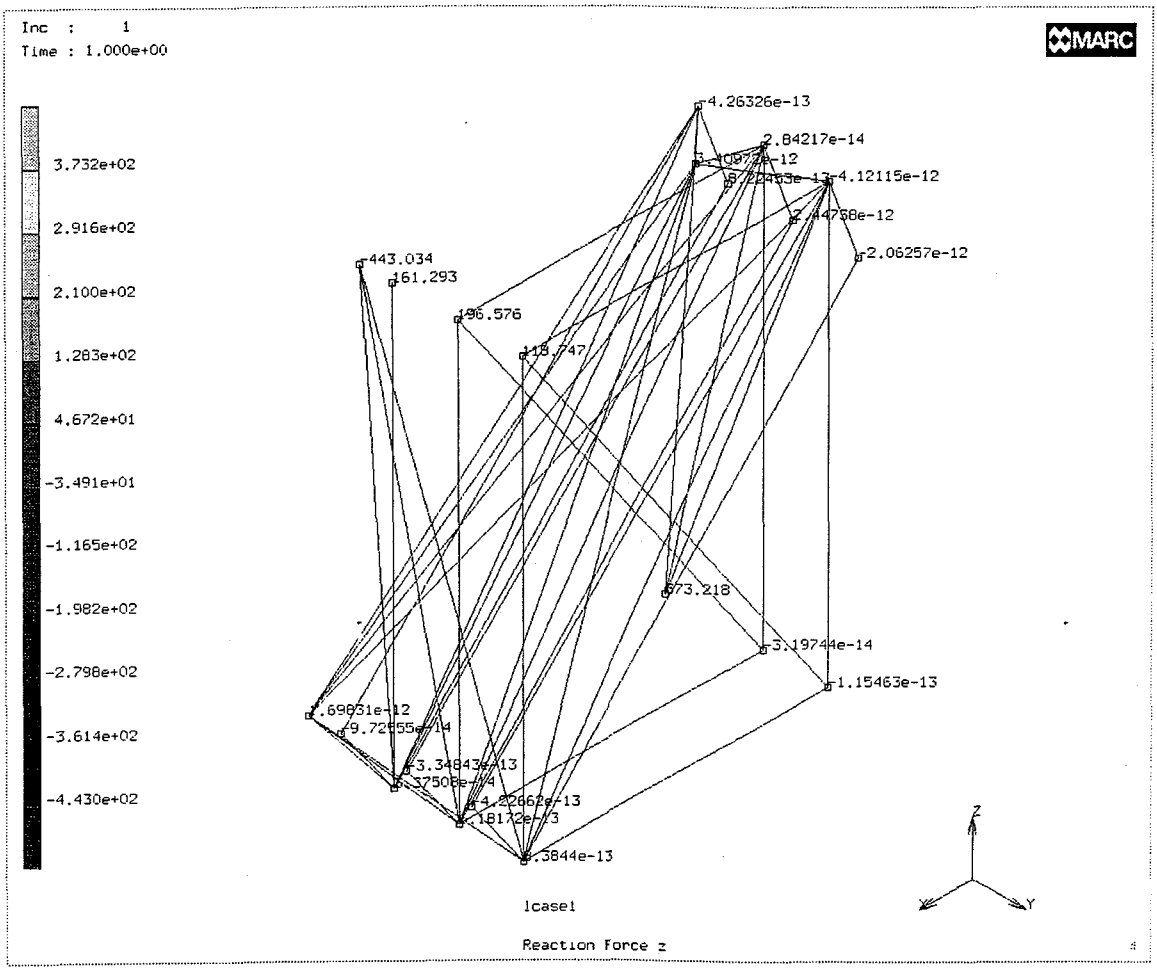

Fig.7.15 (b) Truss analogy representing the force transfer mechanism in specimen C-3 (with the reaction forces at nodes)

7.4.4 Specimen C-4

This type of composite connection is designed with the objective to laterally distribute the forces that usually concentrated at the vicinity of the main girder by adding the diaphragm with top flange, and removing the top flange of the main girder. In this specimen, there is no stud installed on the lateral girder as in case of specimen C-2, and C-3. The force transfer mechanism in this specimen is as shown in Fig. 7.16. Based on this mechanism the strut-and-tie model is constructed. The dimensions of all strut and tie members are pre-determined using the same method as that used for specimen C-1 C-2, and C-3.

In this specimen, since the stud does not exist on the lateral girder, the composite action with the adjacent concrete does not take place. Therefore, system of truss in this case consists of the additional lateral girder strut 1, 2, 3, and 4 that help transfer forces from the pier to the main girder, Fig.7.16. In addition, as included in specimen C-3, the rectangular-shaped truss system is added to the connection's truss system as to simulate the effect of the diaphragm.

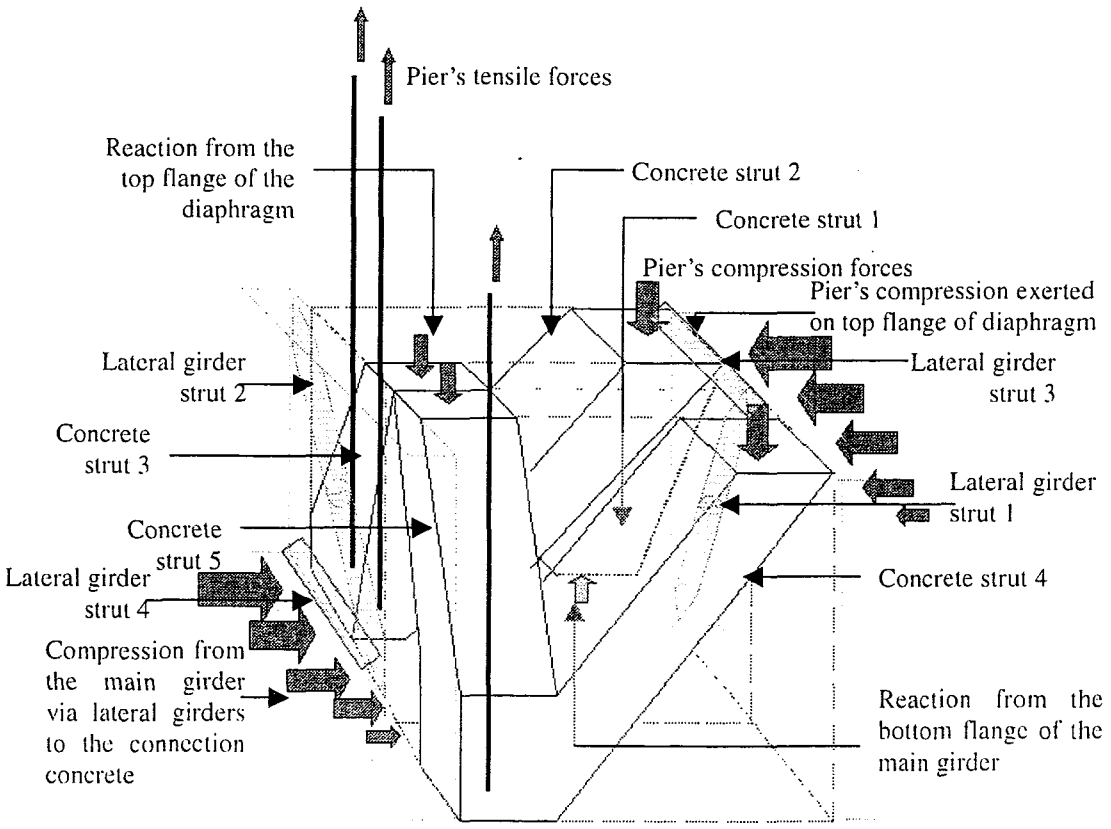

Fig.7.16 (a) Force transfer mechanisms inside the connection concrete of specimen C-4. (established to resist the pier's forces)

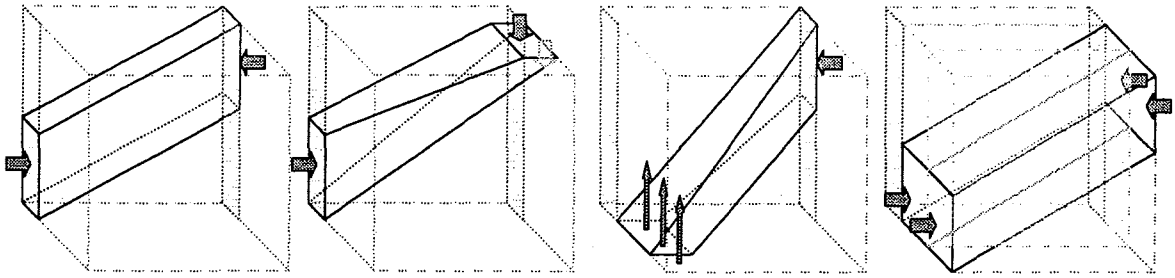

(a) Distributions of the main girder's compressions (left & right) to the connection concrete bounded by flanges and stiffeners

(b) Distributions of the main girder's compression (left) to the connection concrete

(c) Distributions of the main girder's compression (right) to the connection

(d) Distributions of the main girder's forces via lateral girders to the connection concrete

Fig. 7.16(b) Force transfer mechanisms inside connection concrete of specimen C-4. (established to resist main girder's forces)

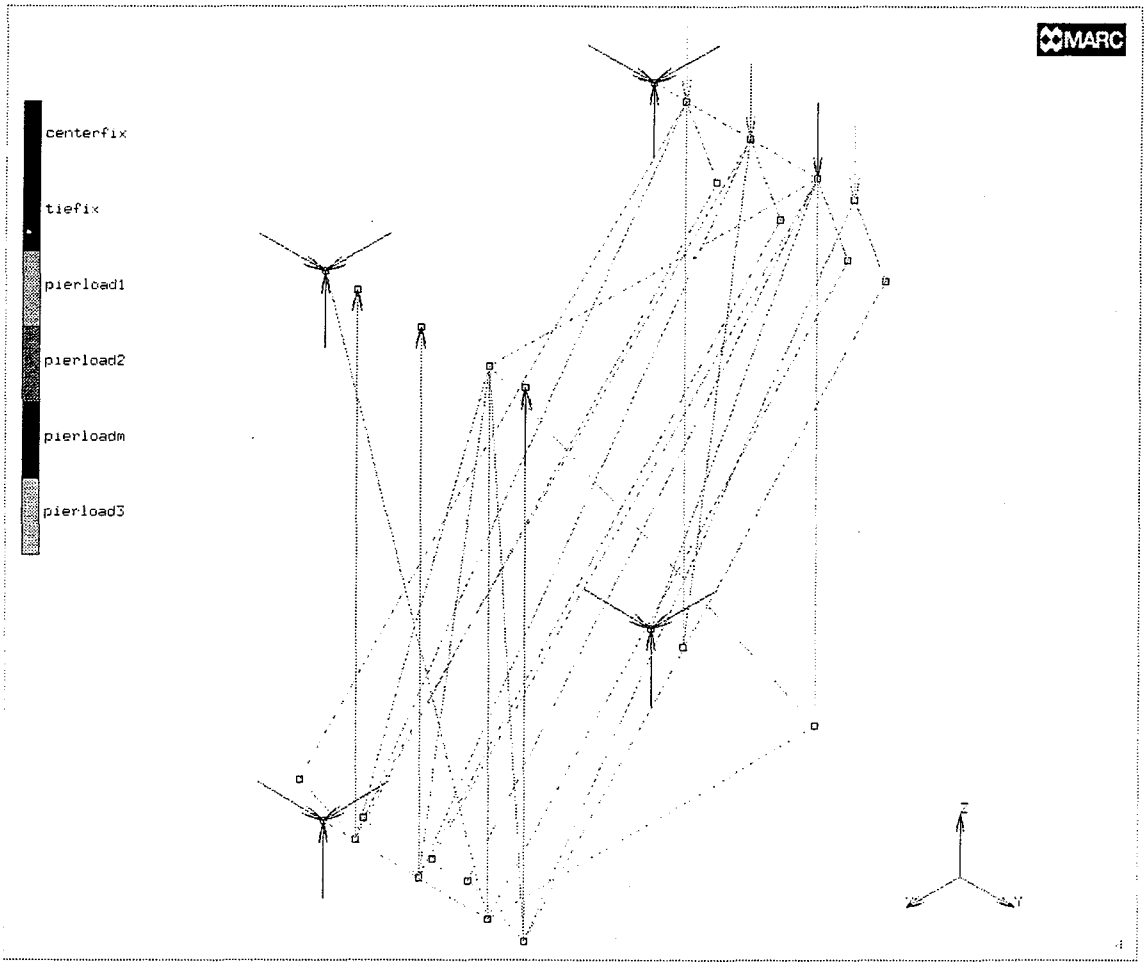

Fig.7.17 (a) Truss analogy representing force transfer mechanism in specimen C-4 (with indications of externally applied forces)

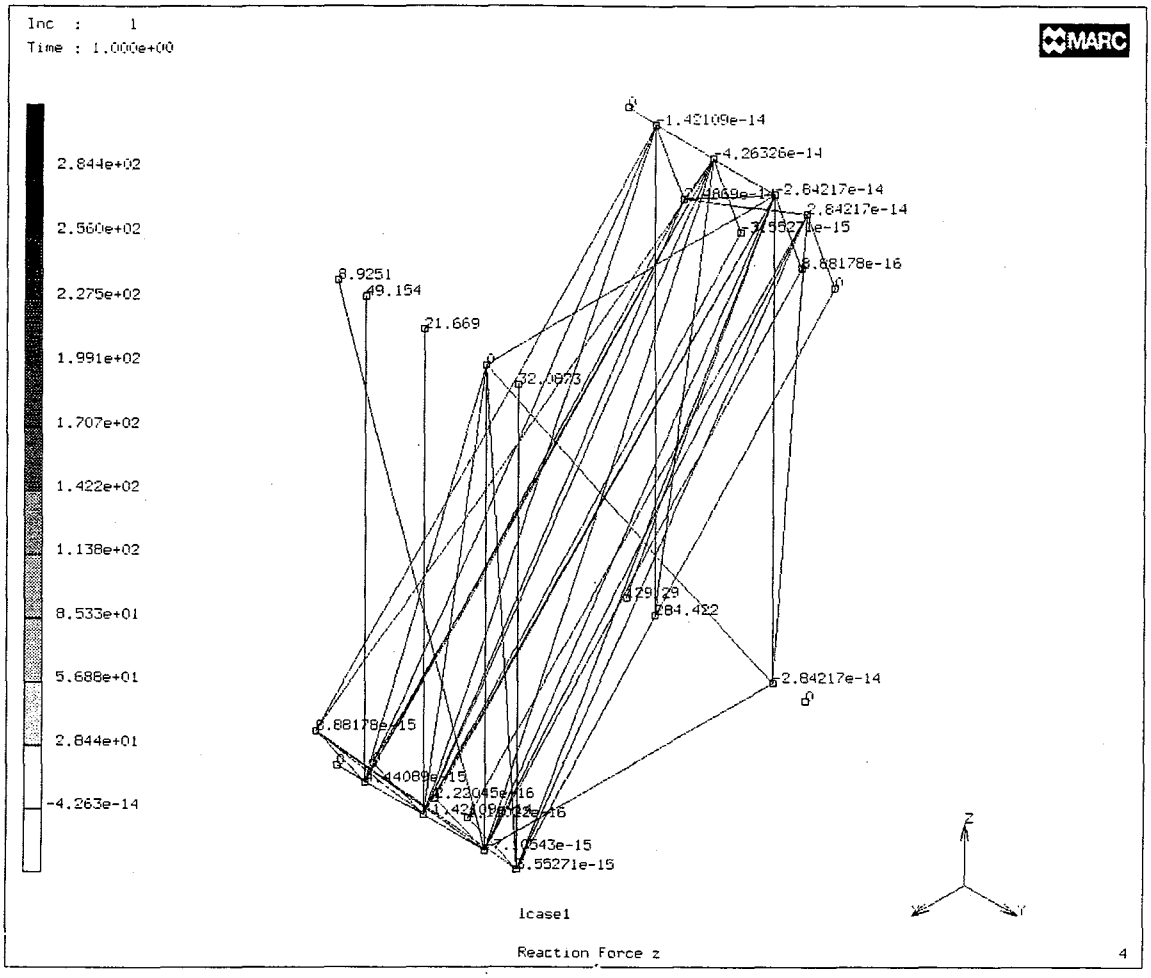

Fig.7.17 (b) Truss analogy representing force transfer mechanism in specimen C-3 (with reaction forces at nodes)

With the same finite element analysis program, MARC, the truss system shown in Fig.7.17 is analyzed. It is noted that since the distribution of forces from pier to the top of the connection is of the same pattern as that shown in Fig.7.9, larger force is, therefore, distributed laterally. It is because on the compression bearing zone which is laterally deviated (top flange of the diaphragm), there is a group of studs welded on. This addition of stud causes the cross-section area of strut that carries the compression force onto the top flange of diaphragm increased. Therefore, this stronger strut will take relatively larger forces than the other struts including the central one in this specimen.

7.5 Comparison between Forces in Reinforcing Bars Obtained from Experiments and from Prediction with Strut-and-Tie Model

So as to prove the applicability of the force transfer mechanism proposed in Chapter 6 to the strut-and-tie model, the distribution of forces in reinforcing bars predicted with the strut-and-tie model are compared with the value obtained from the experiments. To achieve this, in the truss system, all of the reinforcement ties are assumed to have a fixed displacement condition at the top ends. Then, in the analysis, the axial force in every reinforcing bar is computed. The comparisons between the calculated values of forces in reinforcing bars and values obtained in the experiments are shown in Fig.7.18.

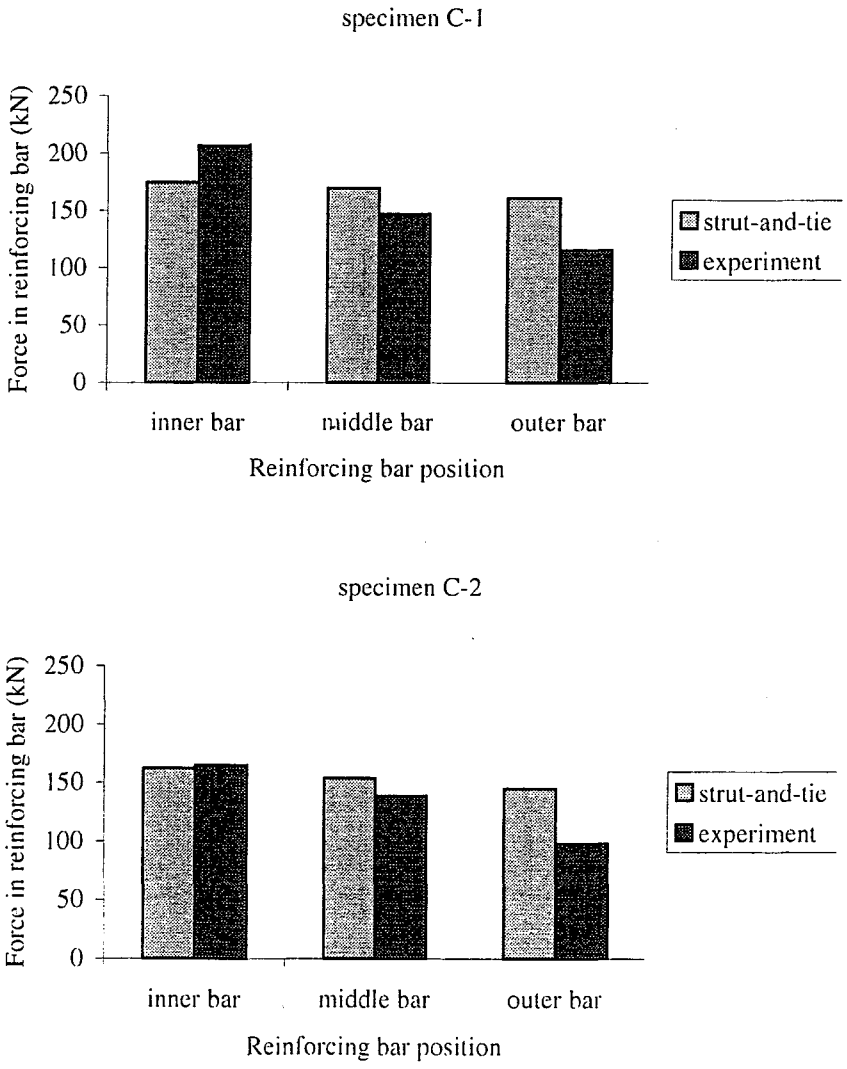

Fig.7.18 Comparisons between forces in reinforcing bar computed in truss analysis and the values obtained from experiments (at horizontal load = 210 kN)

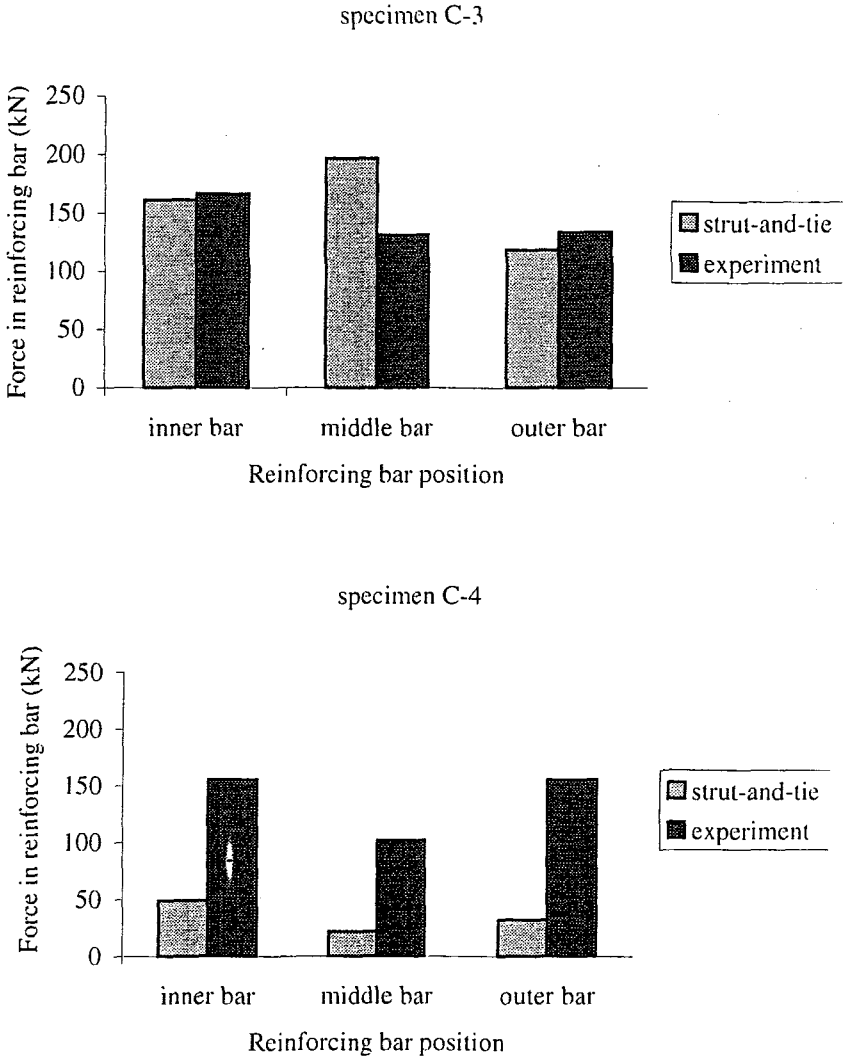

Fig.7.18 Comparisons between forces in reinforcing bar computed in truss analysis and the values obtained from experiments (at horizontal load = 210 kN) (cont.)

From the plot, it can be seen that for specimen C-1, C-2, and C-3, the calculated values agree well with the experimental results except the middle bar of specimen C-3 that shows larger force than the experimental value. This might be due to the assumption used in determining the struts and ties that represent the diaphragm plate. Some dimensions of these struts and ties might be too large. Therefore, when it is subjected to shear-liked forces, the member which is jointed at the same node as the top node of reinforcing bar tie will contribute excessively large upward force to the node.

For specimen C-4, the predicted forces are relatively low compared to the experimental results. This might be caused by the imperfection in determining the dimensions of struts representing the contribution of the lateral girder. Idealizing as the point load is applied on to the cantilever lateral girder, the compression and tension areas at its fixed end could be computed. This point load is the tensile force from pier that is transferred to lateral girder via the diaphragms. The compression and tension areas are then used as the area of lateral girder's struts. In the analysis, this assumed dimension might be too small. So the compression force from the pier, instead of being transferred to the tension side at a right proportion, it is distributed more to the other struts located on compression side. Therefore, the tensile forces in reinforcing bars become smaller than in a real case.

7.6 Composite Connection Design

For a design purpose, in this section, some design considerations are given in the first place. Then the strut-and-tie models derived based on the force transfer mechanisms are simplified. Consecutively, the procedures are suggested for designing the relevant connection components, such as lateral girder and diaphragm. The following chart shows the flow of these design works.

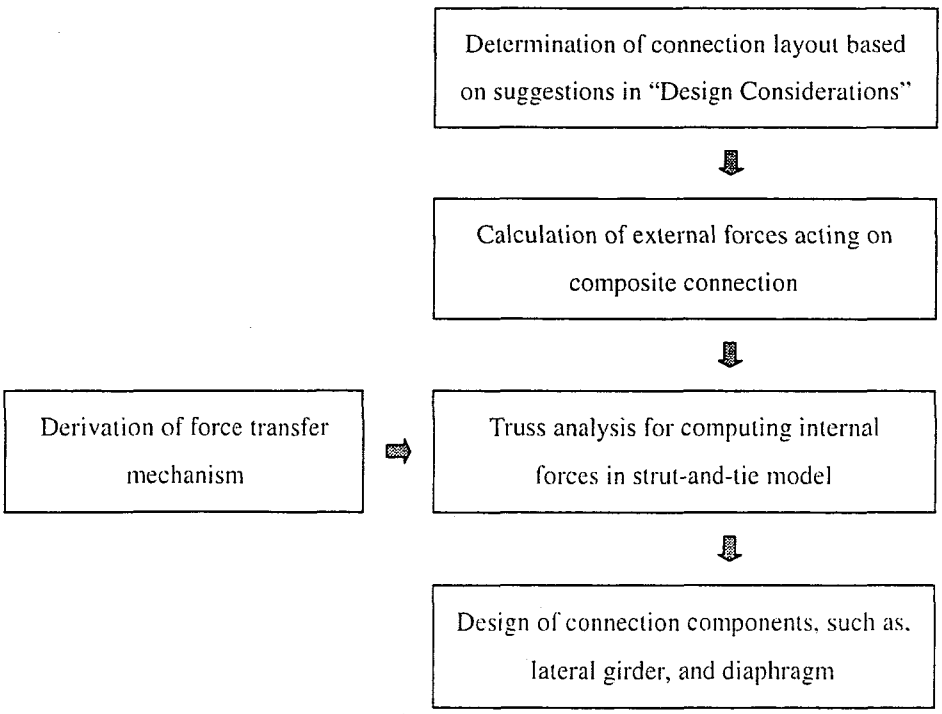

Fig.7.19 Composite connection design procedures

7.6.1 Design Considerations

From series of experiments, behavior of composite connections with different designs could be observed. The results from tests as well as those from analysis were used to derive the force transfer mechanisms. Then the strut-and-tie model was constructed in order to compute the internal forces within the connection and to verify the validity of the mechanism.

In practice, the structure are generally designed such that the failure will not occur primarily inside the connection but in the conjoining member, or more specifically speaking, the pier. However, from the results of strut-and-tie analysis, it was found that in specimen C-1, crushing of connection concrete also occurred at the ultimate state. It leads to the excessive rotation of the connection and the lower ultimate load carrying capacity compared to the other specimens. Therefore, in the proper design, to prevent this kind of detrimental phenomenon in the connection, some points that worth taking into consideration are given as follows.

7.6.1.1 Stress Concentration at Vicinity of Main Girder

Fig.7.20 illustrates the locations where the concrete is highly stressed in specimen C-1.

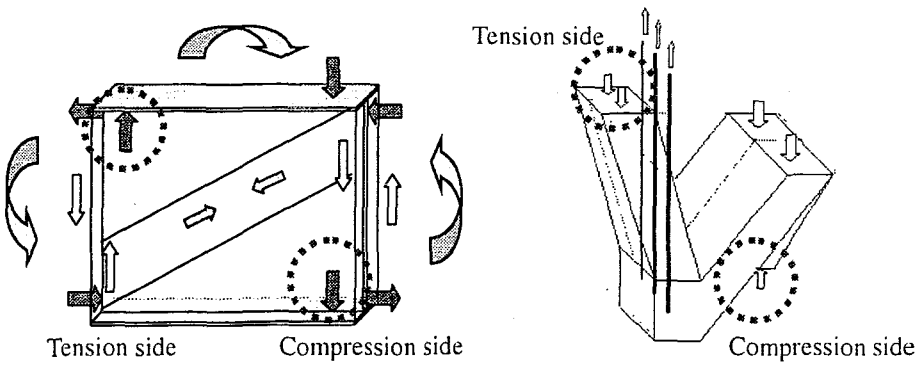

Fig.7.20 Stress concentration at vicinity of the main girder in specimen C-1

On compression side, the pier's compressive force possibly becomes concentrated at the bottom flange of the main girder. On tension side, only the top flange of the main girder will carry the entire pier's tensile force. Therefore, the concrete in these zones is likely to be crushed by the high stress concentration. In addition, since flange of the main girder will also be subjected to high stress, in design, the strength of the welded joint

should be carefully checked. In specimen C-4, as, inside the connection, the top flange of the main girder is removed and the others are added on the top of the diaphragms, thus the stress concentration should also be checked at vicinity of the diaphragm's flange on the tension side.

7.6.1.2 Transverse Tensile Force in Compressive Strut

The damaging effect may occur due to an excessive tensile stress in transverse direction of strut. This transverse stress may cause the diagonal tension crack in strut and reduce the strength of connection. The locations that are prone to this phenomenon are, concrete strut series 1 on compression side, inclined concrete strut series 2 at the middle of the connection, the concrete strut series 3 on tension side, and strut 4 which is located at vicinity of the main girder.

7.6.1.3 Roles of Connection Components

Accordingly to the magnitude of externally applied forces and the predefined dimensions of the connection, the behavior of connection can be predicted by some analytical methodologies, such as, finite element analysis or strut-and-tie model. If the concrete alone can safely carry the compressive forces in strut1, 2, 3, and 4, the connection may be designed as simple as specimen C-1. However, if it cannot carry such forces, the lateral girder may be added so that the forces will be better distributed throughout the connection and the concentration of stress at vicinity of the main girder may be avoided. In addition, in case that the pier is rather wide comparing to the width of the main girder, adding diaphragms will help strengthen the lateral girder, thus, more forces will be carried by the connection components located farther away from the main girder, as a result, the concrete around the main girder will not be overly stressed.

Another alternative design is as that of specimen C-4. By distinguishingly arranging the connection components, the force transfer mechanism is differed. A proper arrangement can greatly reduce the problem of stress concentration thus reduce the potential local deterioration inside the connection. In specimen C-4, forces from pier will be transferred to the main girder mainly via the lateral girder especially on the tension side. Since tensile force from pier is resisted mostly by the diaphragm's flange, thus, in this type of connection, the concrete stress at vicinity of the diaphragm's flange should rigorously be checked. As well, the strength of lateral girder should be appropriately designed as it is the only component which carries forces from the pier to the main girder particularly on tension side.

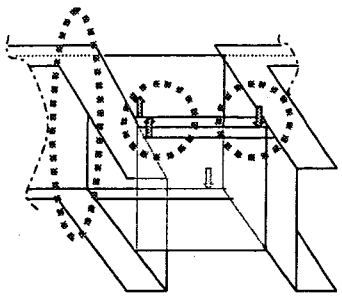

Fig.7.21 Locations where high stress is expected in specimen C-4

7.6.2 Determination of External Forces Applied to Connection

Considering the connection as the system, the external forces applied to the system can be divided into two parts regarding the source of force. These two groups of forces are forces from the pier and forces from the main girder. Forces in these groups consist of flexural compression and tension, and shear forces. A quantitative determination of these forces is as described earlier in section 7.3.

7.6.3 Truss Analysis and Its Simplifications

The simulation of the force transfer mechanism within the composite connection by a system of truss members was shown previously in section 7.4. However, if the main purpose is only to roughly predict the behavior of a newly designed connection at the ultimate state, it may be inconvenient to conduct the analysis of the full model due to its complication. Therefore, the simplified models are proposed in this section. The simplified models for specimen C-1 and C-2 are as shown in Fig.7.22 and 7.23. Instead of dividing the connection into three parallel portions as in the full model, the forces which flow in the same direction are represented by only one flow path or only one truss member. The cross-sectional area of this representative member is assumed to be equal to a summation of areas of all three members that run along the similar path. Additionally, this member is relocated at the center of all three members. By doing so, number of truss element in the preliminary analysis can be reduced to approximately one-third of the original amount in the full model. This simplified truss model can predict exactly the same total forces in the truss members, for example, on compression side, the same reaction from the main girder's bottom flange, as well as on the tension side where the similar reaction force from the main girder's top flange is predicted. It should be noted, however, that for the connection which posses the complicated force transfer mechanism like specimen C-3, it is not appropriate to conduct the simplified truss analysis. This is because, merging three compression strut or tension tie together

will change the effective location of the diaphragm, thus, the contribution of the diaphragm might be wrongly predicted. This inaccurate simulation will lead to a significant discrepancy in the prediction of the connection's behavior at the ultimate state. Furthermore, by collapsing three members into one, the non-uniform distribution of forces in the lateral direction cannot be reproduced. Hence, the stress in strut laid near the main girder may be underestimated, while, in strut located far from main girder, the predicted stress may become too high. For example, in the inclined strut series 2, stress in strut 21 might be underestimated and the stress in strut 23 would be overestimated. It is suggested that the simplified model should be used only to roughly check the capability of the newly designed connection. After coming up with the most appropriate design, the full model should be constructed and analyzed to get the more reliable results.

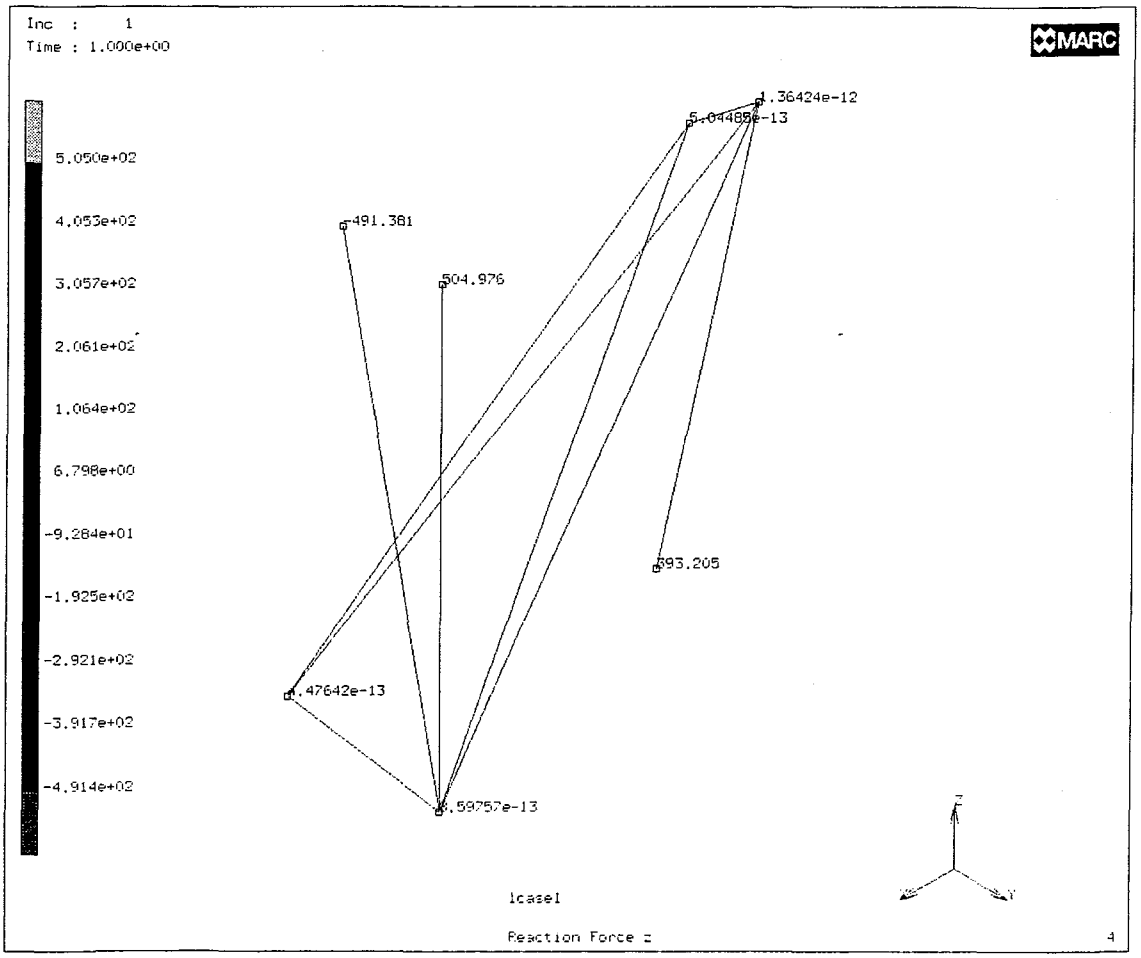

Fig.7.22 Simplified truss model of specimen C-1

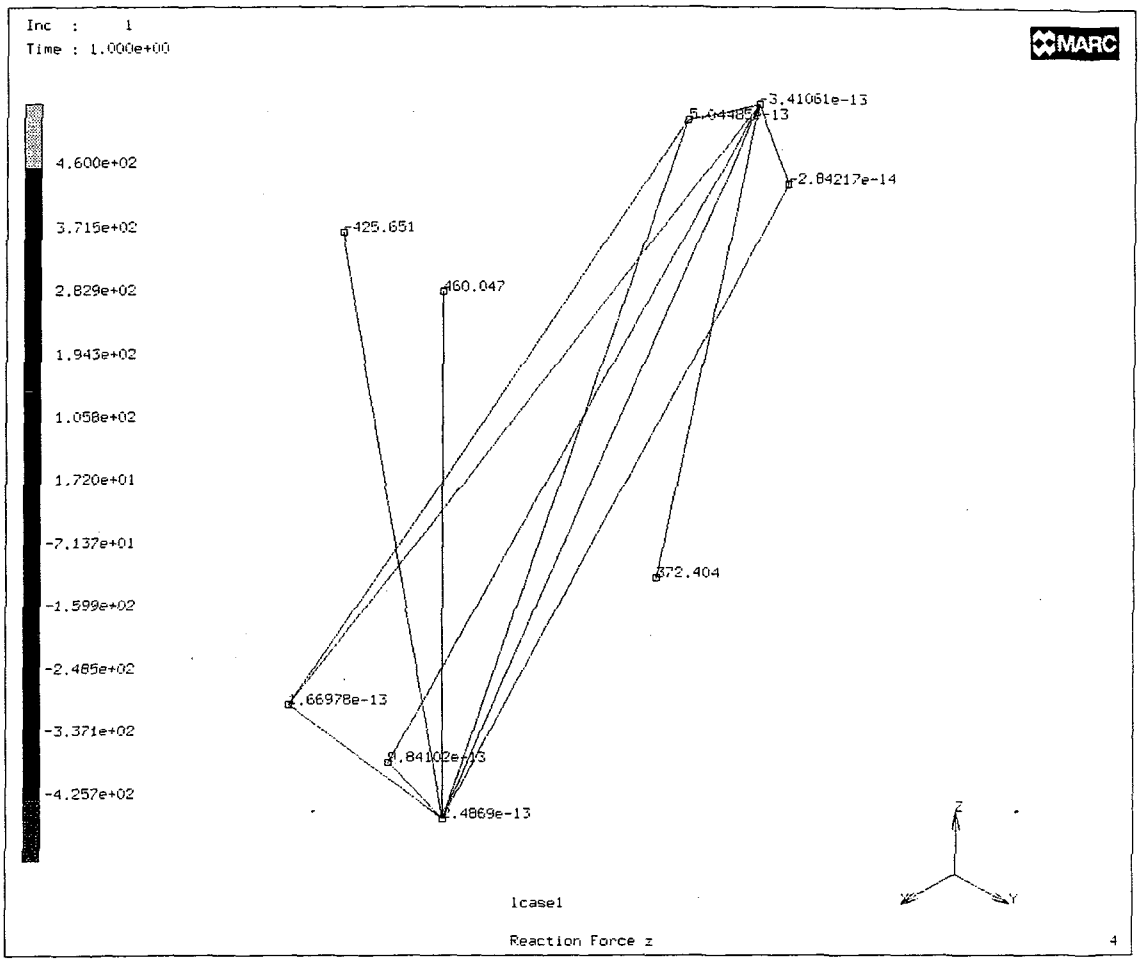

Fig.7.23 Simplified truss model of specimen C-2

7.6.4 Designs of Connection Components

To satisfy the ultimate strength requirements (no failure within the connection), the connection may be strengthened with some additional components such as the lateral girder, and the diaphragm. The suggestions for designs of these two components are given in Table 7.1.

Table 7.1 Suggestions for design of lateral girder and diaphragm

Lateral Girder	**Design Suggestion**
Flange width	Since the flange will help distribute forces from the main girder laterally throughout the connection, therefore, the wider the flange is, the better the forces will be spread out.
Flange thickness	Thickness of flange can be designed by taking into account the horizontal components of the main girder's forces
Web thickness	Assumption of a full composite action between lateral girder and adjacent concrete may be applied. Then by truss analysis, the internal forces of the truss members can be obtained. The transformed section method is consecutively used to calculate a portion of force which is carried by lateral girder's web to the main girder. Finally, based on the allowable stress of steel, the thickness of web can be determined.
Diaphragm	Thickness of the diaphragm can be determined by assuming that all of the truss members that represent the diaphragm will be yielded at the same load. By assuming further that one-third of the cross-sectional area of diaphragm along the diagonal truss is equal to two times of one truss's cross-sectional area, the dimension of truss member can be calculated. It should be noted that in experiment, strain measured on diaphragm was approximately 10% of the yielding strain. Thus the truss cross-sectional area used in calculation example is taken as 10% of the value computed based on aforementioned assumptions. The truss analysis is then carried out. Internal forces obtained can be used to determine the thickness of the diaphragm. This process may need some iterative calculations.

7.7 Conclusions

In this chapter, the force transfer mechanisms proposed for specimen C-1, C-2, C-3, and C-4 are applied to construct the strut-and-tie model. The mechanisms suggest the flow paths of forces within the composite connection and determine the positions of the strut and tie members in the system. Accordingly to the proposed calculation procedures for strut-and-tie model, the dimensions of the strut and tie members are determined. These

members' dimensions along with the assumption of elastic material properties, are implemented to the truss elements which represent the struts and ties in the model. By using the Finite Element Analysis program, the truss analysis is carried out. Comparing to the three-dimensional nonlinear analysis of this type of structure, the calculation time is considerably reduced due to the simplicity of the model. The result from truss analysis is then compared with the experimental result in terms of forces in reinforcing bars. A fair agreement could be observed in the case of specimen C-1, C-2, and C-3. However, for specimen C-4, the underestimated result is obtained from the truss analysis. This might be due to the inappropriate assumption used for determining dimensions of truss members that represent the lateral girder. It is also noted that with the method proposed by Siao [70], the transverse stress in the compressive concrete struts are calculated. Nevertheless, it was found that the tensile stresses did not reach the cracking limit in any concrete struts except the one located at vicinity of the main girder (strut 4 in specimen C-1), while in the experiment, at the ultimate state, the cracks could be observed on the connection surfaces of specimen C-1. This might be due to the inapplicability of the stress prediction method by Siao, or it is possibly due to the inappropriate assumptions used to determine the dimensions of strut and tie members.

Another behavior of the connection that can be predicted by the strut-and-tie model is the stress concentration at the vicinity of the main girder. In specimen C-1, at the top-left node or the top end of concrete strut series 1, Fig.7.8, the force becomes concentrated in this zone. From the strut-and-tie calculation, the stress at this position is equal to 0.0574 kN/mm^2. Comparing to the concrete strength under multi-axial load computed using the equation derived by A. Muttoni, et al.[1], and assuming that the confining stress is one-fifth of the major stress, fc' = 0.06041 kN/mm^2, the stress in this zone is much closed to compressive strength of concrete. Thus, at the ultimate state, the concrete in this zone is possibly crushed. The softening of concrete will reduce the rotational resistance of the connection and the connection concrete will be twisted apart from the main girder. It was also observed in the experiment of specimen C-1 that during approaching the ultimate state, the disintegration between the concrete and steel girder at the connection occurred. For specimen C-2 and C-3, since there exist the lateral girder connected to the concrete, the force in this zone will be partly carried by the lateral girder and transferred to the main girder. Therefore, at the bottom of strut 1 and at the top of strut 2, the stress in concrete will be reduced. By using the transform section method, the proportion of force carried by the lateral girder can be calculated. Stresses on the bearing area of concrete in specimen C-2 is σc = 0.0433 kN, and in

specimen C-3 is, σc = 0.0347 kN. It is obvious that stress becomes less concentrated at this location when the lateral girders are added, thus, these two specimens are less prone to the stress concentration problem that may finally lead to an excessive rotation of the connection like in specimen C-1. For specimen C-4, although, the results from strut-and-tie model is not correlated well with the experimental results, qualitatively, it can be concluded based on the force transfer mechanism that, on tension side, the force will be transferred to the main girder only by the lateral girder strut 2, Fig.7.16., thus care must be taken in designing the thickness of lateral girder. On the compression side, the compressive force from pier will be partially transferred straightforwardly to the bottom flange of the main girder, and the rest to the bearing area on the flange of diaphragm. The later portion of the compressive forces will be conveyed further to the main girder via the lateral girder. So comparing to specimen C-1 the stress concentration on the compression side will be less severe due to the existence of the lateral girder. Notation is given here that, in practices, the reparation of lateral steel girder will be easier than to let the local failure occur in concrete and repair it. It is due to the fact that the concrete is encased inside the lateral girder it will be difficult to assess the failure and properly fix it. This shows the benefits of using type C-4 design.

For the design works, the simplified strut-and-tie models are derived. In these models, the number of truss elements is reduced to, at most, one-third of the full model. It, therefore, helps save time while the designer is trying to find the optimum arrangement of the connection components. However, it is suggested that after the connection components and their positions were finalized, the full truss model should be constructed and analyzed. It is because with the simplified model, the non-uniform distribution of forces in lateral direction cannot be determined. Therefore, the internal forces of some strut and tie members may have been either overestimated or underestimated. Finally, some considerations as well as suggestions for composite connection design are given in the last section of this chapter.